

UNIVERSITY OF BELGRADE

FACULTY OF CHEMISTRY

Adejumo Temiloluwa Timothy

**SYNTHESIS, CHARACTERIZATION AND EVALUATION
OF CATALYTIC PROPERTIES OF Zn(II) COMPLEXES
WITH HYDRAZONE LIGANDS**

Doctoral Dissertation

Belgrade 2024

UNIVERZITET U BEOGRADU

HEMIJSKI FAKULTET

Adejumo Temiloluwa Timothy

**SINTEZA, KARAKTERIZACIJA I ISPITIVANJE
KATALITIČKIH SVOJSTAVA KOMPLEKSA Zn(II) SA
HIDRAZONSKIM LIGANDIMA**

doktorska disertacija

Beograd, 2024

Supervisor

Dr. Božidar Čobeljić,
University of Belgrade – Faculty of Chemistry

Committee members:

Prof. Katarina Anđelković
University of Belgrade – Faculty of Chemistry

Dr Maja Gruden,
University of Belgrade – Faculty of Chemistry

Dr Matija Zlatar
University of Belgrade – Institute of Chemistry,
Technology and Metallurgy

Defense date _____ **2024**

Acknowledgement

I wish to extend my heartfelt gratitude to my father late Pastor E.K. Adejumo and my mother, Assistant Pastor C. Adejumo, for providing me with a remarkable opportunity to pursue professional studies and research. My appreciation also goes to Pastor and Pastor Mrs. Olagunju for their unwavering support.

I am profoundly thankful for the exceptional guidance of my supervisor, Božidar Čobeljić. His consistent encouragement, insightful guidance, and genuine care for his students mark him as an exceptional educator and mentor.

A special note of appreciation is reserved for Professor Katarina Anđelković, whose invaluable contributions greatly enriched this research. May her efforts be rewarded by the divine.

I extend my gratitude to the Faculty of Chemistry at the University of Belgrade, including the faculty's leadership and staff, for fostering an environment conducive to learning and exploration.

Warm appreciation is also due to my colleagues in Lab 527. Marko and Dara's kindness and camaraderie made my time in this group joyful and effortless.

I am indebted to my siblings for their enduring support, encouragement, prayers, and financial assistance.

I am thankful for the gracious assistance I received from various individuals during the course of my research. My sincere thanks go to friends and colleagues who made significant contributions to the success of this project. Your efforts are deeply valued.

I would also like to acknowledge the ministries and institutions that generously supported this research financially.

In closing, I offer my deepest gratitude to the Almighty God, the epitome of compassion and mercy, for granting me the strength to bring this project to fruition.

SYNTHESIS, CHARACTERIZATION AND EVALUATION OF CATALYTIC PROPERTIES OF Zn(II) COMPLEXES WITH HYDRAZONE LIGANDS

Abstract

In this study, a series of novel zinc complexes have been synthesised and thoroughly characterized. Two of the complexes were prepared from the ligands obtained from derivatives of 2-acetylthiazole, and another two from the derivative of Girard's reagents T and P. These complexes featured tridentate coordinating ligands of hydrazone with NNS or NNO donating atoms and were characterized by elemental analysis, spectroscopic techniques and single crystal XRD methods. In addition to these new complexes, the study also included a catalytic study of five analogues previously synthesized, each containing ligands with the same donor atom sets.

The primary aim of this research was to evaluate the catalytic potential of these complexes in the coupling reaction of KA^2 , leading to the synthesis of tetrasubstituted propargylamines, which are commonly used as intermediates in organic synthesis, providing easy access to a wide range of structurally complex organic compounds. A number of model reactants were used to optimise the KA^2 reaction conditions. To further investigate the catalytic activity of the Zn(II) complex, additional tests were then carried out on the most reactive compounds using a variety of substrate combinations.

In order to better understand the electronic structure of the complexes and how it correlates with catalytic reactivity, the study employed density functional theory (DFT) calculations. Based on the Conceptual DFT framework the study derived several global molecular reactivity descriptors, including chemical potential (μ), hardness (η), softness (S), electronegativity (χ), and electrophilic index (ω). These descriptors provided valuable insights into how reactive and stable complexes are.

Keywords: hydrazone ligand; Zn(II) complexes; XRD; ketone-amine-alkyne coupling reaction; catalysis; DFT calculations

Scientific Field: Chemistry

Subfield of Science: Inorganic Chemistry

SINTEZA, KARAKTERIZACIJA I ISPITIVANJE KATALITIČKIH SVOJSTAVA KOMPLEKSA Zn(II) SA HIDRAZONSKIM LIGANDIMA

Apstrakt

U ovoj tezi, sintetisana je i detaljno okarakterisana serija novih kompleksa Zn(II). Dva kompleksa su dobijena polazeći od liganda derivata 2-acetiltiazola, a druga dva od derivata Žirarovih T i P reagenasa. Ovi kompleksi sadrže ligande na bazi tridentatnih hidrazona, sa NNO ili NNS donorskim setom atoma, i okarakterisani su elementalnom analizom, infracrvenom (IC) i nuklearno magnetno rezonantnom (NMR) spektroskopijom i metodom difrakcije rendgenskih zraka na monokristalima. Pored novih kompleksa Zn(II), studija je takođe uključila i pet prethodno sintetisanih analoga, koji sadrže ligande sa istim donorskim setom atoma.

Glavni cilj ovog istraživanja bio je evaluacija katalitičkog potencijala kompleksa Zn(II), u reakciji keto-amin-alkin (KA^2) kuplovanja, koja kao proizvod daje tetrasupstituisane propargilamine. Propargilamini se najčešće koriste kao intermedijeri u organskim sintezama, omogućavajući lak pristup širokom spektru kompleksnih organskih jedinjenja. Prilikom optimizacije KA^2 reakcije korišćeni su različiti model sistemi. Kako bi se dodatna ispitala katalitička aktivnost kompleksa Zn(II), za nejreaktivnija jedinjenja, se potom pratio uticaj promenom polaznih supstrata na reaktivnost.

DFT proračuni su izvedeni da bi se razjasnila elektronska struktura ispitivanih kompleksa Zn(II), odlično povezujući strukturu kompleksa sa njihovom katalitičkom aktivnošću. Na osnovu Konceptualne teorije funkcionala gustine, izračunati su globalni molekularni deskriptori reaktivnosti, kao što su hemijski potencijal (μ), tvrdoća (η), mekoća (S), elektronegativnost (χ) i indeks elektrofilnosti (ω). Ovi deskriptori su pružili uvid u to koliko su proučavani kompleksi reaktivni i stabilni.

Ključne reči: Hidrazonski ligandi, kompleksi Zn(II), Rendgenska strukturna analiza, Keto-amin-alkil reakcija, Kataliza, DFT proračuni.

Naučna oblast: Hemija

Uža naučna oblast: Neorganska hemija

List of abbreviations

ADF:	Amsterdam Density Functional
ATR:	Attenuated Total Reflection
CIF:	Crystallographic Information File
COSY:	Correlated Spectroscopy
CSD:	Cambridge Structural Database
DFT:	Density Functional Theory
DMSO:	Dimethyl sulfoxide
DMSO-d ₆ :	Deuterium dimethyl sulfoxide
FT-IR:	Fourier Transform Infrared spectroscopy
HL ¹ Cl:	(<i>E</i>)- <i>N,N,N</i> -trimethyl-2-oxo-2-(2-(1-(thiazol-2-yl)ethylidene)hydrazinyl)ethan-1-aminium chloride
HL ² Cl:	(<i>E</i>)-2-(1-(thiazol-2-yl)ethylidene)hydrazine-1-carbothioamide
HL ³ Cl:	(<i>E</i>)- <i>N,N,N</i> -trimethyl-2-oxo-2-(2-(1-(pyridin-2-yl)ethylidene)hydrazinyl) ethan-1-aminium Chloride
HL ⁴ Cl:	(<i>E</i>)-1-(2-oxo-2-(2-(1-(pyridin-2-yl)ethylidene)hydrazinyl)ethyl)-pyridine-1-ium chloride
HL ⁵ Cl:	(<i>E</i>)- <i>N,N,N</i> -trimethyl-2-oxo-2-(2-(quinolin-2-ylmethylene)hydrazinyl)ethan-1-aminium chloride
HL ⁶ Cl:	(<i>E</i>)-1-(2-oxo-2-(2-(quinolin-2-ylmethylene)hydrazineyl)ethyl)pyridin-1-ium chloride
IR:	Infrared spectroscopy
MeOH:	Methanol
EtOH:	Ethanol
NMR:	Nuclear magnetic resonance spectroscopy
ORTEP:	Oak Ridge Thermal Ellipsoid Plot
SD:	Standard deviation
TMS:	Tetramethylsilane
KA ² :	Ketone-Amine-Alkyne
GC/MS:	Gas Chromatography-Mass Spectrometry

Table of contents

1.	Introduction	1
2.	Literature review	2
2.1	Hydrazones	2
2.2	Girard's reagent	2
2.3	Hydrazone ligands and their metal complexes	3
2.4	Catalytic applications of metal complexes of hydrazones	10
2.5	Propargylamines	11
3.	Experimental part	13
3.1	Materials and methods	13
3.2	Synthesis of the Ligands	13
3.2.1	Ligand HL ¹ Cl synthesis	13
3.2.2	Ligand HL ² synthesis	13
3.2.3	Ligand HL ³ Cl synthesis	14
3.2.4	Ligand HL ⁴ Cl synthesis	14
3.2.5	Ligand HL ⁵ Cl synthesis	14
3.2.6	Ligand HL ⁶ Cl synthesis	14
3.3	Synthesis of Complexes	15
3.3.1	Synthesis procedure of [ZnL ¹ (NCS) ₂]·H ₂ O complex 1	15
3.3.2	Synthesis procedure of [Zn(L ²) ₂] complex 2	15
3.3.3	Synthesis procedure of [ZnL ³ (NCS) ₂]·0.5CH ₃ OH complex 3	15
3.3.4	Synthesis procedure of [ZnL ¹ (N ₃) ₂] complex 4	16
3.3.5	Synthesis procedure of [ZnL ² (N ₃) ₂] complex 5	16
3.3.6	Synthesis procedure of [ZnL ⁴ (N ₃) ₂] complex 6	16
3.3.7	Synthesis procedure of [ZnL ⁵ (N ₃) ₂] complex 7	16
3.3.8	Synthesis procedure of [ZnL ⁵ (NCO) ₂] complex 8	16
3.3.9	Synthesis procedure of [ZnL ⁶ (NCS) ₂]·2H ₂ O complex 9	17
3.4	X-ray structural analysis	17
3.4.1	Complexes 1 and 2 X-ray structural analysis	17
3.4.2	Complexes 5 and 6 X-ray structural analysis	18
3.5	Catalysis Procedure	19
3.5.1	Catalysis general procedure for complex 1-3	19
3.5.2	Synthesized propargylamines characterization data for 1-3	20
3.5.3	Catalysis general procedure for complexes 4-9	21
3.5.4	Synthesized propargylamines characterization data for 4-9	21
3.6	DFT Calculations	22
3.6.1	DFT Calculations for complexes 1-3	22
3.6.2	DFT Calculations for complexes 4-9	22
3.6.3	Conceptual DFT	22
4.	Result and discussion	24
4.1	Synthesis	24
4.2	FT-IR Spectroscopy of complexes 1, 2, 5 and 6	30
4.3	NMR Spectroscopy of complexes 1, 2, 5 and 6	30
4.4	Crystal structures of complex 1 and 2	31
4.5	Crystal structures of complex 5 and 6	37
4.6	Assessment of the catalytic activity of complex 1-3 in the coupling reaction of KA ²	39
4.6.1	Computational results for complexes 1-3	42
4.7	Assessment of the catalytic activity of complex 4-9 in the coupling reaction of KA ²	45
4.7.1	Computational results for complexes 4-9	47
5.	Conclusion	41

6.	References	52
	Appendix	60
	Personal and Academic Background	85

1. Introduction

Hydrazone ligands possess remarkable versatility and flexibility as polydentate ligands, with exceptional chelating capabilities with various metal ions. These ligands, classified as azomethine compounds and represented by the general structure $R_2C = NNR_2$, differ from similar compounds such as imines and oximes due to their interconnected nitrogen atoms [1]. The ability of hydrazones to coordinate to metal ions is affected by a number of factors, which include the pH of the solution, the substituents on the hydrazone molecule, and its position relative to other functional groups in the molecule [2,3]. Furthermore, upon the ligand's complexation, the -NH group undergoes deprotonation, resulting in the formation of distinct anionic tautomeric species ($=N-N^--C=O$ or $=N-N=C-O^-$) with unique coordination features [4,5]. Potential applications of metal complexes containing hydrazone-based ligands as catalysts are captivating [6]. Zn(II) exhibits a remarkable capacity to create complexes with varying coordination numbers and diverse geometric arrangements, ranging from trigonal bipyramidal, square pyramidal, or octahedral geometry [7]. Examining ligands previously synthesized featuring NNO or NNS chromophores and other hydrazone ligands and their corresponding Zn(II) complexes has revealed an underexplored landscape in terms of their catalytic potential. Detailed catalytic assessments have been conducted sporadically, leaving a substantial gap in our understanding of their catalytic capabilities [7].

In this research, we synthesized and fully characterized four novel complexes of Zn(II), which were formed through the reaction of various zinc(II) salts with hydrazone ligands. The hydrazone ligands were derived from the following compounds; Girard's reagent T and 2-acetylthiazole; thiosemicarbazide and 2-acetylthiazole; 2-acetylpyridine and Girard's reagent T; Girard's reagent P with 2-acetylpyridine; as well as 2-quinolinecarboxaldehyde and Girard's reagent T. The structures were ascertained using spectroscopic analysis, and single crystal XRD, and their catalytic activities in the coupling reaction of KA^2 were also determined. To evaluate the electronic structure of the complexes and their catalytic reactivity, DFT calculations were performed.

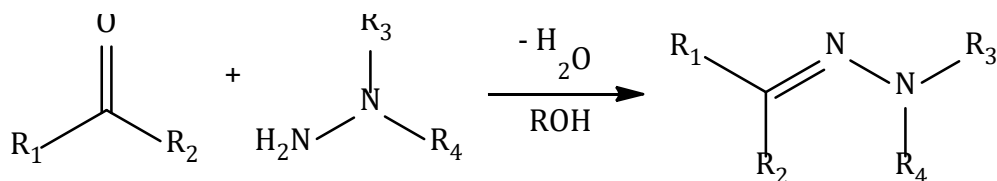
This paper is divided into four main sections:

- A literature review that surveys prior research relevant to the study.
- An experimental segment detailing the methods and materials employed in the research.
- Results and discussion, which thoroughly analyze the findings.
- A conclusive section summarizing the entirety of the work.

2. Literature review

2.1 Hydrazones

Hydrazones belong to a category of organic compounds characterized by a general formula $R_1R_2C=NNR_3R_4$ (Scheme 1). These compounds are considered Schiff bases and fall under the broader category of imines. The traditional approach to synthesizing hydrazones entails a condensation reaction between hydrazine or hydrazide and an aldehyde or ketone in protonated solvents such as ethanol, methanol, or butanol.



Scheme 1: Synthesis of hydrazone

Hydrazones' properties are primarily governed by the active centers of hydrazine, namely the carbon and nitrogen atoms [8].

Hydrazones derived from hydrazides offer increased versatility and potential application as ligands in coordination chemistry due to the presence of an additional donor site, C=O (Figure 1). This characteristic expands their potential to form complexes, and these complexes can exhibit notable catalytic activity [8, 9].

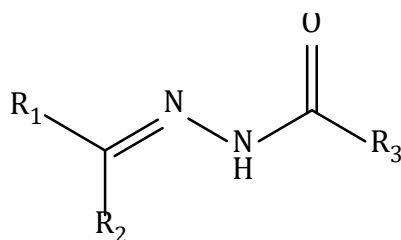


Figure 1: Molecular structure of hydrazone derived from hydrazides

2.2 Girard's reagent

Girard reagents are a class of compounds that are derivatives of glycine hydrazide. These reagents have the ability to form hydrazones when combined with carbonyl compounds, resulting in water-soluble products. The group comprises three primary types (Figure 2): Girard reagent T, also known as trimethylacetylhydrazide hydrochloride [HGT]Cl; Girard's reagent D, with IUPAC name *N,N*-dimethylglycine hydrazide hydrochloride [H₂GD]Cl; and Girard's reagent P, which is pyridinium aceto-hydrazide chloride [HGP]Cl.

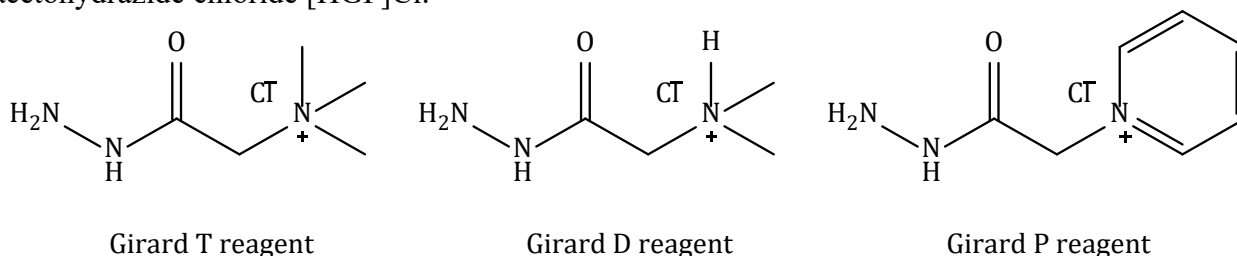


Figure 2: Structural representation of various Girard's reagent

Girard and Sandulesko were the original researchers who synthesized Girard's T and P reagents in 1936. These reagents were obtained by reacting ethyl chloroacetate with trimethylamine or pyridine, resulting in the formation of quaternary ammonium esters. These esters, upon reaction with hydrazine,

yielded the corresponding Girard reagents ([HGT]Cl and [HGP]Cl). Later, Girard's D reagent was synthesized by reacting *N,N*-dimethylglycine ethyl ester and hydrazine hydrate with concentrated hydrochloric acid [10].

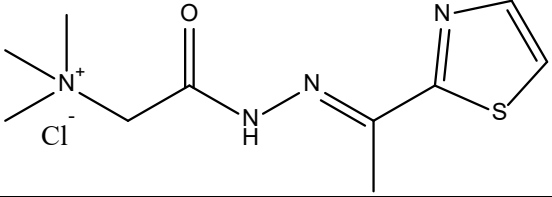
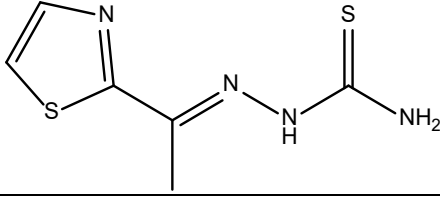
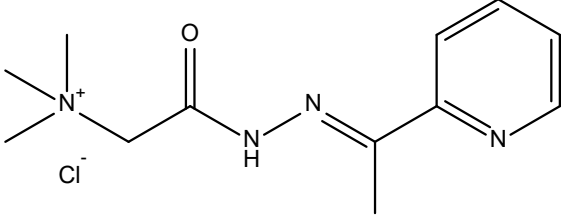
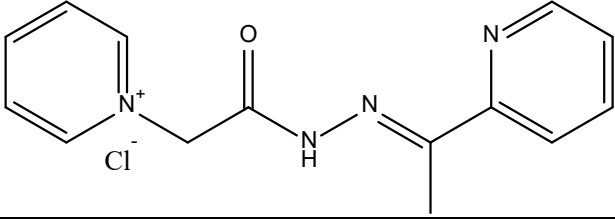
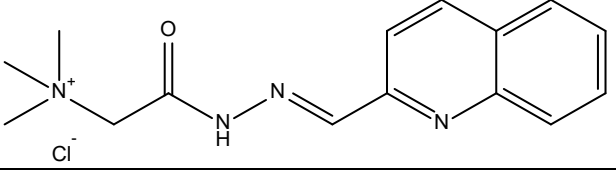
Hydrazone ligands derived from Girard reagents are characterized by having three or more potential donor atoms [11]. These compounds can exist in keto-enol tautomeric forms and have the ability to coordinate metal ions in two distinct ways: either as deprotonated species with a positive charge or as non-protonated, neutral zwitterionic forms. The inclusion of a positively charged group in metal complexes containing hydrazones derived from Girard reagents improves their water solubility [12].

2.3 Hydrazone ligands and their metal complexes

The unique coordination properties of hydrazone ligands, which are influenced by factors such as pH, substituents, and tautomeric forms, make them versatile catalysts [13,14].

Table 1 presents complexes of hydrazone ligands. These highlighted ligands of hydrazone results from the reaction of Girard's reagent T and acetyl thiazole (**HL¹Cl**), 2-acetylthiazole and thiosemicarbazide (**HL²**), 2-acetylpyridine and Girard's reagent T (**HL³Cl**), 2-acetylpyridine and Girard's reagent P (**HL⁴Cl**), as well as 2-quinolinecarboxaldehyde and Girard's reagent T (**HL⁵Cl**). These ligands possess multiple donor atoms, enabling coordination with various central metal ions. The coordination of hydrazone ligands to metal ions can occur in either their neutral or unprotonated forms. This usually depends on the conditions of the reaction, such as the ligand nature and metal ion, the ratio of metal to ligand, and the utilized solvent. Mononuclear or polynuclear complexes with various geometries can be formed under different conditions.

Table 1: Condensation products of selected hydrazone ligands

Ligand	Label	complex	Ref.
	HL¹Cl	(1) [CuL ¹ (N ₃)(CH ₃ OH)]BF ₄ (2) [Ni ₂ L ¹ ₂ (μ-1,1-N ₃) ₂ (N ₃) ₂]·4H ₂ O	15 16
	HL²	(3) FeL ² ₂ , (4) Mn(L ²) ₂ (5) [CoL ² ₂]BF ₄ ·H ₂ O	17 17 18
	HL³Cl	(6) [CdHL ³ (NCS) ₂ (SCN)] (7) [CoL ³ ₂] (8) [Ni ₂ L ³ ₂ (μ-1,1-N ₃) ₂ (N ₃) ₂] (9) [FeL ³ (NCS) ₃] (10) [CuL ³ Cl]ClO ₄ (11) [Cu ₂ L ³ (μ-1,1-N ₃) ₂]	19 20 21 22 14 14
	HL⁴Cl	(12) [Co(L ⁴)(N ₃) ₃]	18
	HL⁵Cl	(13) [Ni ₂ L ⁵ (μ-1,1-N ₃) ₂ (N ₃) ₂] (14) [CoHL ⁵ (N ₃) ₃] (15) [Co ₂ L ⁵ ₂ (μ-1,1-N ₃) ₂ (N ₃) ₂]	3 2 2

A reported literature study [15] describes the interaction involving **HL**¹Cl ligand along with Cu(BF₄)·6H₂O, including NaN₃ in methanol, resulting in a complex seen in Figure 3. Several characterization techniques were used to examine the compound. In this complex, the ligand coordinates in a nonprotonated form *via* NNO atoms. This coordination occurs in conjunction with a molecule of methanol and one azido ligand. The structural arrangement of the complex was characterized as a square-based pyramidal shape, albeit a distorted one [15].

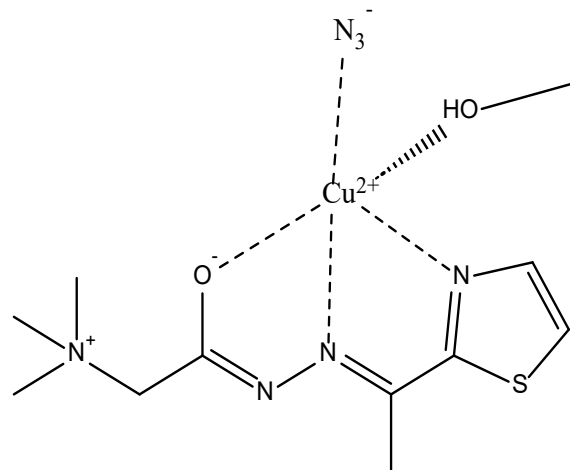


Figure 3: Representation of (1) [CuL¹(N₃)(CH₃OH)]BF₄

In another reference [16], ligand **HL**¹Cl was reacted with chloride salt of nickel(II) and NaN₃ in a mixture of acetonitrile and methanol with a molar ratio of 1:1:3, forming a dinuclear doubly bridged end-on azido complex of nickel (Figure 4). Different methods of characterization were employed in the analysis of the compound. The nickel(II) complex was described to exhibit an octahedral geometry [16].

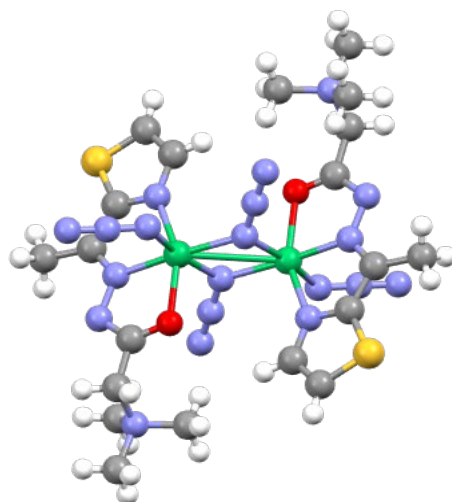


Figure 4: Representation of (2) [Ni₂L²(μ-1,1-N₃)₂(N₃)₂]

In the reference [17], **HL**² was utilized to synthesize Fe(III) and Mn(II) (Figures 5 and 6, respectively). Various characterization techniques show that both complexes exhibit coordination of the deprotonated **HL**² ligand *via* the NNS donor atoms. The manganese and iron complexes adopt trigonal-prismatic and octahedral geometry, respectively. In both cases, the ideal coordination is distorted [17].

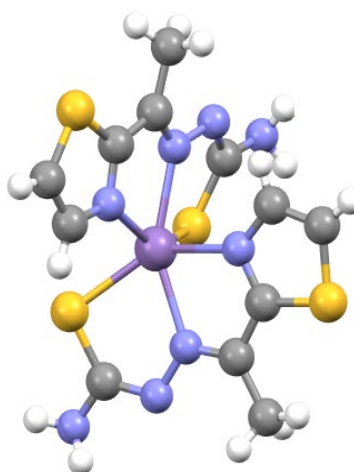


Figure 5: Representation of (3) $[\text{Fe}(\text{L}^2)_2]$

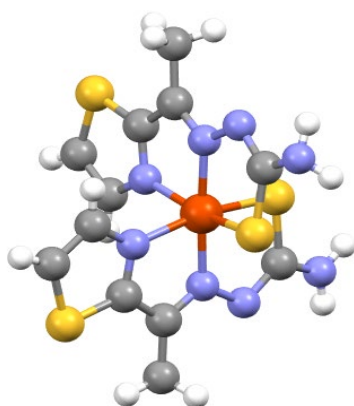


Figure 6: Representation of (4) $[\text{Mn}(\text{L}^2)_2]$

As stated in reference [18], $[\text{Co}(\text{L}^2)_2]\text{BF}_4 \cdot \text{H}_2\text{O}$ (Figure 7) was synthesized from HL^2 and $\text{Co}(\text{BF}_4)_2 \cdot 6\text{H}_2\text{O}$ in a solution mixture of methanol/water. Different analytical techniques were utilized in the characterization. The complex featured two non-protonated hydrazone ligands L^2 bonded to cobalt ion located in the center of the complex in a mer configuration. The formed complex has an octahedral geometry, with chelation involving nitrogen and sulfur atoms [18].

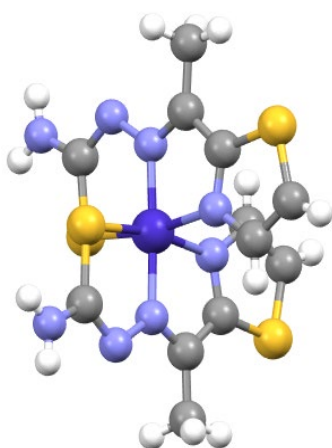


Figure 7: Representation of (5) $[\text{Co}(\text{L}^2)_2]\text{BF}_4 \cdot \text{H}_2\text{O}$

Cobeljic *et al.* [19] reported the synthesis of a cadmium(II) complex derived from the HL^3Cl ligand. Complex 6 (Figure 8) was obtained by the reaction of HL^3Cl with cadmium(II) nitrate and NH_4SCN . The reaction was carried out in an acetonitrile solution. Characterization techniques revealed that the

complex exhibits an octahedral coordination environment. The ligand coordinates to the cadmium *via* NNO donor atoms [19].

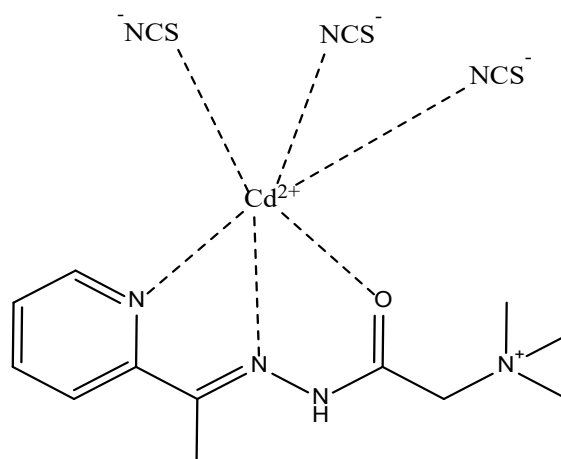


Figure 8: Representation of (6) $[\text{CdHL}^3(\text{NSC})(\text{SCN})]$

As documented in the literature [20], the reaction of HL^3Cl , copper(II) tetrafluoroborate alongside ammonium thiocyanate in a ratio of 1 to 1 to 3.6, gave rise to a compound with the general formula $[\text{CoL}^3_2][\text{Co}(\text{NCS})_4]\text{BF}_4$ (complex 7, Figure 9). In this compound, the Co(III) ion is coordinated by two molecules of the ligand. The ligands coordinate through N and O atoms, resulting in an octahedral complex cation. The compound also contains two anions, namely the tetrahedral isothiocyanato complex anion Co(II) and the BF_4^- anion [20]

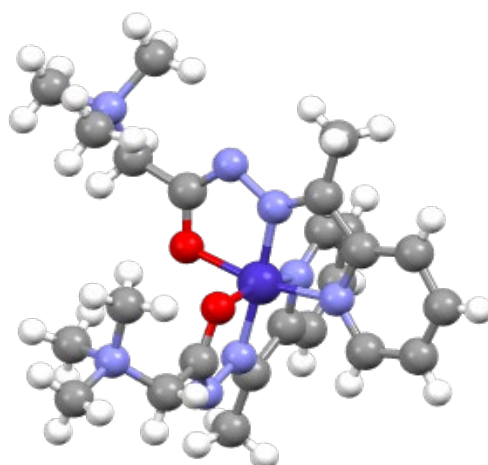


Figure 9: Representation of (7) $[\text{CoL}^3_2]$

In the article [21], the synthesis of a complex of Ni(II) with the composition shown in Figure 10. The reaction was carried out by mixing $\text{Ni}(\text{BF}_4)_2 \cdot 6\text{H}_2\text{O}$, NaN_3 along with HL^3Cl in a mixture of water and methanol as solvents. HL^3Cl coordinates *via* the NNO donor atoms. Each nickel ion in the complex is hexacoordinated with the tridentate ligand and triple azido ligands. The geometry is denoted as a dioctahedral geometry [21].

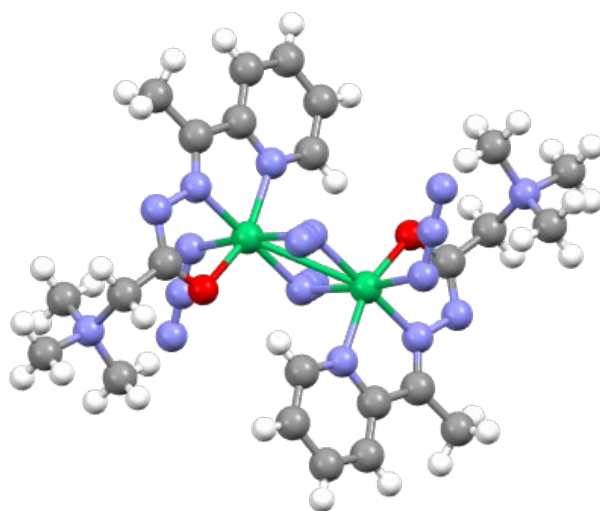


Figure 10: Representation of (**8**) $[\text{Ni}_2\text{L}^3_2(\mu\text{-}1,1\text{-N}_3)_2(\text{N}_3)_2]$

In a report [22], the reaction of HL^3Cl alongside iron nitrate as well as NH_4SCN in a methanol/water solvent mixture yielded a mononuclear isothiocyanato complex of Fe(III) with the composition $[\text{FeL}^3(\text{NCS})_3]$ (complex **9**, Figure 11). The metal ion in the complex is hexacoordinated, with coordination occurring *via* N and O atoms. Along with this, triple thiocyanato ligands are coordinated to the central metal ion. The geometry around the iron is ascertained as octahedral [22].

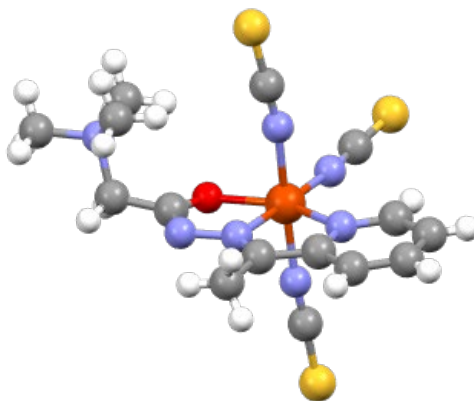


Figure 11: Representation of (**9**) $[\text{FeL}^3(\text{NCS})_3]$

In [14], the authors report the synthesis of mononuclear (**10**) and dinuclear doubly bridged end-on azido (**11**) copper complexes. The synthesis of (**10**) took place in the reaction between $\text{Cu}(\text{ClO}_4)_2 \cdot 6\text{H}_2\text{O}$ and HL^3Cl in methanol, while synthesis of (**11**) was carried out by reacting $\text{Cu}(\text{ClO}_4)_2 \cdot 6\text{H}_2\text{O}$, HL^3Cl , as well as NaN_3 in a mixture of methanol and water. The mononuclear complex (**10**) and the dinuclear complex (**11**) were characterized through various techniques. The complexes exhibit a zwitterionic coordination mode of the hydrazone ligand. Furthermore, the complexes demonstrate efficient catalytic activity in *N*-arylation reactions [14].

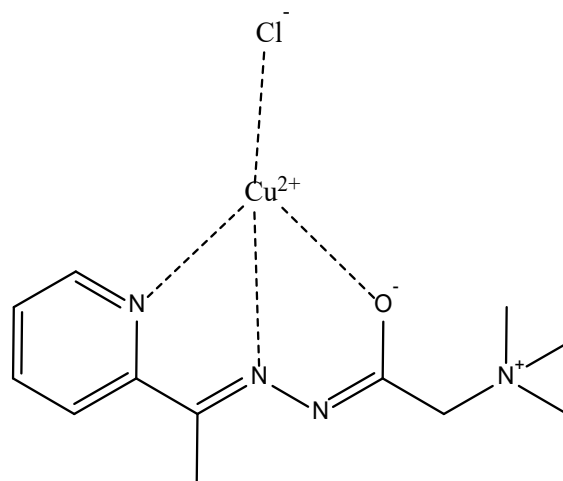


Figure 12: Representation of **(10)** $[\text{CuL}^3\text{Cl}]\text{ClO}_4$

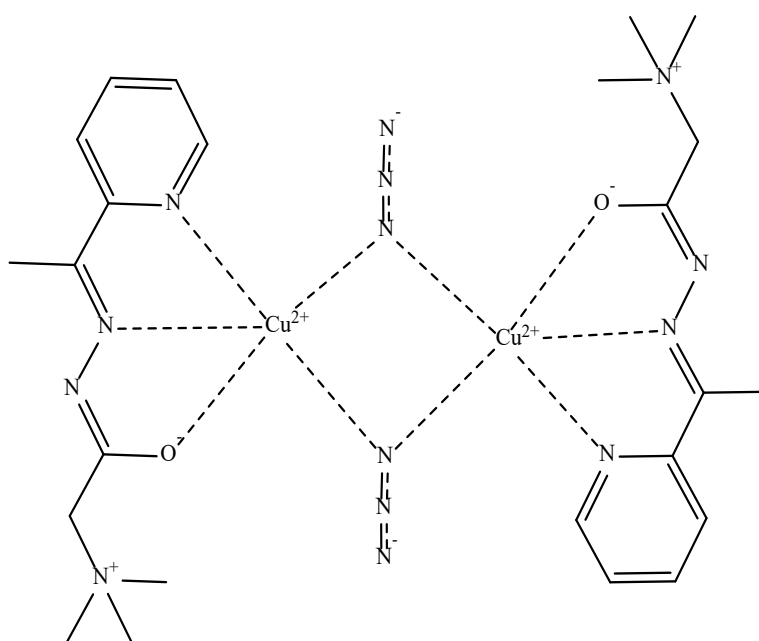


Figure 13: Representation of **(11)** $[\text{Cu}_2\text{L}^3_2(\mu\text{-}1,1\text{-N}_3)_2]$

The synthesis and characterization of the Co(III) complex **(12)**, Figure 14) derived from the HL^4Cl ligand is reported in [18]. The complex, $[\text{Co}(\text{L}^4)(\text{N}_3)_3]$, was characterized using various techniques, including spectroscopic, elemental, and XRD analysis. It was affirmed that HL^4Cl coordinates to the Co(III) ion in an unprotonated form, exhibiting a tridentate NNO coordination mode, and triple azide anions also coordinate to the center metal ion in a meridional arrangement [18].

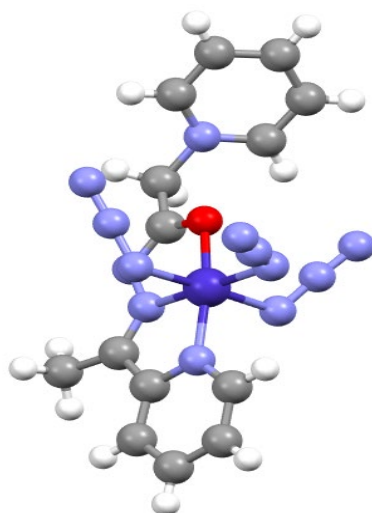


Figure 14: Representation of **(12)** $[\text{Co}(\text{L}^4)(\text{N}_3)_3]$

Romanović *et al.* [3] reported the synthesis of a Ni(II) complex (**13**, Figure 15), which was obtained from a reaction of $\text{Ni}(\text{BF}_4)_2 \cdot 6\text{H}_2\text{O}$ with the ligand HL^5Cl in the presence of NaN_3 . Characterization techniques revealed that the complex is a dinuclear doubly bridged with azido ligands in an end-on fashion. Each of the Ni(II) centers exhibits an octahedral coordination consisting of a hydrazone ligand, which is deprotonated coordinating in an NNO fashion, an azido ligand coordinated through a single binding site, accompanied by a pair of azido ligands forming bridging connections [3].

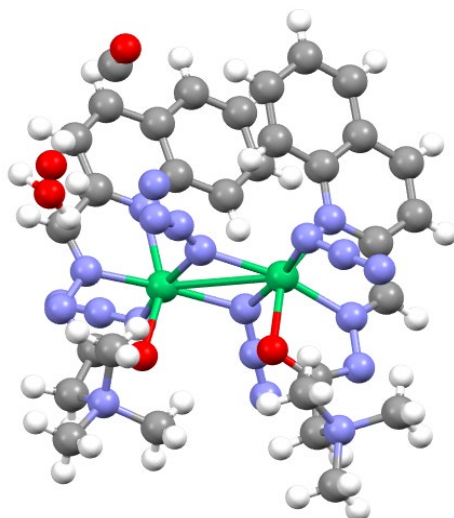


Figure 15: Representation of **(13)** $[\text{Ni}_2\text{L}^5_2(\mu\text{-}1,1\text{-N}_3)_2(\text{N}_3)_2]$

Another report [2] describes the synthesis of Co(II) complexes (**14**) and (**15**) derived from the ligand HL^5Cl . $\text{Co}(\text{BF}_4)_2 \cdot 6\text{H}_2\text{O}$ in reaction with HL^5Cl along with NaN_3 in a ratio 1 to 1 to 2 taking place in acetonitrile and methanol mixture as solvent yielded (**14**), while similar reaction conditions in a ratio of 1 to 1 to 4 yielded (**15**). Analytical characterization shows that (**14**) is a mononuclear azido complex of Co(II), and (**15**) forms a dinuclear complex with bridging azido ligands, oriented in an end-on manner, containing cobalt(II). Complex (**14**) exhibits an octahedral coordination geometry with three meridionally aligned azido ligands. Complex (**15**) features octahedral coordination around each Co(II) center, consisting of a hydrazone ligand coordinated in an NNO fashion, a monodentate azido ligand, and two azido ligands forming bridges [2].

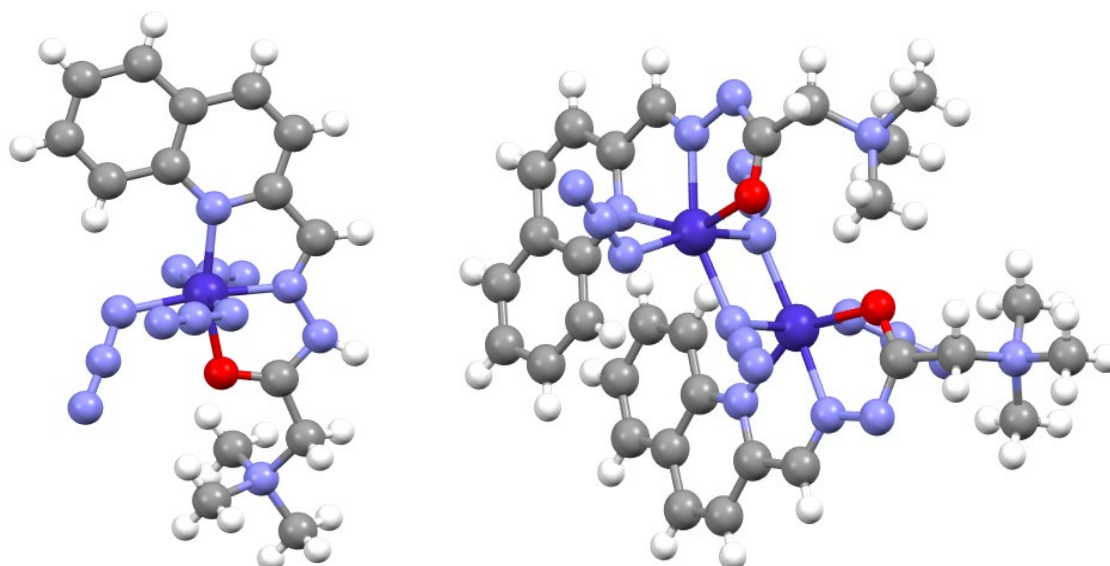


Figure 16: Representation of (14) $[\text{CoHL}^5(\text{N}_3)_3]$ and (15) $[\text{Co}_2\text{L}^5(\mu\text{-}1,1\text{-N}_3)_2(\text{N}_3)_2]$ respectively

2.4 Catalytic applications of metal complexes of hydrazones

Catalytic applications of complexes of hydrazone ligands have been a subject of extensive interest and research. These complexes have found catalytic applications in various organic reactions such as alkylation, arylation, polymerization and oxidation [23, 24]. The catalytic activity of iridium complexes (Figure 17) containing hydrazone ligands was found to be remarkably high in alkylation reactions involving a wide variety of alcohols and aniline derivatives [9]. Hydrazone ligands coordinated to copper(II) ions (Figures 12 and 13) demonstrated exceptional catalytic efficiency in promoting the *N*-arylation reactions of benzimidazole and imidazole [14]. The catalytic activity of molybdenum complexes containing salicylidene 2-picoloyl ligand of hydrazone was found to be remarkably high in the olefin's epoxidation reactions [25]. The titanium complex of bis(2-hydroxybenzylidene)oxalohydrazone (Figure 19) exhibited exceptional activity and selectivity in catalytic oxidation reactions of hydrocarbons, including benzylalcohol, cyclic alkanes, and cycloalkenes [26]. The catalytic activity of oxidovanadium(V) complexes derived from hydrazone ligand, *N'*-(4-bromo-2-hydroxybenzylidene)-3-methyl-4-nitrobenzohydrazone was evaluated and found to be active in the epoxidation of styrene [27].

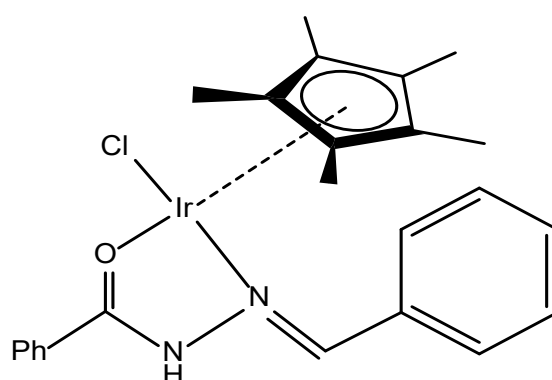


Figure 17: Structure of iridium hydrazine complex [9]

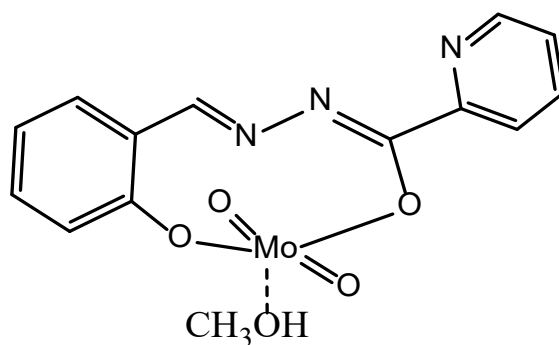


Figure 18: Structure of molybdenum complexes of salicylidene 2-picoloyl hydrazone ligand [24]

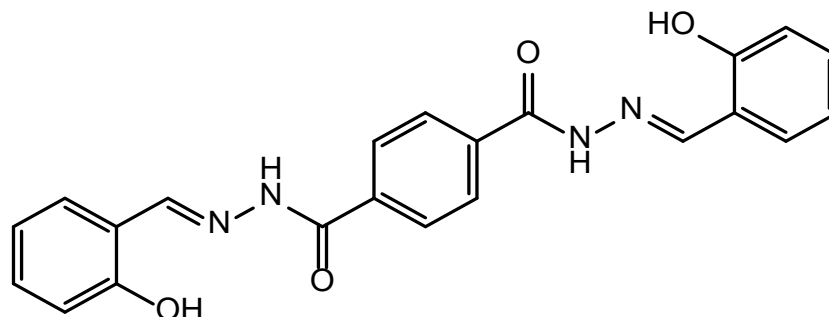


Figure 19: Structure of bis(2-hydroxy benzylidene)oxalohydrazide

2.5 Propargylamines

Propargylamines possess a distinctive structural characteristic, as they combine an alkyne (propargyl) group with an amino group. This structural motif gives propargylamines distinct chemical properties and reactivity, making them a subject of considerable interest in the scientific community [28].

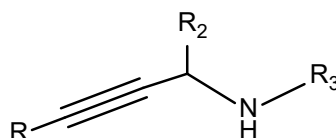
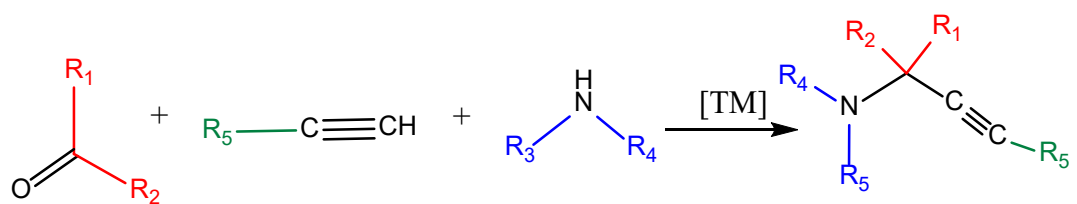


Figure 20: General structure of propargylamine

The bioactive properties exhibited by certain propargylamine derivatives have significantly contributed to their growing importance. Furthermore, the field of pharmaceutical chemistry has witnessed exponential growth in the application of propargylamines, further highlighting their significance [29-31]. Additionally, propargylamines play a crucial role as valuable intermediates in organic synthesis, offering pathways to create structurally intricate compounds. Besides, they have utility as essential starting materials in the synthesis of organic substances and medicinal pharmaceuticals [32,33]. The remarkable versatility of propargylamines stems from their unique structure, characterized by an amine group situated adjacent to another group termed alkyne. The triple bond between carbon atoms confers unique reactivity, allowing propargylamines to function as both electrophilic substrates and electron sources in nucleophilic reactions [34]. Furthermore, the amine moiety of propargylamines is amenable to nucleophilic reactions, enhancing their susceptibility to a wide range of chemical transformations. This combination of structural elements enables propargylamines to participate in diverse chemical reactions and contributes to their broad synthetic utility [29]. Within the propargylamine class, tetrasubstituted propargylamines remain relatively unexplored but hold promise [35]. The Ketone-Amine-Alkyne (KA²) reaction offers a direct synthetic route to these molecules, with several catalytic systems reported in the last decade [35-38]. Despite numerous research reported on the KA² coupling reaction [39-41], it is only recently that the first publication has emerged on a zinc-based homogeneous catalytic system for this process [35]. Consequently, the objective of this research is to explore and investigate the zinc-based homogeneous catalytic system for the KA² coupling in greater detail.



Scheme 2: Multicomponent KA² Coupling Reaction

3. Experimental

3.1 Materials and methods

Chemicals of analytical grade were used without need for additional purification. The IR spectra within the range of 4000-400 cm^{-1} were obtained using FT-IR spectrometer named Nicolet 6700 utilizing the ATR technique (bs-broad signal, w-weak, m-medium, s-strong, vs-very strong). Bruker Avance Ultrashield 500 plus, 200 MHz Varian Mercury spectrometer and 400 MHz Bruker Avance were utilized to obtain the ^{13}C and ^1H NMR spectra. TMS was used as internal standard in all cases. Chemical shifts are expressed in the unit of parts per million (ppm) relative to the standard reference. Coupling constants are measured in the unit of hertz (Hz).

Elemental analyses for carbon, hydrogen, nitrogen, and sulfur were carried out using standard micro-methods on an ELEMENTAR Vario ELIII C.H.N.S.O analyzer. The determination of molar conductivity was done at 25°C using a digital conductivity meter tagged JENWAY-4009. The GC/MS spectra were acquired using a chromatograph mass spectrometer, specifically, the Shimadzu R GCMS-QP2010 Plus, and it was equipped with a MEGAR column (Column ID# 11475, Tmax: 350°C, L: 30 m, I.D.: 0.25 mm, F.T: 0.25 μm , MEGA-5.). The internal standard used in the GC/MS analysis was n-octane.

3.2 Synthesis of the Ligands

3.2.1 Ligand HL^1Cl synthesis

By reacting Girard's reagent T (10 mmol, 1.676 g) with 2-acetylthiazole (10 mmol, 1036 μL) in 20 mL of water, HL^1Cl was successfully synthesized. By adding 3-4 drops of HCl (2M) the reaction was made acidic, thereafter, the mixture was refluxed for 3 hours. After cooling to room temperature, a precipitate formed. The solution containing white-colored precipitate was subjected to filtration followed by a thorough water wash. The product yield was 92% (2.54 g).

Elemental analysis calculated for $\text{ClC}_{10}\text{H}_{17}\text{N}_4\text{SO}$ (%): S 11.58, N 20.24, H 6.19, C 43.40; found (%): S 11.52, N 20.20, H 6.21 C 43.45. IR(ATR, cm^{-1}): 552(w), 585(w), 684(w), 748(w), 787(w), 914(m), 945(w), 976(w), 1135(w), 1201(s), 1300(w), 1401(m), 1487(s), 1550(vs), 1612(w), 1702(vs), 2955(s), 3018(m), 3092(m), 3129(w), 3387(w).

^1H -NMR(DMSO- d_6 , 500 MHz), δ (ppm), (atoms numbering in accordance with scheme 3): 11.86(N-H, 1H, s); 11.61(N-H, 1H, s); 7.932(1H, C3-H, $J_{\text{C2-H/C3-H}} = 5$ Hz, d); 7.926(1H, C3-H, $J_{\text{C2-H/C3-H}} = 5$ Hz, d); 7.854(1H, C2-H, $J_{\text{C2-H/C3-H}} = 5$ Hz, d); 7.848(1H, C2-H, $J_{\text{C2-H/C3-H}} = 5$ Hz, d); 4.82(C7-H, 2H, d); 4.60(C7-H, 2H, s); 3.34(C8-H, 9H, s); 3.30(8-H, 9H, s); 2.53(C5-H, 3H, s); 2.41(C5-H, 3H, s). ^{13}C -NMR(DMSO- d_6 , 125 MHz), δ (ppm): 167.0(C6), 167.3(C6), 166.8(C1), 161.2(C1), 150.8(C4), 147.00(C4), 144.00(C3), 143.9(C3), 123.6(C2), 123.3(C2), 63.8(C7), 63.0(C7), 53.9(C8), 53.6(C8), 15.05(C5), 13.9(C5).

3.2.2 Ligand HL^2 synthesis

By reacting thiosemicarbazide (1.00 mmol, 0.911 g) and 2-acetylthiazole (1.00 mmol, 1.040 mL) in 20 mL of water, the ligand HL^2 was synthesized. By adding 3 drops of HCl (2M), the resulting mixture became acidic, subsequently refluxed at 85 °C. The reaction ended after 180 minutes. As a result of the reaction, a white precipitate formed. The obtained solid precipitate was thoroughly washed using cold H_2O and subsequently filtered. 91% Product yield was obtained.

Calculated elemental analysis of $\text{S}_2\text{N}_4\text{H}_8\text{C}_6$ (%): S 32.02, N 27.98, H 4.03, C 35.98; found (%): S 31.98, N 27.88, H 4.26. C 35.74. IR(ATR, cm^{-1}): 638(w), 712(w), 755(w), 847(w), 881(w), 958(w), 1039(m), 1069(m), 1107(m), 1166(m), 1282(m), 1365(m), 1425(s), 1452(m), 1482(s), 1510(s), 1589(s), 1648(w), 2066(w), 2983(m), 3071(m), 3099(m), 3188(s), 3248(s), 3436(s).

$^1\text{H-NMR}$ (DMSO- d_6 , 400 MHz), δ (ppm), (atoms numbering in accordance to scheme 4): 10.67(s, 1H, NH), 8.53(NH2, s), 2.43(C5-H, 3H, s), 7.89(C2-H, 1H, d), 7.80(C3-H, 1H, d). $^{13}\text{C-NMR}$ (DMSO d_6 , 125 MHz), δ (ppm): 179.4 (C6), 167.5 (C1), 143.7 (C2), 144.7 (C4), 123.1 (C3), 14.1 (C5).

3.2.3 Ligand HL³Cl synthesis

HL³Cl was obtained by reacting Girard's reagent T and 2-acetylpyridine in methanol, as reported in the literature [19].

Calculated elemental analysis of C₁₂H₁₉ N₄ClO (%): H 7.07, N 20.69, C 53.23; found (%): H 7.38, N 20.49, C 53.34. IR(ATR, cm⁻¹): 683(w), 748(w), 914(m), 944(w), 975(w), 1073(m), 1095(w), 1135(m), 1153(w), 1200(s), 1253(w), 1300(w), 1400(m), 1485(m), 1549(s), 1612(w), 1700(vs), 2950(s), 3016(m), 3049(m), 3090(m), 3127(m), 3387(w).

$^1\text{H-NMR}$: 8.12(C2-H, d), 7.91(C3-H, td), 7.45(C4-H, m), 8.62(C5-H, m), 2.37(C7-H3, s), 3.35(C10-H9, s), 4.92(C9-H2, s), 11.41(N-H, s).

3.2.4 Ligand HL⁴Cl synthesis

Synthesis of HL⁴Cl was carried out in ethanol. 2-Acetylpyridine (3.00 mmol, 0.363 g) and Girard's reagent P (3.00 mmol, 0.563 g) were dissolved in 40 mL of the solvent, acidified with a few drops of HCl. This was followed by 120 minutes of reflux. After allowing the solution to cool, precipitate with white color was obtained, subsequently filtered and properly washed with ethanol. Yield = 52% (0.451 g).

Calculated elemental analysis of C₁₄H₁₅N₄ClO (%): N 19.27, H 5.20, C 57.83; found (%): N 19.25, H 5.23, C 57.80. IR (ATR, cm⁻¹): 569(w), 600(w), 646(m), 702(m), 725(w), 774(m), 790(m), 848(w), 1081(w), 1111(m), 1150(w), 1197(m), 1221(m), 1263(s), 1323(w), 1384(s), 1433(s), 1453(m), 1485(vs), 1582(m), 1630(s), 1699(vs), 2949(w), 3054(s), 3125(m), 3273(m), 3425(s).

$^1\text{H-NMR}$ (DMSO- d_6 , 400 MHz), δ (ppm), (atoms numbering in accordance to scheme 6): 11.55(NH, 1H, s), 9.09(C9-H, 2H, d), 8.67(C11-H, 1H, t), 8.60(C5-H, 1H, d), 8.21(C10-H, 2H, t), 8.13(C2-H, 1H, d), 7.85(C3-H, 1H, t), 7.41(C4-H, 1H, t), 6.14(C8-H, 2H, s), 2.37(C7-H, 3H, s). ^{13}C NMR(DMSO- d_6 , 125 MHz), δ (ppm): 168.19 (C12), 154.99 (C1), 150.94 (C6), 149.15 (C5), 146.89 (C9), 146.67 (C11), 137.09 (C3), 128.01 (C10), 124.76 (C4), 120.66 (C2), 62.35 (C8), 12.76 (C7).

3.2.5 Ligand HL⁵Cl synthesis

In the synthesis of HL⁵Cl, a solution of Girard's reagent T together with 2-quinolinecarboxaldehyde was refluxed as reported in the literature [3].

Elemental analysis calculated for C₁₅H₁₉ClN₄O (%): N 18.26, H 6.24, C 58.73, found: N 18.02, H 6.13, C 58.96 IR(ATR, cm⁻¹): 533(w), 633(w), 656(w), 758(m), 832(w), 868(w), 916(w), 950(w), 989(w), 1135(m), 1230(m), 1301(m), 1340(w), 1379(w), 1414(m), 1497(m), 1562(w), 1595(m), 1699(s), 2831(m), 2939(m), 2970(m), 3062(m), 3414(m).

$^1\text{H-NMR}$ (CD₃OD, 500 MHz), δ (ppm): 7.78(C6-H, 1H, t), 8.03(C7-H, 1H, d), 7.62(C5-H, 1H, t), 7.94(C4-H, 1H, d), 8.36(C3-H, 1H, d), 8.18(C2-H, 1H, d), 8.17(C8-H, 1H, s), 4.94(C10-H, 2H, s), 3.47(C11-H, 9H, s).

3.2.6 Ligand HL⁶Cl synthesis

HL⁶Cl was produced by reacting Girard's reagent P with 2-quinolinecarboxaldehyde in an ethanolic solution, following procedure report[42].

Elemental analysis calculated for C₁₇H₁₅N₄ClO: N 17.15%, H 4.63%, C 62.48%; found: N 17.11%, H 4.65%, C 62.50%, IR(ATR, cm⁻¹): 750(w), 773(m), 1125(m), 1274(s), 1389(s), 1428(w), 1487(s), 1695(vs), 2958(s), 3065(s), 3133(s), 3418(s).

$^1\text{H-NMR}$ (DMSO- d_6 , 400 MHz), δ (ppm): 9.07(C12-H, 2H, d), 8.69(C14-H, 1H, t), 8.47(C4-H, 1H, d), 8.32(C9-H, 1H, s), 8.23(C13-H, 2H, t), 8.12(C3-H, 1H, d), 8.01(C8-H, C5-H, 2H, m), 7.79(C7-H, 1H, t), 7.64(C6-H, 1H, t), 6.13(C11-H, 2H, s)

3.3 Synthesis of Complexes

3.3.1 Synthesis procedure of $[\text{ZnL}^1(\text{NCS})_2]\cdot\text{H}_2\text{O}$ complex 1

Complex 1 synthesis involved the reaction of HL^1Cl , $\text{Zn}(\text{OAc})_2\cdot 2\text{H}_2\text{O}$ and NH_4SCN in a molar ratio of 0.3 mmol, 0.3 mmol, 0.78 mmol respectively (75 mg, 83 mg, 60 mg). This took place in 10 mL mixture of water and 10 mL methanol as solvent. The resulting solution underwent refluxing for 4 hours and was allowed to cool afterwards, then placed in a refrigerator at a temperature of -8°C for a duration of two weeks. This forms crystals with a pale-yellow appearance which were appropriate for X-ray analysis. Yield: 83% (0.11 g).

Elemental analysis calculated for $\text{ZnS}_3\text{C}_{12}\text{H}_{20}\text{N}_6\text{O}_3$ (%): S 24.51, N 21.41, H 5.13, C 36.71; found (%): S 24.31, N 21.27, H 5.15, C 36.55. IR(ATR, cm^{-1}): 556(w), 746(w), 880(w), 923(w), 988(w), 1012(w), 1064(w), 1095(w), 1151(w), 1237(w), 1290(w), 1341(m), 1402(s), 1424(s), 1475(s), 1536(s), 1610(s), 2088(vs), 2959(w), 3055(w), 3123(m), 3383(s), 3502(s).

$^1\text{H-NMR}$ (DMSO- d_6 , 500 MHz), δ (ppm), (atoms numbering in accordance to scheme 9): 8.16(1H, C3-H, $J_{\text{C2-H/C3-H}}=2.2$ Hz, d), 8.06(1H, C2-H $J_{\text{C2-H/C3-H}}=2.2$ Hz, d), 4.20(C7-H, 2H, s), 3.27(C8-H, 9H, s), 2.54(C5-H, 3H, s). $^{13}\text{C-NMR}$ (DMSO- d_6 , 125 MHz), δ (ppm): 171.7(C6), 166.2(C1), 147.3(C4), 142.5(C2), 134.3(C9), 125.7(C3), 66.7(C7), 53.8(C8), 15.4(C5).

3.3.2 Synthesis procedure of $[\text{Zn}(\text{L}^2)_2]$ complex 2

The second complex (2) was prepared through the reaction of HL^2 , $\text{Zn}(\text{BF}_4)_2\cdot 6\text{H}_2\text{O}$ and NaN_3 in the following quantity, respectively (0.20 mmol, 40 mg), (0.20 mmol, 72 mg) and (0.46 mmol, 30 mg). It was carried out in a solution containing 5 mL water with 15 mL acetonitrile. The resulting solution, after being refluxed for 4 hours and refrigerated for one week at -8°C , produced crystals with yellow color that were well-suited for X-ray analysis. The yield was 87% (0.08 g).

Elemental analysis calculated for $\text{ZnS}_4\text{C}_{12}\text{H}_{14}\text{N}_8$ (%): S 32.18, N 28.12, H 3.54, C 36.16; found (%): S 32.07, N 28.02, H 3.56, C 36.04. IR(ATR, cm^{-1}): 480(w), 547(w), 596(w), 644(w), 677(m), 726(w), 783(m), 882(w), 1029(m), 1097(s), 1162(s), 1198(vs), 1298(s), 1375(vs), 1425(vs), 1496(s), 1569(m), 1589(m), 1632(m), 2078(m), 2185(w), 2255(w), 2925(w), 3109(s), 3169(s), 3308(vs), 3436(m), 3496(w), 3571(w).

$^1\text{H-NMR}$ (DMSO- d_6 , 500 MHz), δ (ppm), (atoms numbered in accordance to scheme 10): 7.94(C3-H, 1H, d); 7.88(C2-H, 1H, d); 7.45(NH₂, 2H, s); 2.43(C5-H, 3H, s). $^{13}\text{C-NMR}$ (DMSO- d_6 , 125 MHz), δ (ppm): 181.7(C6), 167.3(C1), 142.4(C2), 139.2(C4), 122.5(C3), 15.9(C5).

3.3.3 Synthesis procedure of $[\text{ZnL}^3(\text{NCS})_2]\cdot 0.5\text{CH}_3\text{OH}$ complex 3

Complex 3 was formed through the combination of HL^3Cl to a reaction with NH_4SCN and $\text{Zn}(\text{OAc})_2\cdot 2\text{H}_2\text{O}$, following a documented procedure as previously outlined [19].

IR (ATR, cm^{-1}): 749(w), 782(w), 914(w), 975(w), 1019(m), 1074(m), 1145(w), 1200(w), 1302(m), 1339(m), 1366(m), 1397(m), 1437(m), 1464(m), 1535(s), 1566(m), 1592(w), 1620(w), 1639(w), 2067(vs), 3030(w).

$^1\text{H-NMR}$ (DMSO- d_6 , 500 MHz), δ (ppm): 8.55(C6-H, $J^3=5$ Hz, d), 7.77(C5-H, 1H, m), 8.23(1H C4-H, $J^3=10$ Hz $J^4=5$ Hz, td), 8.07(C3-H, 1H, m), 2.55(C8-H₃, 3H, s), 3.28(C11-H₃, 3H, s), 4.19(C10-H₂, 2H, s)

3.3.4 Synthesis procedure of [ZnL¹(N₃)₂] complex 4

Following the procedure described in the reference, a combination of **HL**¹Cl, NaN₃ and Zn(BF₄)₂·6H₂O in methanol yielded complex 4 [43].

Elemental analysis calculated for ZnSC₁₀H₁₆N₁₀O (%): S 8.23, N 35.94, H 4.14, C 30.82; found (%): S 8.21, N 35.83, H 4.18, C 30.76. IR(ATR, cm⁻¹): 80(w), 1079(w), 1116(w), 1153(w), 1203(w), 1285(w), 1339(m), 1407(w), 1433(w), 1481(w), 1540(s), 1600(w), 2057(vs), 3378(w).

¹H-NMR(DMSO-*d*₆, 400 MHz), δ (ppm): 8.04(C3-H, 1H, d), 7.92(C2-H, 1H, d), 4.13(C7-H, 2H, s), 3.23(C8-H, 9H, s), 2.53(C5-H, 3H, s).

3.3.5 Synthesis procedure of [ZnL²(N₃)₂] complex 5

In the synthesis of complex 5, 0.040 g **HL**² (0.20 mmol) was solubilized in water and methanol (5/25 mL). This was followed by the addition of solid Zn(BF₄)₂·6H₂O (0.20 mmol, 0.069 g). After the Zn(BF₄)₂·6H₂O had been allowed to dissolve, NaN₃ (0.80 mmol, 0.052 g) dissolved in 5 mL H₂O was introduced into the solution. The resulting solution underwent refluxing for a duration of 2 hours. After we allowed the solvent to evaporate slowly at ambient temperature for a period of 24 hrs, yellow crystals, which were well suited for single X-ray analysis were collected. Yield = 87% (60 mg).

Elemental analysis calculated for ZnS₂C₆H₇N₇ (%): S 20.91, N 31.97, H 2.30, C 23.50; found (%): S 20.87, N 31.91, H 2.33, C 23.47. IR(ATR, cm⁻¹): 472(w), 495(w), 596(w), 643(w), 684(m), 746(m), 790(m), 886(w), 998(w), 1035(w), 1112(m), 1167(m), 1204(m), 1301(m), 1342(m), 1369(m), 1388(s), 1428(s), 1499(m), 1585(m), 1625(s), 1997(m), 2048(s), 2084(s), 3089(m), 3104 (m), 3169(m), 3227(w), 3291(m), 3399(m), 3419(s).

¹H-NMR(DMSO-*d*₆, 400 MHz), δ (ppm), (atoms are numbered in accordance to scheme 12): 7.89(C3-H, 1H, d), 7.83(C2-H, 1H, d), 7.38(NH₂, 2H, s), 2.38(C5-H, 3H, s). ¹³C-NMR(DMSO-*d*₆, 125 MHz), δ (ppm): 181.61(C6), 167.08(C1), 142.27(C2), 138.93(C4), 123.18(C3), 15.75(C5).

3.3.6 Synthesis procedure of [ZnL⁴(N₃)₂] complex 6

The reaction between 0.30 mmol of **HL**⁴Cl (87 mg) along with 0.30 mmol of Zn(BF₄)₂·6H₂O (104 mg) and NaN₃ (78 mg, 1.20 mmol) in a solvent mix of water, acetonitrile and methanol (5/10/20 mL) as a solvent, yielded complex 6. The mixture, which underwent refluxing in 2 hours, was allowed to cool and thereafter allowed to slowly evaporate at ambient temperature for a day. Yellow-colored crystals were harvested. Yield = 87 mg (67 %).

Calculated elemental analysis of ZnOC₁₄H₁₄N₁₀ (%): N 34.69, C 41.65, H 3.49; found: N 34.61, C 41.45, H 3.51. IR(ATR, cm⁻¹): 634(w), 677(w), 724(w), 785(w), 1021(w), 1091(w), 1153(w), 1189(w), 1208(w), 1261(w), 1320(w), 1362(m), 1440(w), 1462(m), 1485(w), 1538(m), 1569 (w), 1595(w), 1630(w), 2055(s), 2079(s), 2937(w), 2997(w), 3092(w), 3137(w), 3390(w)

¹H-NMR(DMSO-*d*₆, 400 MHz), δ (ppm), (numbering of atoms according to scheme 13): 9.03(C9-H, 2H, d), 8.61(C11-H, 1H, t), 8.43(C5-H, 1H, d), 8.13(C10-H, 2H, t), 8.08(C3-H, 1H, t), 7.89(C2-H, 1H, d), 7.62(C4-H, 1H, dd), 5.48(C8-H, 2H, s), 2.31(C7-H, 3H, s). ¹³C-NMR(DMSO-*d*₆, 125 MHz), δ (ppm): 172.52(C12), 161.39(C6), 149.32(C1), 148.79(C5), 146.53(C9), 146.21(C11), 140.62(C3), 127.77(C10), 126.1(C4), 123.26(C2), 62.77(C8), 12.74(C7).

3.3.7 Synthesis procedure of [ZnL⁵(N₃)₂] complex 7

Complex 7 was synthesized as reported previously; the reaction was carried out in methanol solution involving Zn(BF₄)₂·6H₂O, ligand **HL**⁵Cl and NaN₃ [44]

Elemental analysis calculated for ZnOC₁₅H₁₈N₁₀ (%): N 33.37, H 4.32, C 42.92, found: N 33.35, H 4.56, C 43.03. IR(ATR, cm⁻¹): 589(w), 632(w), 757(m), 785(w), 833(w), 873(w), 925(m), 972(w),

1032(w), 1086(s), 1125(w), 1232(w), 1300(s), 1344(w), 1398(m), 1535(s), 1566(s), 1612(w), 1645(w), 1748(w), 1923(w), 2067(s), 2169(w), 2817(w), 2939(w), 3027(w), 3310(w).

¹H-NMR(DMSO-*d*₆, 400 MHz), δ (ppm): 8.70(C7-H, 1H, d), 7.91(C6-H, 1H, m), 7.91(C5-H, 1H, m), 8.70(C4-H, 1H, d), 8.09(C3-H, 1H, d), 7.71(C2-H, 1H, d), 8.38(C8-H, 1H, s), 4.17(C10-H, 2H, s), 3.28(C11-H, 9H, s).

3.3.8 Synthesis procedure of [ZnL⁵(NCO)₂] complex 8

In the synthesis of complex **8**, a mixture of Zn(BF₄)₂·6H₂O, HL⁵Cl ligand together with NaOCN in methanol was refluxed as reported [44].

Elemental analysis calculated for ZnO₃C₁₇H₁₈N₆ (%): N 20.02, H 4.32, C 48.64, found (%): N 19.98, H 4.47, C 48.73. IR(ATR, cm⁻¹): 629(w), 752(w), 785(w), 807(w), 830(w), 931(w), 972(w), 995(w), 102(w), 1080(w), 1124(w), 1203(w), 1242(w), 1305(w), 134(w), 1400(w), 1482(w), 1530(s), 1563(m), 1611(w), 2203(s), 2966(w), 3063(w), 3536(w).

¹H-NMR (400 MHz, DMSO-*d*₆), δ (ppm): 8.66(C7-H, 1H, d), 7.91(C6-H, 1H, m), 7.91(C5-H, 1H, m), 8.66(C4-H, 1H, d), 8.09(C3-H, 1H, d), 7.71(C2-H, 1H, d), 8.34(C8-H, 1H, s), 4.15(C10-H, 2H, s), 3.27(C11-H, 9H, s).

3.3.9 Synthesis procedure of [ZnL⁶(NCS)₂]·2H₂O complex 9

Complex **9** was obtained by reacting HL⁶Cl, NH₄SCN, along with Zn(BF₄)₂·6H₂O in a solution of MeOH, following the method in the previous study [45].

Elemental analysis calculated for ZnS₂C₁₉H₁₅N₆O (%): S 13.56, N 17.75, H 3.20, C 48.26; found: S 13.49, N 17.68, H 3.25, C 48.30. IR(ATR, cm⁻¹): 737(w), 829(w), 1084(m), 1271(w), 1360(m), 1433(w), 1488(s), 1518(s), 1562(m), 2075(vs), 3060(m).

¹H-NMR(DMSO-*d*₆, 400 MHz), δ (ppm): 9.12(C12-H, 2H, d), 8.70(C4-H, 1H, d), 8.65(C14-H, 1H, t), 8.56(C9-H, 1H, s), 8.24(C8-H, 1H, d), 8.19(C13-H, 2H, t), 8.09(C5-H, 1H, d), 7.94(C7-H, 1H, t), 7.85(C3-H, 1H, d), 7.70(C6-H, 1H, t), 5.60(C11-H, 2H, s).

3.4 X-ray structural analysis

3.4.1 Complexes 1 and 2 X-ray structural analysis

XRD using single-crystal was employed in analyzing the structural arrangement of both complexes at a molecular level. Detailed refinement information and crystallographic data obtained from the analysis are presented in Table 2. For complex **1**, data for X-ray intensity was gathered at room temperature using a diffractometer from Nonius Kappa CCD furnished with a graphite-based crystal monochromator utilizing MoK α X-rays as the radiation source (wavelength = 0.71073 Å). Cell refinement and reduction of data were performed utilizing DENZO along with SCALPACK software [46]. In the case of complex **2**, diffraction data was collected at room temperature using a dual-source Agilent SuperNova diffractometer equipped with an Atlas detector and radiation source utilizing MoK α with a mirror-monochromated (wavelength=0.71073 Å). The processing of data was carried out using CrysAlis-PRO software [47]. SIR-92 software was used to solve the structures of both complexes and subsequently refined against F² data through the full-matrix least-squares approach in SHELXL-2014 [49]. Anisotropic refinement was applied to all non-hydrogen atoms. Within complex **1**, hydrogen atoms associated with water molecules were positioned using a disparity map and subsequently refined, following prescribed constraints for distances (DFIX) set at U_{iso}(H)=1.5U_{eq}(O) and O-H =0.96 Å. Hydrogen atoms not explicitly observed were included in the model using geometric calculations and then adjusted using a standard refinement approach. The crystallographic data pertaining to both complexes are archived with the CCDC under deposition codes 2021000 (for complex **1**) and 2021001 (for complex **2**).

Table 2: crystallographic refinement data for complexes **1** and **2**

	Complex 1	Complex 2
Molecular formula	ZnS ₃ C ₁₂ H ₂₀ N ₆ O ₃	ZnS ₄ C ₁₂ H ₁₄ N ₈
Molecular weight (g/mol)	457.89	463.92
Dimensions of crystal (mm)	0.100 × 0.100 × 0.010	0.100 × 0.050 × 0.050
Color of crystal	colourless	yellow
Crystal system	triclinic	monoclinic
Space group	<i>P</i> -1	<i>P</i> 2 ₁ / <i>c</i>
<i>a</i> (Å)	8.8362	9.0503
<i>b</i> (Å)	8.8934	13.6692
<i>c</i> (Å)	14.5684	14.9717
<i>α</i> (°)	81.964	90.00
<i>β</i> (°)	86.941	101.012
<i>γ</i> (°)	61.769	90.00
Unit cell volume (Å ³)	998.65	1818.05
Multiplicity or <i>Z</i> value	2	4
Calculated density (g/cm ³)	1.523	1.695
F(000)	472	944
Number of collected reflections	7430	17333
Number of independent reflections	4532	4133
R _{int}	0.0293	0.0450
Number of reflections observed	3161	3033
Parameters	242	230
R[I > 2σ (I)] ^a	0.0407	0.0356
wR ₂ (all data) ^b	0.0898	0.0760
Goodness of Fit (Goof, <i>S</i> ^c)	1.043	1.018
Minimum/maximum residual electron density (e Å ⁻³)	-0.29/+0.33	-0.34/+0.32

$$^a R = \frac{\sum ||F_o| - |F_c||}{\sum |F_o|}$$

$$^b wR_2 = \left\{ \frac{\sum [w(F_o^2 - F_c^2)^2]}{\sum [w(F_o^2)^2]} \right\}^{1/2}$$

^c $S = \left\{ \frac{\sum [w(F_o^2 - F_c^2)^2]}{(n/p)} \right\}^{1/2}$ Where "n" represents the count of reflections and "p" signifies the total number of parameters refined.

3.4.2 Xray structural analysis of complex **5** and **6**

The crystallographic information and refinement details for complexes **5** and **6** are shown in Table 3. X-ray diffraction data involving a single crystal were obtained at room temperature utilizing a dual-source Agilent SuperNova diffractometer equipped with an Atlas detector, and the diffraction experiments utilized radiation source MoK α with a mirror-monochromated at a wavelength = 0.71073 Å. The data was processed using the software named CrysAlis-PRO [50]. Direct methods were initially used to determine the structures employing SHELXS-2013/1[49]; thereafter, refinement was done using a complete-matrix least-squares approach, which relied on F square, with SHELXL-2018/3 [51]. Anisotropic refinement was applied to other atoms aside from hydrogen. Hydrogen atoms bonded with nitrogen were first identified through a difference map and then optimized with the aid of constraints for distance (DFIX) set at N–H = 0.86 Å. Their isotropic thermal parameters were increased by a factor of 1.2 in relation to the equivalent isotropic displacement parameter of the corresponding nitrogen atom. The remaining hydrogen atoms were incorporated into the model following geometric calculations and subsequently fine-tuned utilizing a riding model. Complexes **5** and **6** crystallographic data was archived with the CCDC under the accession numbers CCDC 2244671 and 2244672, respectively.

Table 3: crystallographic refinement data for complexes **5** and **6**

	Complex 5	Complex 6
Molecular formula	C ₆ H ₇ N ₇ S ₂ Zn	C ₁₄ H ₁₄ N ₁₀ OZn
Molecular weight (g/mol)	306.68	403.72
Size of crystal (mm)	0.500 × 0.300 × 0.100	0.500 × 0.100 × 0.100
Crystal of color	yellow	colourless
Crystal system	monoclinic	monoclinic
Space group	<i>P</i> 2 ₁ / <i>c</i>	<i>P</i> 2 ₁ / <i>c</i>
<i>a</i> (Å)	7.4254	12.3417
<i>b</i> (Å)	18.6798	8.990
<i>c</i> (Å)	7.9925	15.3451
β (°)	100.930	101.169
Unit cell volume (Å ³)	1088.49	1671.99
Multiplicity or <i>Z</i> value	4	4
Calculated density (g/cm ³)	1.871	1.604
F(000)	616	824
Number of collected reflections	10146	15739
Number of independent reflections	2503.0	3828.0
R _{int}	0.03490	0.03200
Number of reflections observed	2190.0	3007.0
Number of parameters	152.0	236.0
R[I > 2σ(I)] ^a	0.02890	0.03310
wR ₂ (all data) ^b	0.07200	0.08230
Goodness of fit (Goof, <i>S</i> ^c)	1.0890	1.0520
Minimum/maximum residual electron density (e Å ⁻³)	-0.54/+0.33	-0.30/+0.38

$$^a R = \frac{\sum ||F_o| - |F_c||}{\sum |F_o|}$$

$$^b wR_2 = \left\{ \frac{\sum [w(F_o^2 - F_c^2)^2]}{\sum [w(F_o^2)^2]} \right\}^{1/2}$$

^c $S = \left\{ \frac{\sum [w(F_o^2 - F_c^2)^2]}{(n/p)} \right\}^{1/2}$ Where "n" represents the count of reflections and "p" signifies the total number of parameters refined

3.5 Catalysis Procedure

3.5.1 General catalytic procedure for complex 1-3

The procedure involved loading a pressure tube or vial sealed with Teflon with the catalyst, typically x mol%, and 0.5 equivalents of the specified additive, typically MgSO₄, except otherwise specified. Subsequently, the amine (0.5 mmol) was introduced into the mixture under ambient air conditions and stirred until the solid catalyst showed signs of partial dissolution. Following that, alkyne (0.5 mmol) was incorporated into the mixture, and it was mixed at room temperature. Subsequently, the ketone (0.5 mmol) was introduced; thereafter, the reaction mixture was allowed to agitate within a preheated oil bath for the designated reaction duration. After reaching and cooling to ambient temperature, the mixture was supplemented with 2 × 5 mL ethyl acetate and stirred for five minutes. To eliminate inorganic impurities, the mixture underwent filtration through a brief silica gel plug, followed by concentration under reduced pressure. The concentrated material was then introduced into a column of silica gel.

The desired products were isolated using gradient column chromatography, employing ethyl acetate/petroleum ether as the eluting solvent. The structural confirmation of the products was accomplished through ¹H-NMR and ¹³C{¹H}-NMR spectroscopy, which not only validated their compositions but also demonstrated consistency with data that were previously reported [35,41].

3.5.2 Synthesized propargylamines characterization data for 1-3

(IVa) 1 Isolated in oil form with a yield of 91% (0.46 mmol, 115 mg), color: yellow/orange. $^1\text{H-NMR}(\text{CDCl}_3, 200 \text{ MHz}) \delta$ 1.91-1.41(overlapping peaks, 12H, m), 2.13-1.94(2H, m), 2.82(4H, $J = .9$ Hz, t), 7.30(3H, m), 7.44(2H, $J = 6.7, 3.1$ Hz, dd). $^{13}\text{C}\{^1\text{H}\}\text{-NMR}(\text{CDCl}_3, 50 \text{ MHz}) \delta$ 23.0, 23.5, 25.7, 37.8, 47.0, 59.3, 86.1, 90.3, 123.6, 127.6, 128.1, 131.7.

(IVb) Isolated in the form of oil. Color: yellowish. Yield: 87%(0.44 mmol, 116 mg). $^1\text{H-NMR}(\text{CDCl}_3, 400 \text{ MHz}) \delta$ 1.83-1.34(overlapping peaks, 14H, m), 2.11-2.05(2H, m), 2.70(4H, m), 7.28-7.23(3H, m), 7.47-7.36(2H, m). $^{13}\text{C}\{^1\text{H}\}\text{-NMR}(\text{CDCl}_3, 101 \text{ MHz}) \delta$ 23.2, 24.9, 25.8, 26.6, 35.8, 47.3, 59.7, 86.3, 90.6, 124.0, 127.8, 128.4, 131.9.

(IVc) Isolated in the form of oil. Color: yellow, yield: 64% yield(0.32 mmol, 91 mg). $^1\text{H-NMR}(\text{CDCl}_3, 400 \text{ MHz}) \delta$ 78-1.42(overlapping peaks, 14H, m), 2.12-2.09(2H, m), 2.34(3H, s), 2.73(4H, s), 7.10(2H, $J = 7.9$ Hz, d), 7.33 (2H, $J = 7.9$ Hz, D). $^{13}\text{C}\{^1\text{H}\}\text{-NMR}(\text{CDCl}_3, 101 \text{ MHz}) \delta$ 21.5, 23.3, 24.7, 25.8, 26.4, 35.7, 47.3, 59.9, 86.7, 90.4, 120.6, 129.1, 131.7, 137.9.

(IVd) Isolated in oily form. Color: brownish/orangish, yield: 72%(0.36 mmol, 82 mg). $^1\text{H-NMR} (400 \text{ MHz, CDCl}_3) \delta$ 1.05(3H, $J = 7.5$ Hz, t), 1.42(3H, s), 1.74-1.65(2H, m), 1.84-1.79(4H, m), 2.80(4H, $J = 5.8$ Hz, t), 7.32-7.26(3H, m), 7.45-7.38(2H, m). $^{13}\text{C}\{^1\text{H}\}\text{-NMR}(\text{CDCl}_3, 101 \text{ MHz}) \delta$ 8.9, 23.7, 25.1, 33.9, 47.8, 58.6, 84.7, 90.9, 123.5, 127.7, 128.2, 131.7

(IVe) Isolated in the form of oil with yellow color, yield: 67%(114 mg, 0.34 mmol). $^1\text{H-NMR}(\text{CDCl}_3, 200 \text{ MHz}) \delta$ 1.24 (3H, $J = 7.1$ Hz, t), 2.13-1.43(14H, m), 2.42-2.18(3H, $J = 11.0$ Hz, t), 3.15(2H, $J = 11.6$ Hz, t), 4.13(2H, $J = 7.1$ Hz, q), 7.35-7.23(3H, m), 7.42(2H, $J = 6.7, 3.0$ Hz, dd). $^{13}\text{C}\{^1\text{H}\}\text{-NMR}(\text{CDCl}_3, 50 \text{ MHz}) \delta$ 14.3, 22.9, 25.8, 28.9, 35.9, 41.6, 45.8, 59.0, 60.3, 86.2, 90.4, 123.6, 127.8, 128.3, 131.7, 175.4.

(IVf) Isolated in the form of oil with yellow color, yield: 67%(114 mg, 0.34 mmol). $^1\text{H-NMR}(\text{CDCl}_3, 200 \text{ MHz}) \delta$ 1.24 (3H, $J = 7.1$ Hz, t), 2.13-1.43(14H, m), 2.42-2.18(3H, $J = 11.0$ Hz, t), 3.15(2H, $J = 11.6$ Hz, t), 4.13(2H, $J = 7.1$ Hz, q), 7.35-7.23(3H, m), 7.42(2H, $J = 6.7, 3.0$ Hz, dd). $^{13}\text{C}\{^1\text{H}\}\text{-NMR}(\text{CDCl}_3, 50 \text{ MHz}) \delta$ 14.3, 22.9, 25.8, 28.9, 35.9, 41.6, 45.8, 59.0, 60.3, 86.2, 90.4, 123.6, 127.8, 128.3, 131.7, 175.4.

(IVg) Isolated in the form of oil with yellow color, yield: 67%(114 mg, 0.34 mmol). $^1\text{H-NMR}(\text{CDCl}_3, 200 \text{ MHz}) \delta$ 1.24 (3H, $J = 7.1$ Hz, t), 2.13-1.43(14H, m), 2.42-2.18(3H, $J = 11.0$ Hz, t), 3.15(2H, $J = 11.6$ Hz, t), 4.13(2H, $J = 7.1$ Hz, q), 7.35-7.23(3H, m), 7.42(2H, $J = 6.7, 3.0$ Hz, dd). $^{13}\text{C}\{^1\text{H}\}\text{-NMR}(\text{CDCl}_3, 50 \text{ MHz}) \delta$ 14.3, 22.9, 25.8, 28.9, 35.9, 41.6, 45.8, 59.0, 60.3, 86.2, 90.4, 123.6, 127.8, 128.3, 131.7, 175.4.

(IVh) Isolated in the form of oil with yellow color, yield: 67%(114 mg, 0.34 mmol). $^1\text{H-NMR}(\text{CDCl}_3, 200 \text{ MHz}) \delta$ 1.24 (3H, $J = 7.1$ Hz, t), 2.13-1.43(14H, m), 2.42-2.18(3H, $J = 11.0$ Hz, t), 3.15(2H, $J = 11.6$ Hz, t), 4.13(2H, $J = 7.1$ Hz, q), 7.35-7.23(3H, m), 7.42(2H, $J = 6.7, 3.0$ Hz, dd). $^{13}\text{C}\{^1\text{H}\}\text{-NMR}(\text{CDCl}_3, 50 \text{ MHz}) \delta$ 14.3, 22.9, 25.8, 28.9, 35.9, 41.6, 45.8, 59.0, 60.3, 86.2, 90.4, 123.6, 127.8, 128.3, 131.7, 175.4.

(IVi) Prepared according to the standard procedure, the product was acquired in oily form with a yellow appearance and yield pf 70%(0.35 mmol, 96 mg). $^1\text{H-NMR}(\text{CDCl}_3, 400 \text{ MHz}) \delta$ 0.95-0.79(3H, m), 1.78-1.70-1.24(22H, m), 1.93(2H, $J = 11.2$ Hz, d), 2.22(2H, $J = 6.7$ Hz, t), 2.70-2.50(4H, m). $^{13}\text{C}\text{-NMR}(\text{CDCl}_3, 101 \text{ MHz}) \delta$ 14.1, 18.7, 22.7, 23.2, 24.9, 25.9, 29.3, 29.3, 31.4, 36.0, 47.0, 58.9, 80.7, 85.8.

(IVj) Obtained in accordance with the standard procedure in oily form with a yellow appearance and 67% yield(1.34 mmol, 339 mg). $^1\text{H-NMR}(\text{CDCl}_3, 400 \text{ MHz}) \delta$ 1.87-1.44(overlapping peaks, 12H, m), 2.15-2.10(2H, m), 2.75-2.60(4H, m), 7.31-7.25(3H, m), 7.41(2H, $J = 6.5, 3.2$ Hz, dd). $^{13}\text{C}\{^1\text{H}\}\text{-NMR}(\text{CDCl}_3, 101 \text{ MHz}) \delta$ 23.5, 24.5, 26.3, 39.9, 50.4, 67.7, 85.4, 91.6, 123.9, 127.7, 128.3, 131.8

3.5.3 General catalytic procedure for complexes 4-9

The experimental procedures were executed within an argon atmosphere, employing conventional Schlenk techniques to ensure an inert environment. Solvents were included for specific substrates to prevent unintended solidifying of mixtures in the reaction. In these instances, a minimal quantity of toluene in an anhydrous state was introduced. The reactions were conducted inside a flame-dried J Young tube fitted with a stirring bar. To initiate the process, catalyst (5 mol%) and amine (0.5 mmol) were introduced into the tube, and stirring continued until partial dissolution of the solid occurred. Subsequently, alkyne and ketone, both in 0.5 mmol, along with dry toluene if required, were added. Additionally, a desiccant was placed inside the sealed tube. This was followed by stirring the mixture for 16 hrs. at a temperature of 130 °C within an oil bath. After cooling, ethyl acetate was employed, and the resulting mixture was filtrated through a celite pad. Subsequently, the solvent was discharged through vacuum evaporation, leaving behind a residue. To obtain propargylamine substrates that are without impurity, the residue underwent purification through column chromatography, utilizing an eluent composed of petroleum ether/ethyl acetate. The products obtained were then subjected to characterization through ¹H-NMR analysis, and the obtained data agreed with literature references [41, 52-54].

3.5.4 Characterisation data of the propargylamine products

(Va) Isolated in oily form with a yellowish appearance and 85% yield(0.41 mmol, 112 mg). ¹H-NMR(CDCl₃, 200 MHz) δ 1.68-1.37 (overlapping peaks, 14H, m), 2.10 (2H, J=11.4 Hz, d), 2.66 (4H, J=5.4 Hz, t), 7.35-7.23(3H, m), 7.45-7.40(2H, m).

(Vb) Isolated as an orange-colored oil with 67% yield (0.33 mmol, 91 mg). ¹H-NMR (400 MHz, CDCl₃) δ 1.28 (s, 1H), 1.56-1.47 (m, 2H), 1.63 (dd, J = 12.6, 3.1 Hz, 2H), 1.73 (dt, J = 10.3, 5.0 Hz, 2H), 2.07-2.00 (m, 2H), 2.73 (t, J = 4.7 Hz, 4H), 3.77 (t, J = 4.8 Hz, 4H), 7.29 (q, J = 3.3, 2.3 Hz, 3H), 7.43 (dt, J = 6.0, 3.8 Hz, 2H).

(Vc) Isolated in oily form with a yellowish appearance. Yield: 42%(0.20 mmol, 64 mg). ¹H-NMR(CDCl₃, 400 MHz) δ 0.88(3H, m), 1.74-1.07(20H, m), 1.94(2H, J = 11.6 Hz, d), 2.79(2H, J = 7.1 Hz, T), 7.33-7.23(3H, m), 7.42(2H, J=6.7, 3.1 Hz, dd).

(Vd) Oil isolated with orange appearance in 40% yield(0.20 mmol, 57 mg). ¹H-NMR(CDCl₃, 200 MHz) δ 0.87 (6H, J=7.3 Hz, t), 1.76-1.42 (12H, m), 2.05(2H, J=11.8 Hz, d), 2.62(4H, J=7.8 Hz, t), 7.33-7.24(3H, m), 7.47-7.37(2H, m).

(Ve) Isolated as a yellow-colored oil with 50% yield (0.49 mmol, 67 mg). ¹H-NMR(CDCl₃ 400 MHz) δ 1.70-1.60(8H, m), 1.84-1.81(4H, m), 2.04-1.98 (2H, m), 2.35(3H, s), 2.90(4H, J=6.3 Hz, d), 7.11(2H, J=7.8 Hz, d), 7.32(2H, J=7.8 Hz, d).

(Vf) Isolated as an orange-colored oil with 38% yield(0.20 mmol, 54 mg). ¹H-NMR(CDCl₃, 200 MHz) δ 1.81-1.38 (12H, m), 2.00-1.88(2H, m), 2.76-2.67(4H, m), 7.22-7.18(2H, m), 7.40-7.31(2H, m).

(Vg) Oil with an orange appearance was isolated in a yield of 96%(0.48 mmol, 142 mg). ¹H-NMR(CDCl₃, 400 MHz) δ 1.78-1.37(overlapping peaks, 15H, m), 2.10(2H, J = 11.8 Hz, d), 2.73(4H, s), 3.81(3H, s), 6.83(2H, J=8.5 Hz, d), 7.37(2H, J=8.6 Hz, d).

(Vh) Oil with yellow color isolated in 43% yield(0.23 mmol, 62 mg). ¹H-NMR(CDCl₃, 400 MHz) δ 0.91(7H, J=12.8, 6.8 Hz, dt), 1.67-1.43(14H, m), 1.78(4H, s), 1.89(2H, J=11.6 Hz, d), 2.23(2H, J=6.8 Hz, t), 2.78 (4H, J=6.1 Hz, d).

(Vi) Oil with yellow appearance. Isolated in 75% yield(0.38 mmol, 94 mg). ¹H-NMR(CDCl₃, 400 MHz) 0.96(6H, J=7.5 Hz, t), 1.76(8H, m), 2.76(4H, s), 7.28(4H, J=5.4 Hz, d), 7.45-7.38(2H, m).

3.6 DFT Calculations

3.6.1 DFT Calculations for complexes 1-3

Geometry optimization was carried out for complexes **1-3** using DFT calculations. The calculations were performed in the gaseous phase using the Gaussian 09 program [55], employing the B3LYP/6-31G theoretical level [56-59]. All computational tasks for complexes **1-3** were executed utilizing the supercomputing facility PARADOX [60].

3.6.2 DFT Calculations for complexes 4-9

Computational studies for complexes **4-9** were conducted utilizing the ADF engine [61, 62] integrated into the Amsterdam modeling suite [63]. Scalar-relativistic effects were considered by employing the zeroth-order regular approximation (ZORA) [64-66] method. Hydrogen atoms were optimized by employing the fast inertial relaxation engine [67] optimizer in Cartesian coordinates, while the other atomic positions were fixed based on the geometries of the complexes determined via X-ray analysis. The optimization of hydrogen atoms incorporated Becke's exchange [68] and Perdew's correlation [69], complemented by Grimme's fourth-generation dispersion energy corrections [70] (BP86-D4). Double-zeta Slater-type orbitals (STO) with an extra polarization function (DZP) were used as the basis sets for all-electron calculations.

3.6.3 Conceptual DFT

Conceptual DFT descriptors [71, 72] were utilized to interpret and anticipate the reactivity of the molecules. These descriptors are inherent properties directly derived from the DFT computations [73, 74]. In this research, we examined global reactivity descriptors, including the electronic chemical potential (μ), molecular hardness (η), molecular softness (S), electrophilicity index (ω), and electronegativity (χ). These descriptors serve as vital tools for comprehending and forecasting the reactivity of the molecules under investigation. These global reactivity descriptors are assessed through two distinct methodologies: finite difference linearization (FDL) and the frontier molecular orbital approximation (FMO) [73], Eqs 1-5.

$$\eta = E_e(N + 1) - 2E_e(N) + E_e(N - 1) \approx e_{LUMO} - e_{HOMO} \quad (1)$$

$$\mu = (E_e(N + 1) - E_e(N - 1)) / 2 \approx (e_{HOMO} + e_{LUMO}) / 2 \quad (2)$$

$$S = 1/\eta \quad (3)$$

$$\omega = \mu^2 / 2\eta \quad (4)$$

$$\chi = -\mu \quad (5)$$

The FDL approach is based on the calculation of energies of complexes with an additional or one less electron. The FMO approximation is based on the evaluation of energies of the frontier molecular orbitals (HOMO, LUMO). Molecules with a larger orbital energy gap are considered "hard" and exhibit higher chemical stability, while those with a smaller energy gap are referred to as "soft" and display greater polarizability. Soft molecules require less energy for excitation [71,75].

For complexes **1-3**, HOMO-LUMO energies were determined by the time-dependent DFT (TD-DFT) using the Gaussian 09 program [55]. Several TD-DFT calculations were utilized, encompassing B3LYP/6-31G, B3LYP/6-311G(d,p), and BVP86/6-311G(d,p) [68,69,76] under vacuum conditions. Additionally, investigations of HOMO-LUMO energy were extended to include toluene as the solvent, employing TD-DFT with the polarizable continuum model (PCM) [77] at the B3LYP/6-31G level of theory.

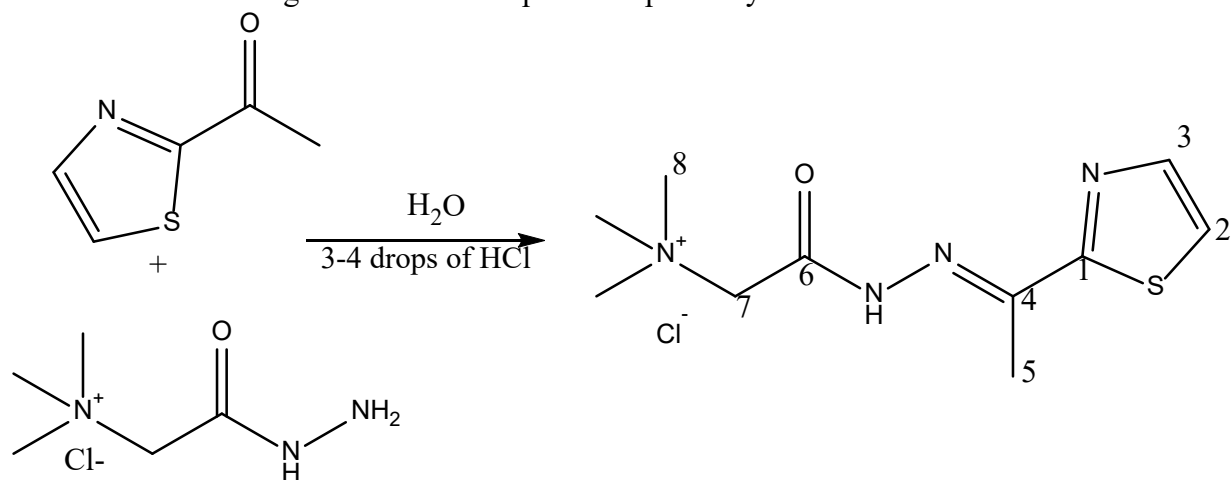
For complexes **4-9**, FDL and FMO approaches are compared from single-point calculations with the ADF engine from the Amsterdam modeling suite [62]. Range-separated hybrid CAM-B3LYP functional [78], all-electron triple-zeta STO basis set with an added polarization function (TZP), and an enhanced numerical grid ("Becke grid Quality good" in ADF) was employed. The LibXC [79]

library was utilized for calculations involving the CAM-B3LYP functional [78]. The unrestricted formalism was used for the calculations regarding the species with an unpaired number of electrons.

4. Results and discussion

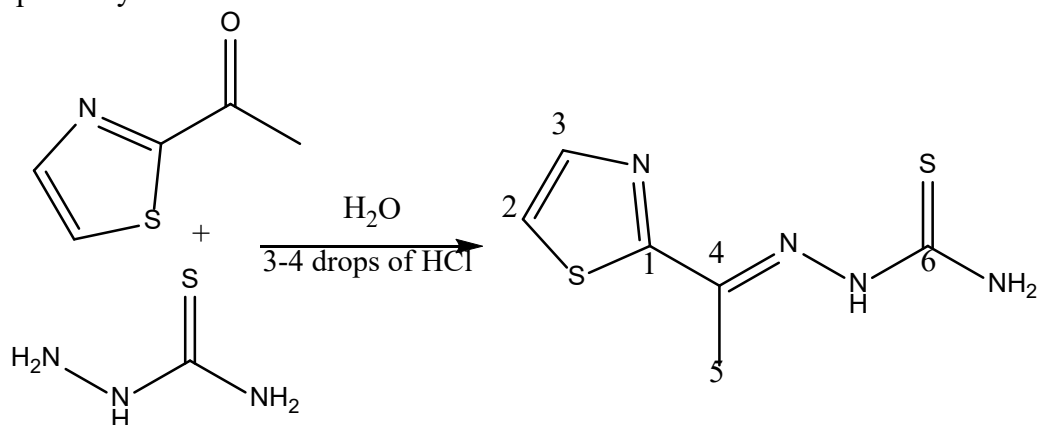
4.1 Synthesis

HL¹Cl was synthesized by reacting Girard's reagent T with 2-acetylthiazole in water, using an equal molar ratio. Precipitate with a white appearance was formed after the reaction. The obtained product was characterized through elemental and spectroscopic analysis.



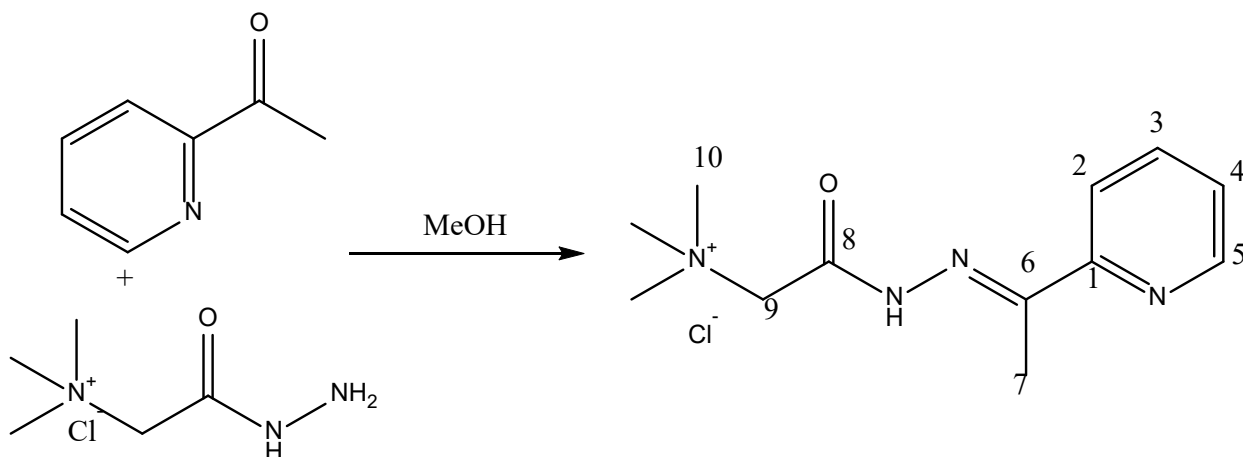
Scheme 3: Synthesis of **HL¹Cl**

HL² was synthesized by reacting 2-acetylthiazole with thiosemicarbazide under similar reaction conditions to **HL¹Cl**. The resulting reaction produced a precipitate with a white appearance. Various analytical techniques were employed to characterize the product, including elemental and spectroscopic analysis.



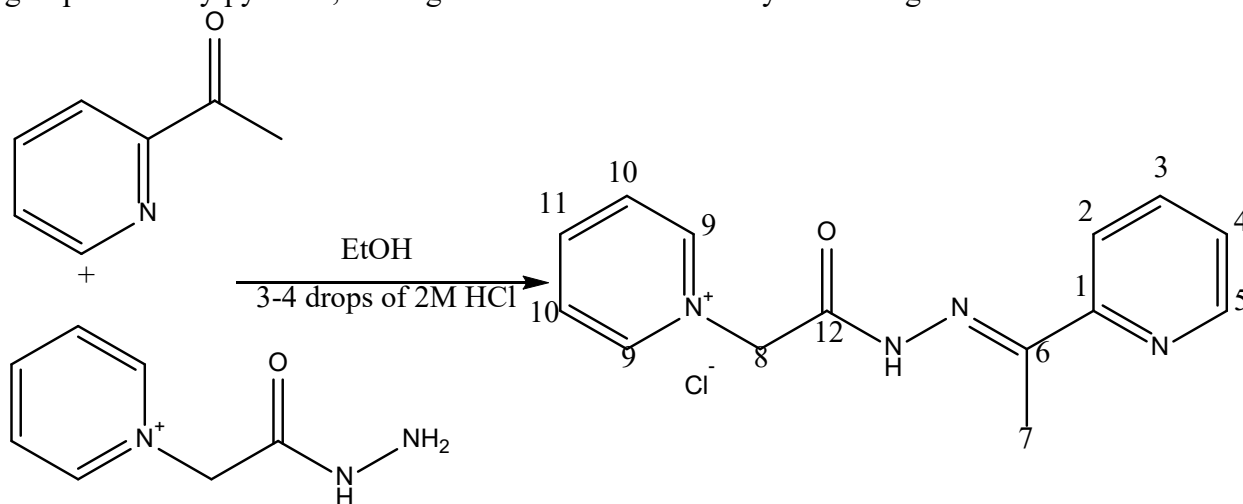
Scheme 4: Synthesis of **HL² Ligand**

The ligand **HL**³Cl was synthesized as reported in literature [19], and outlined in Scheme 5



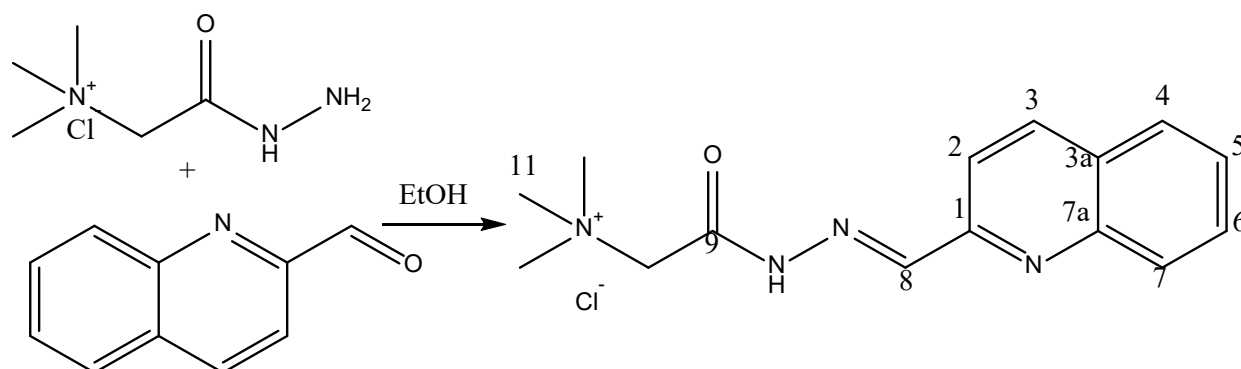
Scheme 5: Synthesis of **HL**³Cl ligand

HL⁴Cl was synthesized through a reaction between Girard's reagent P and 2-acetylpyridine, as shown in Scheme 6. During the reaction, the aldehyde moiety of Girard's P reagent reacts with the ketone group of 2-acetylpyridine, leading to the formation of the hydrazone ligand **HL**⁴Cl.



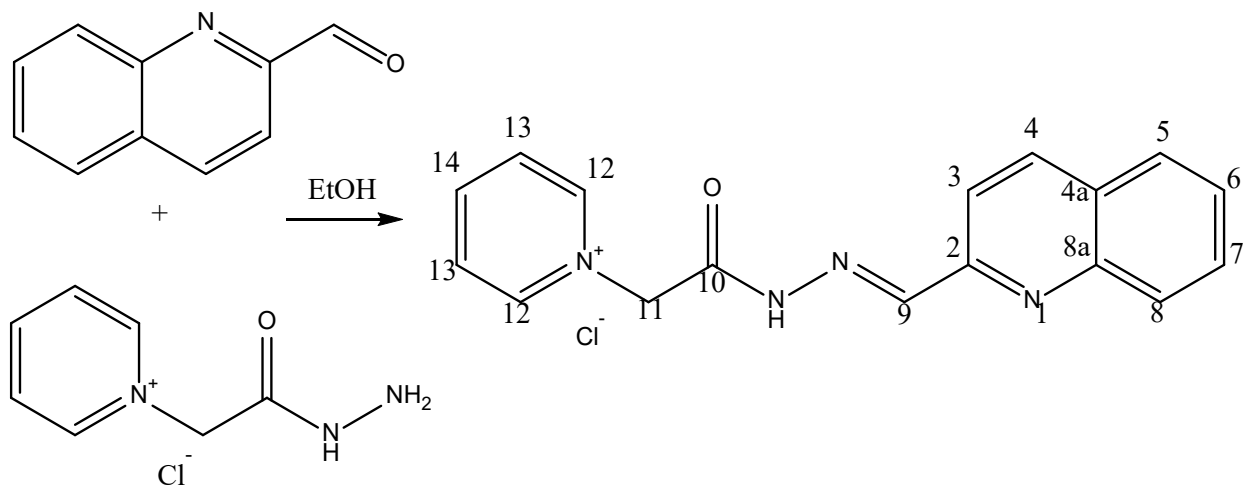
Scheme 6: synthesis of **HL**⁴Cl

HL⁵Cl was synthesized as previously outlined in the reported literature [3] (scheme 7).



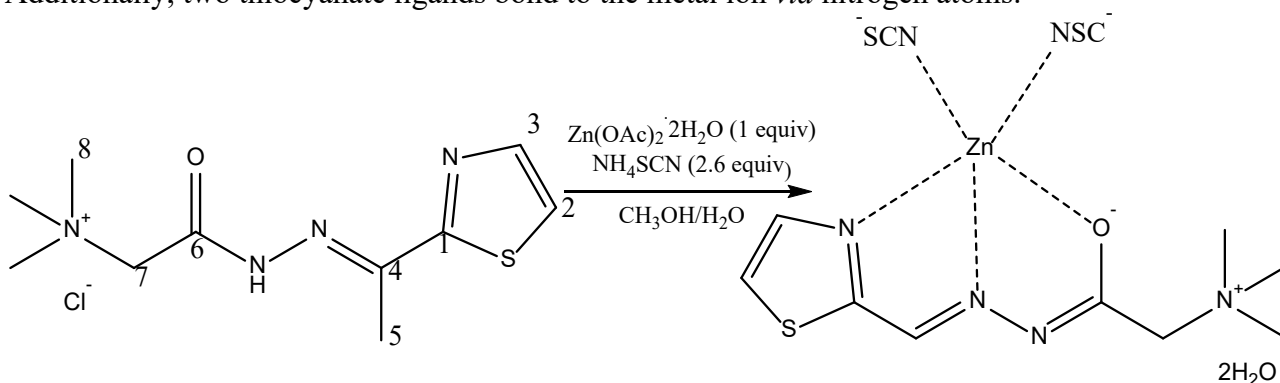
Scheme 7: synthesis of **HL**⁵Cl

The ligand **HL**⁶Cl was synthesized as previously outlined in the reported literature [42] (scheme 8).



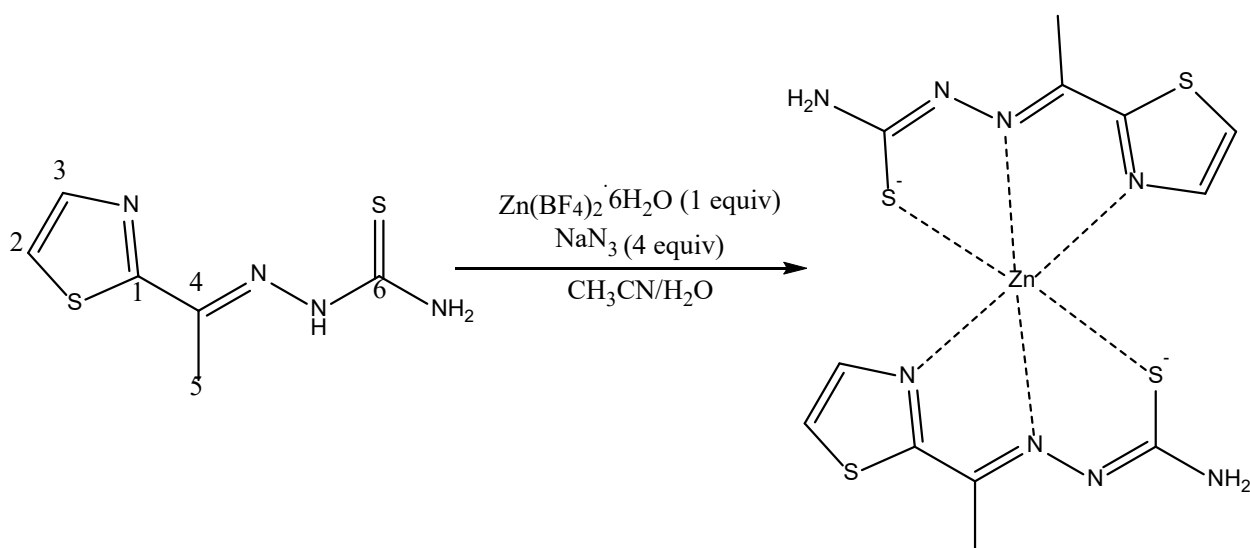
Scheme 8: synthesis of **HL**⁶Cl

Mononuclear complex **1** was synthesized in accordance with Scheme 9. In the complex, the central zinc ion exhibits a fivefold coordination geometry, wherein it coordinates with various atoms from the ligand. The nitrogen from the thiazole and azomethine group, alongside the oxygen from the carbonyl group, all originating from the non-protonated ligand, establish bonds with the ion of Zn(II). Additionally, two thiocyanate ligands bond to the metal ion *via* nitrogen atoms.



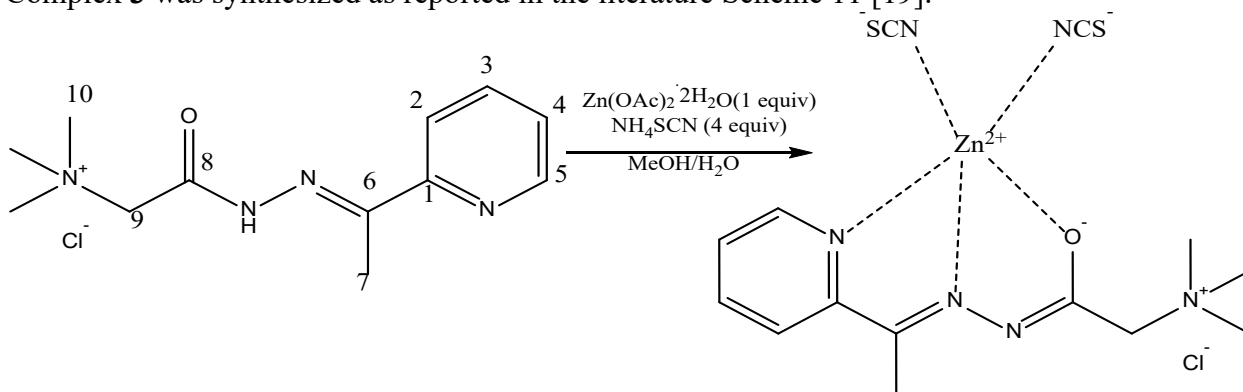
Scheme 9: synthesis of complex **1**

The mononuclear complex, denoted as complex **2** was successfully synthesized, as represented in Scheme 10. It is composed of [Zn(L²)₂]. In complex **2**, two nonprotonated ligands **L**², coordinate to the Zn(II) ion *via* various atoms, resulting in the formation of a distorted octahedral complex. The coordination atoms involved include the nitrogen from imine and thiazole, along with S-atoms of thiolate from each ligand.



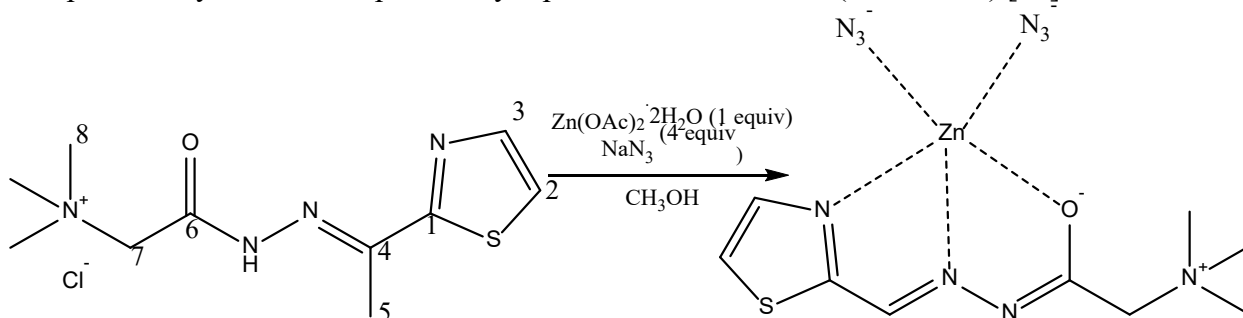
Scheme 10: Synthesis of complex **2**

Complex **3** was synthesized as reported in the literature Scheme 11 [19].



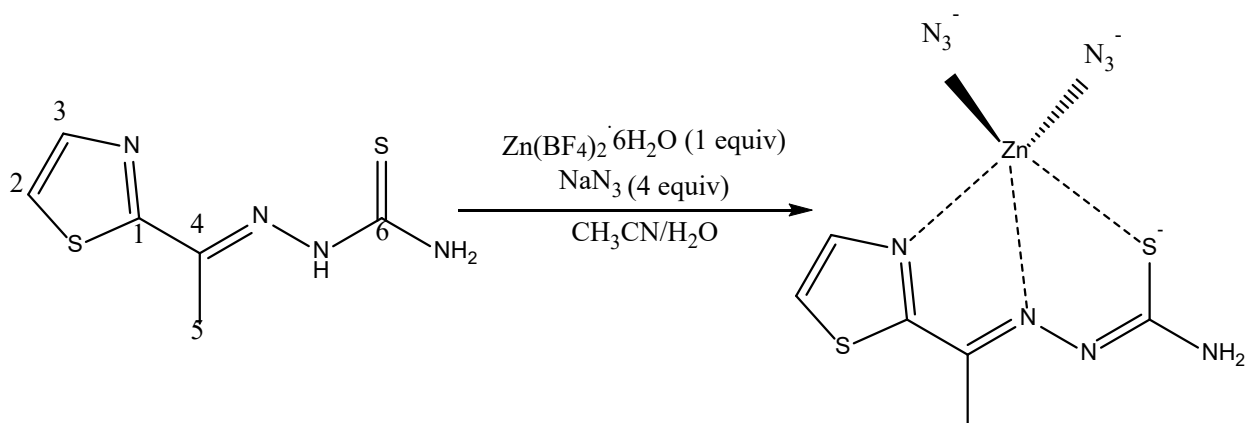
Scheme 11: Synthesis of complex **3**

Complex **4** is synthesized as previously reported in the literature (Scheme 12) [43].



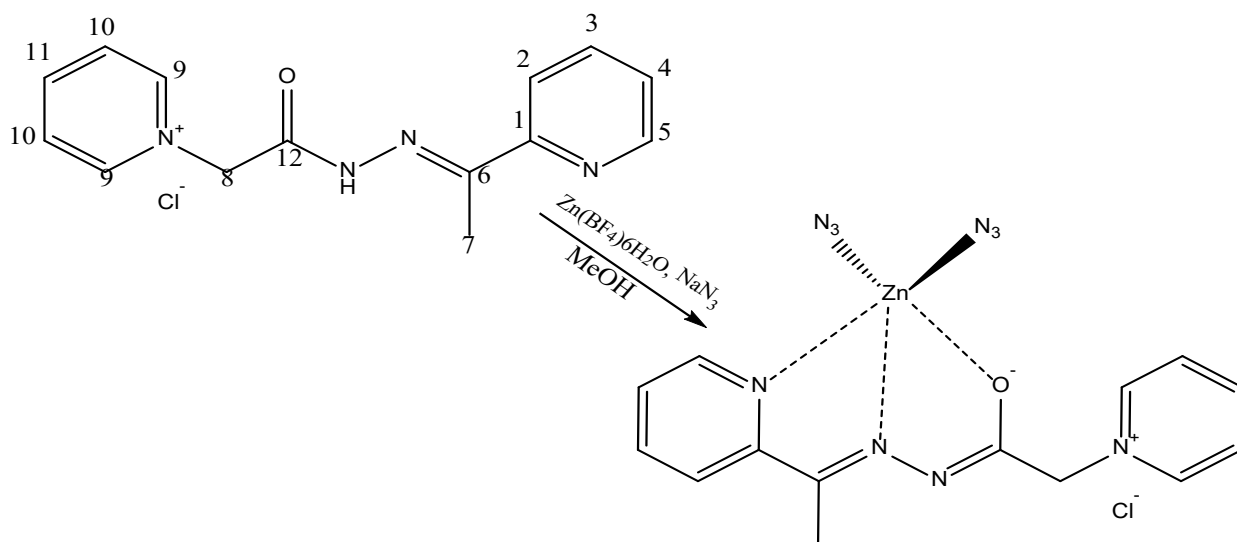
Scheme 12: Synthesis of complex **4**

Mononuclear complex **5** composing $\text{ZnL}^2(\text{N}_3)_2$ was synthesized as depicted in Scheme 13. In complex **5**, Zn(II) exhibits pentacoordination. The coordination involved both the thiazole and azomethine nitrogens, as well as the sulfur atoms from the thiolate, which originated from the non-protonated ligand. Additionally, coordination occurred with the presence of double azido ligands.



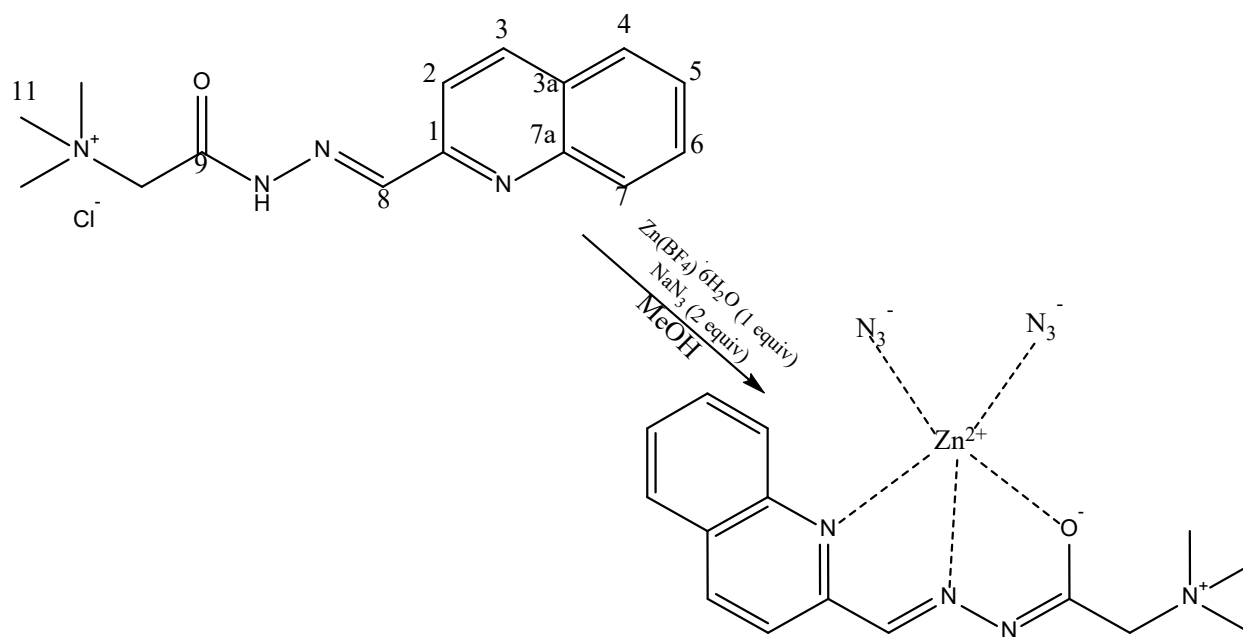
Scheme 13: Synthesis of complex **5**

Mononuclear complex **6**, composing $[\text{ZnL}^4(\text{N}_3)_2]$, is synthesized as depicted in Scheme 14. Within complex **6**, L^4 assumes its deprotonated, formally neutral, zwitterionic state as it coordinates to the $\text{Zn}(\text{II})$ ion. This coordination occurs *via* the N-atoms of imine and pyridine groups, O-atoms from the carbonyl group, in addition to two azido ligands. Thereby a pentacoordinated complex is formed.

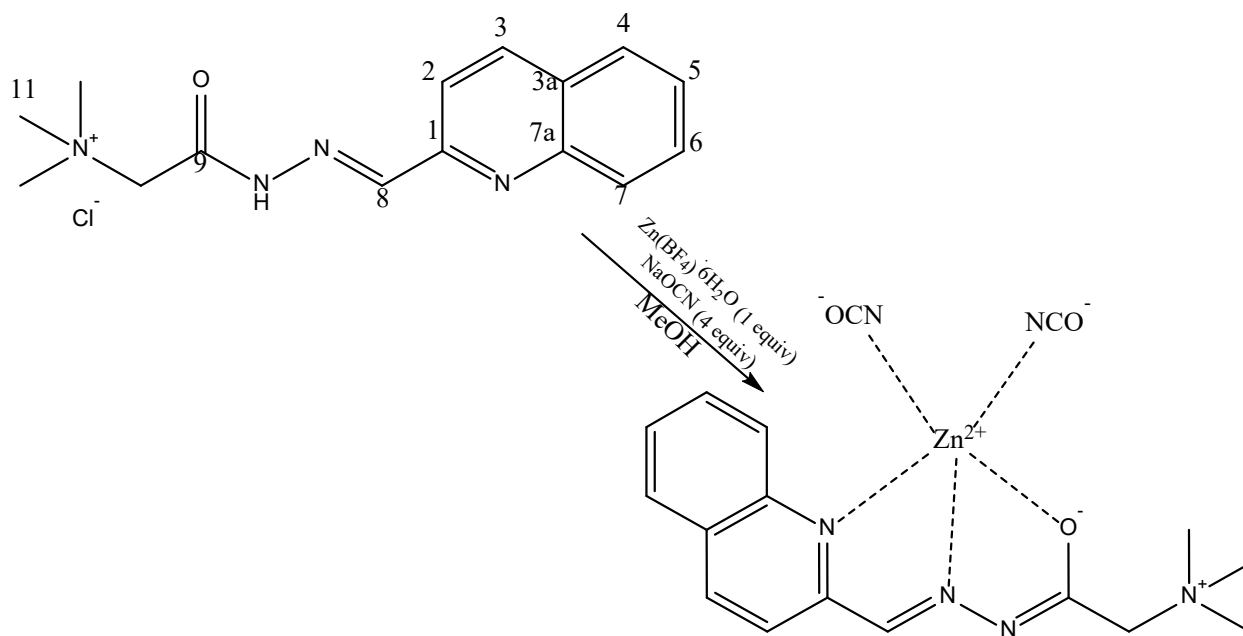


Scheme 14: Synthesis of complex **6**

As previously reported, complexes **7** and **8** were synthesized according to Schemes 15 and 16, respectively [44].

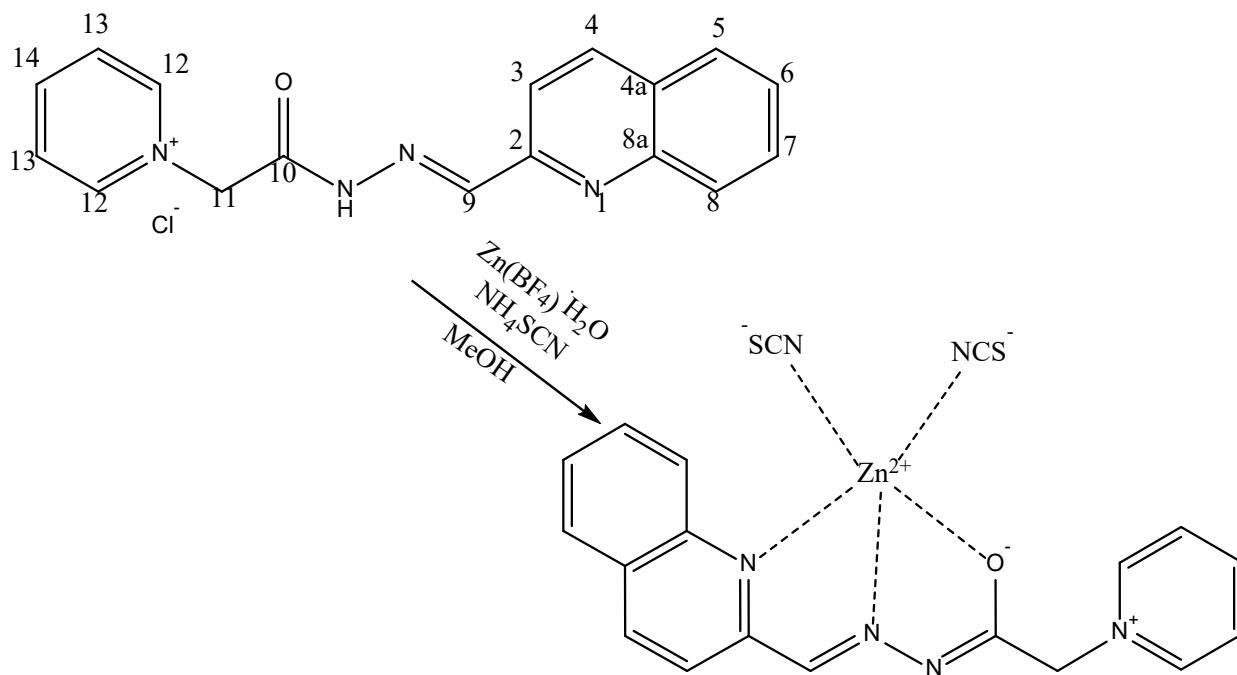


Scheme 15: Synthesis of complex **7**



Scheme 16: Synthesis of complex **8**

Complex **9** was synthesized following the method previously studied, scheme 17 [45].



Scheme 17: Synthesis of complex **9**

The previously reported ligands and complexes that were synthesized, were subjected to characterization through elemental analysis, as well as IR and NMR spectroscopy, confirming their purity.

4.2 FT-IR Spectroscopy of complexes **1**, **2**, **5** and **6**

The absence of the 1702 cm^{-1} band in complex **1**, attributed to the carbonyl moiety of the noncoordinated HL^1Cl , is indicative of coordination through the O-atom. Furthermore, the emergence of a 2088 cm^{-1} band in the spectrum of the same complex indicates coordination of the SCN^- group through the nitrogen atom.

The shifts in the band from 1648 cm^{-1} in the noncoordinated ligand HL^2 to 1632 cm^{-1} in complex **2** indicated coordination through the azomethine group of the $\text{C}=\text{N}$ group.

The IR spectra of complex **5** provide evidence for the coordination of HL^2 in its non-protonated form, as indicated by the absence of the 3435 cm^{-1} N-H band. In contrast, when examining the spectra of the free ligand HL^2 , $\text{C}=\text{S} + \text{CH}$ and $\text{C}=\text{S} + \text{C}=\text{N}$ bands were seen at 1068 and 1481 cm^{-1} , respectively.

Within the spectra of **6**, a noticeable band at approximately 1629 cm^{-1} emerges. This band is assigned to the vibration of $-\text{O}-\text{C}=\text{N}$, suggesting the non-protonated coordination of α -oxyazine ligand. This contrasts the carbonyl group band observed in the uncoordinated HL^4Cl ligand around 1699 cm^{-1} [80].

4.3 NMR Spectroscopy of complexes **1**, **2**, **5** and **6**

NMR spectra of the prepared complexes (**1**, **2**, **5**, and **6**) reveal notable shifts in the chemical shifts of both hydrogen and carbon atoms when compared to the values detected in the uncoordinated ligands. These shifts strongly suggest the occurrence of coordination between the ligand and the metal ion in each respective complex.

Within complex **1**, the coordination involving the N-group of the thiazole induces a shift in the C3-H signal from 7.926 to 8.06 ppm in the downfield direction. The absence of the NH signal at 11.61

ppm in the ligand within the complex implies deprotonation and coordination *via* N-atoms. Furthermore, coordination through azomethine nitrogen causes a shift in the downfield direction of the C4 signal from 147 ppm to 147.3 ppm, while coordination through thiazole nitrogen leads to a shift in the upfield direction of the C3 signal from 143.9 ppm to 125.7 ppm.

Within the spectrum of **2**, a downfield shift is observed in the C3-H signal, shifting from 7.80 ppm to 7.94 ppm in ligand and complex, respectively. This shift is attributed to coordination through the thiazole nitrogen. Additionally, the hydrazide NH signal at 10.67 ppm in the ligand is not detected in the complex, indicating deprotonation and coordination. Coordination through the S-group results in a shift towards the downfield direction of the C6 carbon signal, moving from 179.4 ppm to 181.7 ppm. Furthermore, coordination through N-azomethine induces an upfield shift in the C4 signal, transitioning from 144.7 ppm in the ligand to 139.2 ppm in **2**, while coordination through N-thiazole group leads to a shift in the downfield direction in the C3 signal, changing from 123.1 ppm to 122.5 ppm.

The analysis of the ^1H NMR spectrum revealed that the NH signal at 10.6 ppm, present in the ligand **HL**², was absent in the complex **5** spectrum. This absence strongly suggests that **HL**² is coordinated in a non-protonated form known as **L**². It was evident in the ^{13}C NMR spectrum that **5** exhibited coordination via N-thiazole and N-azomethine, as well as with sulfur atoms of the thiolate group. Notably, thiolate carbon (C6) displayed a downfield shift, transitioning from 179.4 ppm in **HL**² spectrum to 181.6 ppm in the **5** spectrum, indicating the coordination via S-atom of the same group.

The analysis of the ^1H NMR spectrum for complex **6** indicated that **HL**⁴Cl is also coordinated without the H-atom, as evidenced by the absence of the NH signal at 11.5 ppm. **HL**⁴Cl coordination via O- from the carbonyl group led to a downfield shift of the signals of the C8-H protons, moving from 6.1 ppm to 5.4 ppm in the spectra of **6**. ^{13}C NMR spectrum reveals the C1 resonated at 154.9 ppm in **HL**⁴Cl, whereas in complex **6**, the same carbon could be seen at 149.3 ppm. N-azomethine coordination induced an upfield shift of the C6 signal, shifting from 150.9 ppm to 161.3 ppm in the spectrum of **6**. Furthermore, coordination of the O-carbonyl resulted in a C12 upfield shift, from 168.1 ppm in the **HL**⁴Cl spectra to 172.5 ppm in the spectrum of **6** [81,82].

It is important to emphasise that the purity of the previously synthesised complexes (3,4,7,8 and 9) was checked by recording the corresponding IR and NMR spectra and comparing the values with those reported in the literature.

4.4 Crystal structure of complex **1** and **2**

Figure 21 illustrates the molecular arrangement of complex **1**, while precise bond angles and lengths are detailed in Table 4. The non-charged compound is found in a dihydrate form and undergoes crystallization in the crystal system known as triclinic with the space group P-1. Within **1**, the zinc ion in the 1st position displays fivefold coordination, establishing connections with the tridentate coordination of ligand **L**¹ and a pair of N-atoms (N5, N6) originating from the SCN⁻ ligands.

The coordination of ligand with zinc takes place in the form of zwitterionic, where the donor atoms create an NNO-set configuration. This leads to the formation of two interconnected chelate rings with five members each, specifically the Zn- N-C -C -N and Zn-N -N -C -O rings.

The dihedral angle, which measures approximately 4 degrees between these two five-membered chelate rings, indicates that the metal-ligand arrangement in **1** is not coplanar. To quantify this distortion in a five-coordinated system, it is common to employ the trigonality index τ , calculated as $\tau = (\beta - \alpha)/60$, where β represents the largest basal angle, and α is the second largest angle. In regular square-based pyramidal structures, τ equals 0, while in trigonal bipyramidal structures, τ equals 1 [83].

In the case of **1**, the calculated value of $\tau = 0.36$ shows that the coordination geometry around Zn1 exhibits approximately 36 percent trigonal distortion from an ideal square –

based pyramidal shape. The largest basal angles, N2 -Zn1 -N5 and O1 -Zn1 -N1, measure 127.42(10)° and 149.20(7)° respectively. Zinc in the first position is situated outside the plane formed by the L atoms (N1, N2, N5 and O1), which consist of four atoms, by a distance represented as ρ measuring 0.6091(3) angstrom.

1 displays a slight increase in trigonal distortion from the usual configuration of a square – based pyramidal compared to other zinc complexes with five coordination. These complexes utilize N-heteroaromatic monohydrazones of Girard's reagent T as ligands, along with monodentate pseudohalide/halide ligands (NCO⁻, N³⁻, Cl⁻ or NCS⁻). The estimated τ values for these complexes spread from 0.31 to 0.34, as presented in Table 5.

The τ values observed for **1** fall within the span of values typically seen in similar zinc complexes (Table 5) [84-88].

In **1**, it's evident zinc forms a stronger bond with the N-atom of the imine moiety in **L**¹ in comparison to the N-atom of the 1,3-thiazole ring. This distinction is noticeable when observing the bond lengths of Zn1-N1(2.212 angstroms) and Zn1-N2(2.058 angstroms) as documented in Table 4. Similarly, in analogous complexes featuring zinc (II), Girard's hydrazone-T ligands and monodentate ligands such as N₃⁻, NCO⁻, NCS⁻, or Cl⁻, it is consistently observed that the Zn-N(imine) bond lengths (ranging from 2.049 to 2.088 Å are shorter than the Zn-N(quinoline/pyridine) bond lengths (2.240-2.34 /2.206 angstrom). This underscores the stronger interaction of the zinc ion with the N-atoms of the imine moiety compared to those of quinoline or pyridine [19, 44, 89]. Referring to Table 5, the bond distances of Zn-O (enolic) span between 2.146 to 2.222 angstroms. The most compact bond distance Zn-O (enolic) is observed in **3** (refers to Table 5), while the longest is found in **7** (refers to Table 5). In **1**, the SCN ligands coordinate to the Zn in a bent manner, resulting in angles of Zn-N-C measuring 168.5 and 171.7 degrees.

The crystal structure analysis of **1** reveals that complex molecules assemble into supramolecular layers that are oriented parallel to the (0 0 1) lattice plane. These layers are formed through a combination of moderate O1W – H1W ... O1 and weaker C8 – H8A ... S2 and C10 – H10B ... O1W intermolecular bonds of hydrogen [90], as detailed in Table 6 and illustrated in Figure 22a. Furthermore, water molecules in the solvent O1W and O2W play a role in connecting adjacent layers, which are related by symmetry center, through weak intermolecular bonds of hydrogen involving C – H ... OW interactions (as listed in Table 6 and depicted in Figure 22b).

Along the [-1 1 0] direction, the smallest distances between gravity centers of the 1,3-thiazole rings are measured as 4.467 and 4.666 angstrom, respectively.

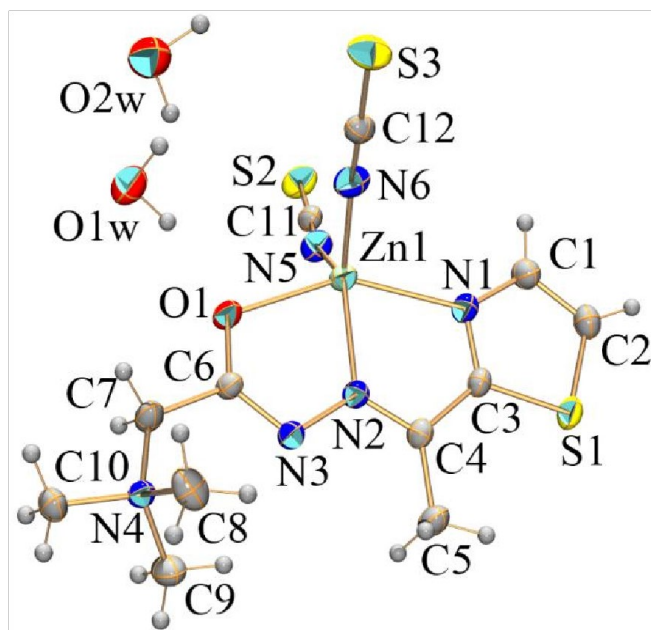


Figure 21: A representation of the structure of complex **1** depicted using an ORTEP diagram, with thermal ellipsoids drawn to illustrate the molecular arrangement at a probability level of 30%

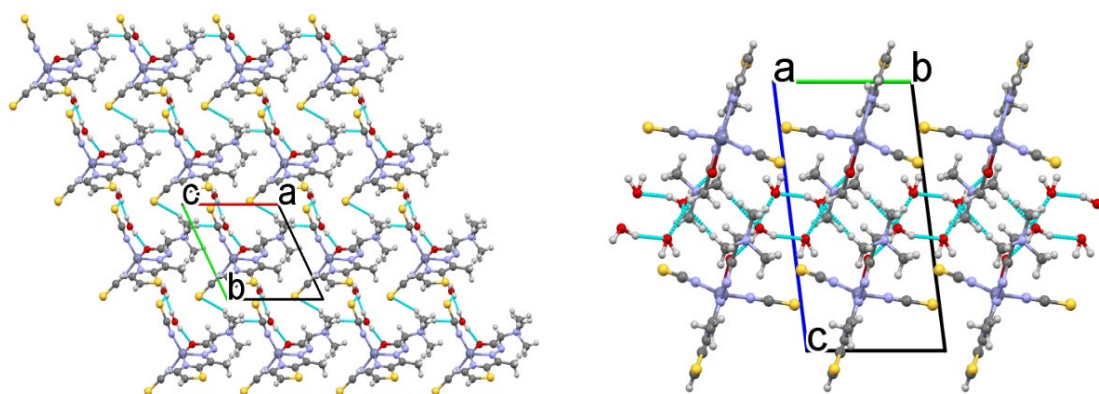


Figure 22a and 22b: a) An illustration of the crystal packing of **1** reveals that molecules are interconnected via hydrogen bonds, including $\text{OW} - \text{H} \cdots \text{O}$, $\text{CMe} - \text{H} \cdots \text{OW}$ and $\text{CMe} - \text{H} \cdots \text{S}$ interactions (indicated by blue dashed lines). These interactions form layers that are oriented parallel to the (0 0 1) lattice plane. (b) When observing the layers parallel to the (0 0 1) lattice plane from a side view, it becomes apparent that these layers, which are related through symmetry centers symmetry, are joined together with the assistance of O1W and O2W water molecules.

Table 4: Selected bond angles ($^\circ$) and lengths (\AA) for complexes **1** and **2**

1		2	
Bond Angles			
O1–Zn1–N1	149.20	N5–Zn1–S4	154.65
N2–Zn1–N1	75.37	N6–Zn1–S4	79.42
N5–Zn1–N1	97.92	N2–Zn1–S4	101.19
N6–Zn1–N1	101.94	N5–Zn1–N1	84.54
N2–Zn1–O1	74.02	N6–Zn1–N1	93.21
N5–Zn1–O1	97.85	N2–Zn1–N1	73.63
N6–Zn1–O1	96.93	N6–Zn1–N5	75.28
N5–Zn1–N2	127.42	N2–Zn1–N5	103.08
N6–Zn1–N2	121.74	N2–Zn1–N6	166.84

N6–Zn1–N5	110.73	N1–Zn1–S4	95.42
Bond Lengths			
N6–C12	1.149	N8–C12	1.360
N5–C11	1.146	N7–C12	1.332
N3–C6	1.317	N6–C10	1.301
N2–N3	1.389	N4–C6	1.360
N2–C4	1.285	N3–C6	1.327
S3–C12	1.624	N6–N7	1.36
S2–C11	1.626	N2–N3	1.370
O1–C6	1.265	N2–C4	1.290
Zn1–N1	2.212	S4–C12	1.712
Zn1–O1	2.1778	S2–C6	1.716
Zn1–N2	2.058	Zn1–S4	2.4109
Zn1–N5	1.959	Zn1–S2	2.4516
Zn1–N6	1.955	Zn1–N1	2.318
		Zn1–N2	2.147
		Zn1–N5	2.1869
		Zn1–N6	2.149

Table 5: Correlation of structural parameters influencing the geometry of pentacoordinate $[\text{ZnLX}_2]$ complexes, where L represents a tridentate ligand of hydrazone, and X can be a halide, pseudohalide, or DMSO

Complex	α ($^\circ$)	β ($^\circ$)	τ^1	ρ^2 (\AA)	References
$[\text{ZnL}^1(\text{NCS})_2] \cdot 2\text{H}_2\text{O}$ (1)	127.42(10)	149.20(7)	0.36	0.6091(3)	This work
$[\text{ZnL}^3(\text{NCS})_2] \cdot 0.5\text{MeOH}^3$ (3)	128.4(3)	147.9(2)	0.32	0.6022(11)	[19]
$[\text{ZnL}^5(\text{NCO})_2]^4$ (7)	126.41(10)	146.98(8)	0.34	0.6462(4)	[44]
$[\text{ZnL}^4(\text{N}_3)_{1.65}\text{Cl}_{0.35}]^4$ (8)	128.68(8)	148.40(6)	0.33	0.5648(2)	[89]
$[\text{ZnL}^5(\text{N}_3)_2]^4$ (I)	129.4(2)	147.68(10)	0.31	0.6165(5)	[44]
$[\text{Zn}(\text{L}^5)\text{Cl}_2] \cdot 0.5\text{H}_2\text{O}^5$ (II)	123.36(5)	147.07(6)	0.40	0.6453(3)	[84]
$[\text{Zn}(\text{L}^6)\text{Cl}_2]^6$ (III)	126.09(5)	146.03(7)	0.33	0.6715(2)	[85]
$[\text{Zn}(\text{HL}^7)(\text{NCS})_2]^7$ (IV)	133.96(8)	151.16(7)	0.29	0.5154(3)	[91]
$[\text{Zn}(\text{HL}^7)_2]^7$ (V)	131.46(6)	148.52(8)	0.28	0.6628(3)	[91]
$[\text{Zn}(\text{HL}^7)\text{Br}_2]^7$ (VI)	131.83(6)	147.91(8)	0.27	0.6528(3)	[91]
$[\text{Zn}(\text{L}^8)\text{Br}_2]^8$ (VII)	129.81(8)	146.06(9)	0.27	0.6677(4)	[86]
$[\text{Zn}(\text{L}^9)\text{Cl}(\text{DMSO})]^9$ (VIII)	134.73(6)	149.56(7)	0.25	0.5025(3)	[87]
$[\text{Zn}(\text{L}^{10})\text{Cl}_2]^{10}$ (IX)	133.36(6)	144.88(7)	0.19	0.6438(3)	[88]
$[\text{Zn}(\text{L}^{11})\text{Cl}_2]^{11}$ (X)	135.35(8)	143.18(9)	0.13	0.6503(4)	[87]

Table 6: Parameters of hydrogen-bond for **1**

D–H...A	D–H (\AA)	H...A (\AA)	D...A (\AA)	D–H...A ($^\circ$)	Symmetry operation on A
Inter layer C9–H9C...O1W	0.96	2.528	3.476(5)	169.8	1–x, 1–y, 1–z
Intra C9–H9B...N3	0.96	2.381	3.022(5)	123.8	
Intra C5–H5B...S1	0.96	2.872	3.253(3)	104.9	
C10–H10B...O1W	0.96	2.686	3.579(5)	155.0	–1+x, y, z
Inter layer C7–H7A...O2W	0.97	2.685	3.575(5)	152.7	1–x, 2–y, 1–z
C8–H8A...S2	0.96	2.896	3.737(5)	146.8	–1+x, 1+y, z
O2W–H4W...S3	0.92(4)	2.81(3)	3.616(6)	147(4)	

O1W–H2W...O2W	0.94(4)	1.96(4)	2.868(5)	162(4)
O1W–H1W...O1	0.91(4)	1.89(4)	2.792(4)	170(3)

The structure of complex **2** is depicted in Figure 23. Specific bond angles and lengths can be found in Table 4. This complex, which in its neutral form is denoted as $[\text{Zn}(\text{L}^2)_2]$, forms a crystal structure system known as monoclinic with the space group $\text{P}2_1/\text{c}$. In **2**, a pair of unprotonated L^2 molecules coordinate in a meridional fashion with the $\text{Zn}(\text{II})$, resulting in an octahedral complex that is distorted. Chelation takes place *via* two sets of donor atoms (NNS), where each of the ligands binds to the metal center via the N-atoms of the imine and thiazole groups and also the S-atom of thiolate. The tridentate coordination from each ligand forms two interconnected chelate rings with five members, namely, $\text{Zn} - \text{N} - \text{N} - \text{C} - \text{S}$ and $\text{Zn} - \text{N} - \text{C} - \text{C} - \text{N}$. These rings, denoted as $\text{Zn1} - \text{N6} - \text{N7} - \text{C12} - \text{S4}$ and $\text{Zn1} - \text{N5} - \text{C9} - \text{C10} - \text{N6}$, exhibit a nearly planar configuration. In contrast, the other pair of chelate rings, $\text{Zn1} - \text{N2} - \text{N3} - \text{C6} - \text{S2}$ and $\text{Zn1} - \text{N1} - \text{C3} - \text{C4} - \text{N2}$, show significant deviations from planarity, with dihedral angles measuring 7.1 and 2.2 degrees, respectively. Furthermore, it's worth mentioning that the two chelating planes, composed of the N-N-S-Zn atoms, exhibit a nearly perpendicular orientation, with a dihedral angle measuring 89.7° . When we compare **2** to a zinc complex featuring 2-acetylthiazole (N4)-phenylthiosemicarbazone [92], we observe more significant distortion in the latter due to a phenyl group present, which is attached to a N-atom in the terminal position of the thiosemicarbazone ligand. This difference is evident in the reduced dihedral angle between the chelating planes N-N-S-Zn (83.9°) [92], compared to that observed in complex **2** (89.7°).

An important parameter to assess the octahedral strain is the average ΔOh value, representing the average deviation of the 12 angles within the octahedral configuration from the ideal 90 degrees. Complex **2** demonstrates reduced octahedral distortion when compared to the similar zinc complex featuring 2-acetylthiazole (N4)-phenylthiosemicarbazone, with estimated ΔOh measurements of 10 and 12 degrees, respectively. Additionally, average bond lengths between Zn and the ligand atoms ($\text{Zn}-\text{N}_{1,3\text{-thiazole}}$: 2.2525 angstroms; $\text{Zn}-\text{S}_{\text{thiolate}}$: 2.4313 angstroms; $\text{Zn}-\text{N}_{\text{imine}}$: 2.148 angstroms) seen in **2** closely resemble those which can be found in similar structures ($\text{Zn}-\text{N}_{1,3\text{-thiazole}}$: 2.2310 angstroms; $\text{Zn}-\text{S}_{\text{thiolate}}$: 2.4331 angstroms; $\text{Zn}-\text{N}_{\text{imine}}$: 2.1877 angstroms).

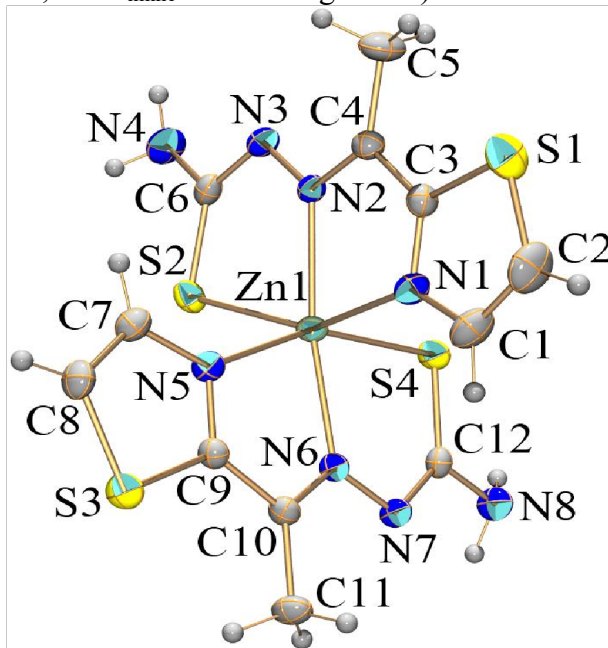


Figure 23: A representation of the molecular structure of $[\text{Zn}(\text{L}^2)_2]$ (complex **2**) depicted using an ORTEP diagram, with thermal ellipsoids drawn to illustrate the molecular arrangement at a 30% probability level

Within crystals of **2**, the molecules exhibit self-assembly, forming layers parallel with (1 0 0) lattice plane. This assembly is facilitated by intermolecular bonds of hydrogen between the NH₂ groups (N4 and N8) in the terminal position, which act as donors of hydrogen bonds, and the sulfur atoms of thiolate moiety S2 at $1 - x, 2 - y, -z$ and S4 at $1 - x, -1/2 + y, -z$, which serve as accepting group (Table 7 and Figure 24a). Moreover, interactions characterized by subtle π -stacking interactions between the 1,3-thiazole rings, which are heteroaromatic, link the complex molecules of adjacent layers, resulting in the formation of a three-dimensional supramolecular structure (Figure 24b and Table 8). Furthermore, molecules of **2** are connected along a specific crystallographic axis through weak C_{aromatic}-H \cdots N_{hydrazone} contacts.

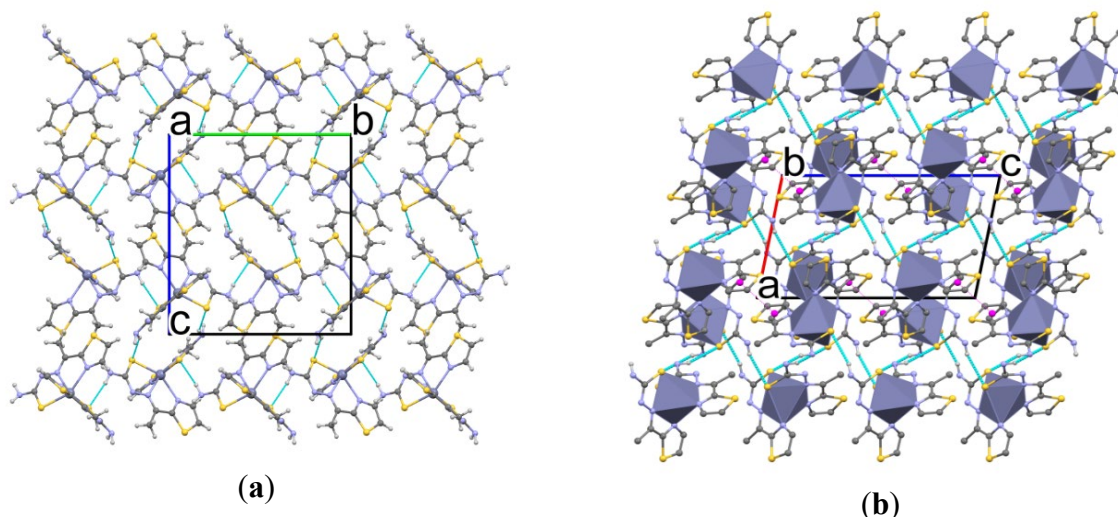


Figure 24a and 24b: (a) An illustration of the crystal packing of **2** demonstrates how molecules are interconnected through N-H \cdots S bonds of hydrogen, indicated by blue dashed lines, forming layers that are parallel to the lattice plane (1 0 0). (b) lateral perspective of the layers reveals $\pi\cdots\pi$ intermolecular interactions that engage the 1,3-thiazole rings. For clarity, H-atoms not participating in H-bonding have been excluded

Table 7: Parameters of hydrogen-bond for **2**

D-H \cdots A	D-H (Å)	H \cdots A (Å)	D \cdots A (Å)	D-H \cdots A (°)	Symmetry operation on A
Intra C11-H11B \cdots S3	0.96	2.76	3.243(3)	111.7	
Intra C5-H5B \cdots S1	0.96	2.68	3.168(4)	112.1	
C8-H8 \cdots N3	0.93	2.73	3.226(3)	114.3	1+x, y, z
N8-H8B \cdots S2	0.87	2.74	3.492(2)	145.7	1-x, 2-y, -z
N4-H4B \cdots S4	0.87	2.74	3.570(3)	159.9	1-x, -1/2+y, 1/2-z

Table 8: Intermolecular $\pi\cdots\pi$ interaction parameters for **2**.

Cg(I) ¹	Cg(J) ¹	Cg(I)–Cg(J) ² (Å)	α^3 (°)	β^4 (°)	γ^5 (°)	Slippage ⁶ (Å)	Sym. code on (J)
Cg(1)	Cg(1)	4.0785(15)	0.02(14)	24.7	24.7	1.703	2-x, 2-y, 1-z

¹ Designation for aromatic rings: (1) = S1, C1–C3, N1.

² Cg(I)–Cg(J) = Gap between centers of the rings (Ang.).

³ α = Dihedral angle measured in degrees between (I) and (J) planes.

⁴ β = Angle measured in degrees between the vector Cg(I)–Cg(J) and the normal to plane (I).

⁵ γ = Angle measured in degrees between the vector Cg(I)–Cg(J) and the normal to plane (J).

⁶ Slippage = Distance between the center of gravity Cg(I) and the perpendicular projection of Cg(J) onto ring I (in angstroms)

4.5 Crystal structure of complexes 5 and 6

Complex **5** exhibits crystallization in the crystal system known as monoclinic, with P21/c space group. Four $[\text{ZnL}^2(\text{N}_3)_2]$ asymmetric units are present in the unit cell of complex **5**. The coordination environment of zinc in **5** exhibits distorted geometry, positioned approximately midpoint between a square pyramid and a trigonal bipyramid, as determined by the calculated τ parameter 0.46. The zinc ion forms coordination bonds with a group of NNS-donor atoms from L^2 , in addition to two N-atoms (N5 and N7 $_i$, where $i = x, 1/2 - y, -1/2 + z$) originating from azide anions related by symmetry. A depiction of the zinc ion's coordination environment is provided in Figure 25. Detailed information regarding bond angles and lengths for complex **5** can be found in Table 9.

In the case of **5**, the azide anions serve as bridging ligands, connecting the Zn(II) ions and forming polymeric zigzag chains that extend parallel to the crystallographic axis c , as shown in figure 26. These zigzag chains further assemble into a three-dimensional network through H-bonds, involving interactions with the NH_2 group in terminal position and N-atoms from thioamide and azide groups, as detailed in Table 10. The tridentate coordination of L^2 results in the creation of two interconnected chelating rings consisting of five members: Zn–N–N–C–S and Zn–N–C–C–N. These chelating rings exhibit an almost planar arrangement, indicated by a dihedral angle of 2.2 degrees. The observed bond lengths for Zn–L in **5** (Zn–N $_{\text{imine}}$ 2.1231 angstrom, Zn–S $_{\text{thiolate}}$ 2.3516 angstrom and Zn–N $_{\text{Ar}}$ 2.1390 angstrom) fall within the reported range of zinc complexes numbering up to five featuring similar tridentate NNS ligands of hydrazone (ranging from 2.125 to 2.227 angstrom, 2.324 to 2.431 angstrom, and 2.03 to 2.156 angstrom, respectively) [93-101]. As for the azide ligands in complex **5**, they adopt a bent coordination mode with N–N–Zn angles of 115.62 and 123.08 degrees.

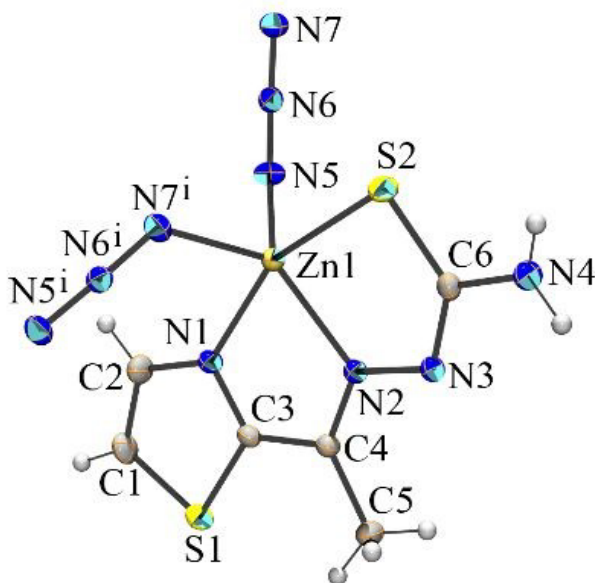


Figure 25: An ORTEP representation displays the structure of **5**. Thermal ellipsoids are depicted at a probability level of 30%

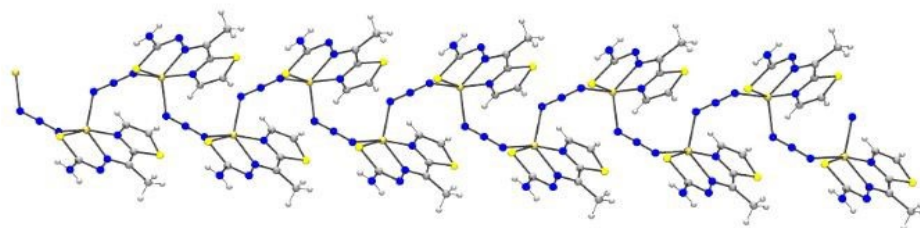


Figure 26: A zigzag polymeric chain is formed through the $\mu_{1,3}$ bridging role played by the azide anions within complex **5**

Complex **6** shares the same P21/c space group as **5**, with its' unit cell consisting of four neutral molecules of $[\text{ZnL}^4(\text{N}_3)_2]$. Bond angles and lengths for **6** is presented in table 9. Figure 27 illustrates the structure of **5** at the molecular level, including the numbering scheme for the atoms. In this complex, zinc showcases penta-coordination through the donor atoms NNO from L^4 , in addition to two N-atoms (N5 and N8) derived from the azide ligands. Calculated $\tau = 0.08$ indicates a slight distortion of the Zn(II) ion's five-coordinate geometry towards a square pyramidal configuration in complex **6**. A 9.2 degrees dihedral angle between the chelating rings consisting of five members (Zn–N–C–C–N and Zn–N–N–C–O) reveals the characteristic of the M-L system as non-coplanar within **6**. The observed bond lengths for Zn–L (Zn–N_{imine} 2.0430 angstrom, Zn–N_{py} 2.1759 angstrom and Zn–O_{enolate} 2.2401 angstrom) in **6** are in line with those reported for zinc complexes with penta-coordination featuring related NNO hydrazone ligands which are tridentate (ranging from 2.044 to 2.088 angstrom, 2.08 to 2.219 angstrom, and 2.079 to 2.21 angstrom, respectively) [101-106]. However, the Zn–O_{enolate} bond in complex **6** appears slightly longer. The bond angles N9–N8–Zn and N6–N5–Zn1, measuring 134.8 and 128.9 degrees, respectively, indicate the bent coordination manner of the azide ligands. Crystal structure of **6**, reveals that the individual $[\text{ZnL}^4(\text{N}_3)_2]$ molecules assemble into a three-dimensional supramolecular structure through weak intermolecular C–H \cdots N and C–H \cdots O bonds of hydrogen, as detailed in Table 11.

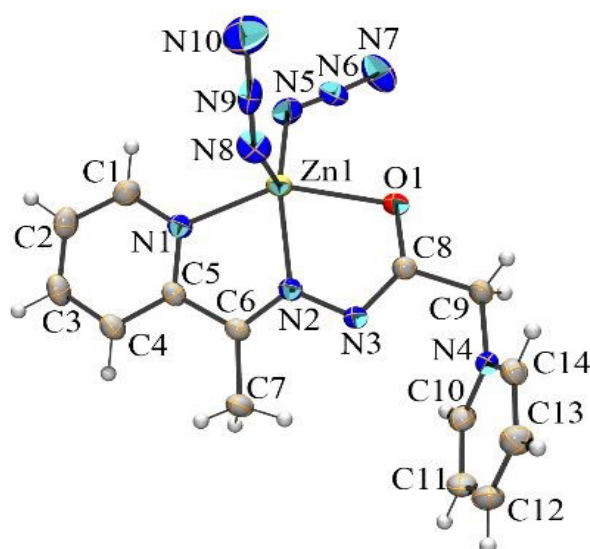


Figure 27: An ORTEP representation illustrates the molecular structure of **6**. Thermal ellipsoids are depicted at the probability level of 30%.

Table 9: Selected bond angles ($^{\circ}$) and lengths (\AA) of complexes **5** and **6**.

5		6	
Bond angles			
N7–N6–N5	178.2	N5–N6–N7	176.5
N6–N7–Zn1 ⁱ	123.08	N9–N8–Zn1	134.8
N6–N5–Zn1	115.62	N6–N5–Zn1	128.9
N7–Zn1–S2 ⁱ	101.34	N8–Zn1–O1	98.46
N2–Zn1–S2	80.82	N2–Zn1–O1	73.94
N1–Zn1–S2	157.65	N1–Zn1–O1	146.89
N7–Zn1–N1 ⁱ	91.80	N8–Zn1–N1	102.44
N2–Zn1–N1	76.83	N2–Zn1–N1	75.55
N5–Zn1–S2	99.27	N5–Zn1–O1	97.96
N5–Zn1–N7 ⁱ	102.90	N5–Zn1–N8	110.75
N5–Zn1–N2	129.83	N5–Zn1–N2	142.25
N7–Zn1–N2 ⁱ	126.50	N8–Zn1–N2	106.92

N5–Zn1–N1	95.26	N5–Zn1–N1	98.26
		N8–N9–N10	177.0
Bond lengths			
N2–C4	1.290	N2–C6	1.289
N2–N3	1.369	N2–N3	1.377
N3–C6	1.327	N3–C8	1.321
S2–C6	1.736	O1–C8	1.263
N5–N6	1.178	N5–N6	1.109
N6–N7	1.167	N6–N7	1.178
		N8–N9	1.015
		N9–N10	1.216
Zn1–N5	2.085	Zn1–N5	1.982
Zn1–N7	2.097	Zn1–N8	2.039
Zn1–N2	2.1231	Zn1–N2	2.0430
Zn1–N1	2.1390	Zn1–N1	2.175
Zn1–S2	2.3516	Zn1–O1	2.2401

Symmetry codes: $i = x, 1/2 - y, -1/2 + z$.

Table 10: Parameters describing hydrogen bonding in the complex **5**

D–H...A	D–H (Å)	H...A (Å)	D...A (Å)	D–H...A (°)	Symm. operation on A
Intra C5–H5B...S1	0.96	2.67	3.212(2)	116	
N4–H4NB...N3	0.86(3)	2.34(3)	3.183(3)	169(2)	1–x, 1–y, –z
N4–H4NA...N5	0.85(2)	2.46(2)	3.232(3)	151(2)	1+x, y, z

Table 11: Parameters describing hydrogen bonding in the complex **6**

D–H...A	D–H (Å)	H...A (Å)	D...A (Å)	D–H...A (°)	Symm. operation on A
Intra C7–H7A...N3	0.96	2.37	2.791(3)	106	
C14–H14...O1	0.93	2.58	3.438(3)	154	–x, 1–y, –z
C10–H10...N7	0.93	2.62	3.303(4)	130	x, 1/2–y, –1/2+z
C9–H9A...N10	0.97	2.56	3.496(4)	163	x, –1+y, z
C1–H1...N7	0.93	2.62	3.308(4)	131	1–x, 1/2+y, 1/2–z

A geometric analysis of zinc complexes with a five-coordinate arrangement featuring tridentate NNO and/or NNS ligands of hydrazone was conducted by searching the CSD and incorporating X-ray data from complexes **5** and **6** presented in this study. This search in the CSD database resulted in thirty structures of zinc complexes featuring NNS ligands and fifty structures with NNO ligands. In all cases, these complexes exhibit a five-coordinate geometry, with the remaining two coordination sites being occupied by monodentate ligands. From the calculated τ values for all these complexes, it can be inferred that the geometries of five-coordinate zinc complexes with NNS hydrazone ligands vary, encompassing a spectrum of shapes from near-square pyramidal to somewhat distorted trigonal bipyramidal configurations. On the other hand, those with NNO hydrazone ligands display variations ranging from perfect square pyramidal to highly distorted square pyramidal forms.

4.6 Assessment of the catalytic activity of complex **1-3** in the coupling reaction of KA^2

In the catalytic study of the complexes **1-3**, pyrrolidine, cyclohexanone and phenylacetylene were selected as a set of substrates to study. In the experiment, it was found that using 10 mol% of complex **1** as a catalyst in toluene resulted in 85% isolated yield of the product after 16 hrs (Table 12, Entry no. 1). As anticipated, in the control experiment where HL^1Cl was utilized as a catalyst, the

propargylamine desired was not formed. Under the same reaction conditions, complex **3** gave a 67% yield, while complex **2** showed average catalytic activity (Table 12, Entries no. 3 and 5). This suggests that the zinc center in complex **2** is not fully coordinated under the reaction conditions. When we reduced the catalyst loading and temperature while removing the solvent, we obtained moderate yields for both complex **1** and complex **3** (Table 12, Entries 6-8). When we elevated the temperature while incorporating MgSO₄ as a water-scavenging additive, we attained the maximum yield when employing complex **1** at a loading of 5 mol% (Table 12, Entry no. 9). Under these conditions, complex **3** also yielded results of moderate proportions. However, when the reaction was allowed to proceed for only 3 hours, incomplete conversion and a reduced yield were observed (Table 12, Entries no. 10 and 11, respectively), indicating optimal conditions for Entry 9. It's important to highlight that complex **1** exhibits a comparable performance in this reaction when assessing the reactivity of basic zinc salts. However, the conditions detailed in this research necessitate a lower catalyst loading than zinc acetate. Zinc acetate requires a 10 mol% loading under dry and inert conditions to achieve yields exceeding 90%.

We investigated various substrate combinations using conditions mentioned earlier, as depicted in Scheme 18. **IVb** was obtained for piperidine in high yield consistent with results obtained in both the ligand-free system based on zinc and a more recent manganese-based system reported in the literature [35, 41]. Propargylamine **IVc** was achieved with a moderate yield, and the combination of pyrrolidine and a linear ketone resulted in **IVd** with 72% yield. **IVe**, featuring an ester group for potential further modification, was successfully synthesized with a good yield. The synthesis of the **IVf** which is derived from primary amine, was successful but yielded moderately due to the intermediate imine's stability. Introducing increased steric hindrance in the linear ketone resulted in a substantial reduction in the yield, underscoring the pivotal role of steric hindrance in this reaction (as seen in **IVg**).

When we combined a particular aliphatic alkyne with N-phenylpiperazine, we achieved a 37% isolated yield of propargylamine **IVh**. To evaluate the impact of using a less functionalized aliphatic alkyne, we employed 1-octyne, resulting in a 70% yield of compound **IVi**. Lastly, we opted for cyclopentanone as a coupling partner, and as expected from reactivity trends, we obtained compound **IVj** with a moderate yield [35, 41].

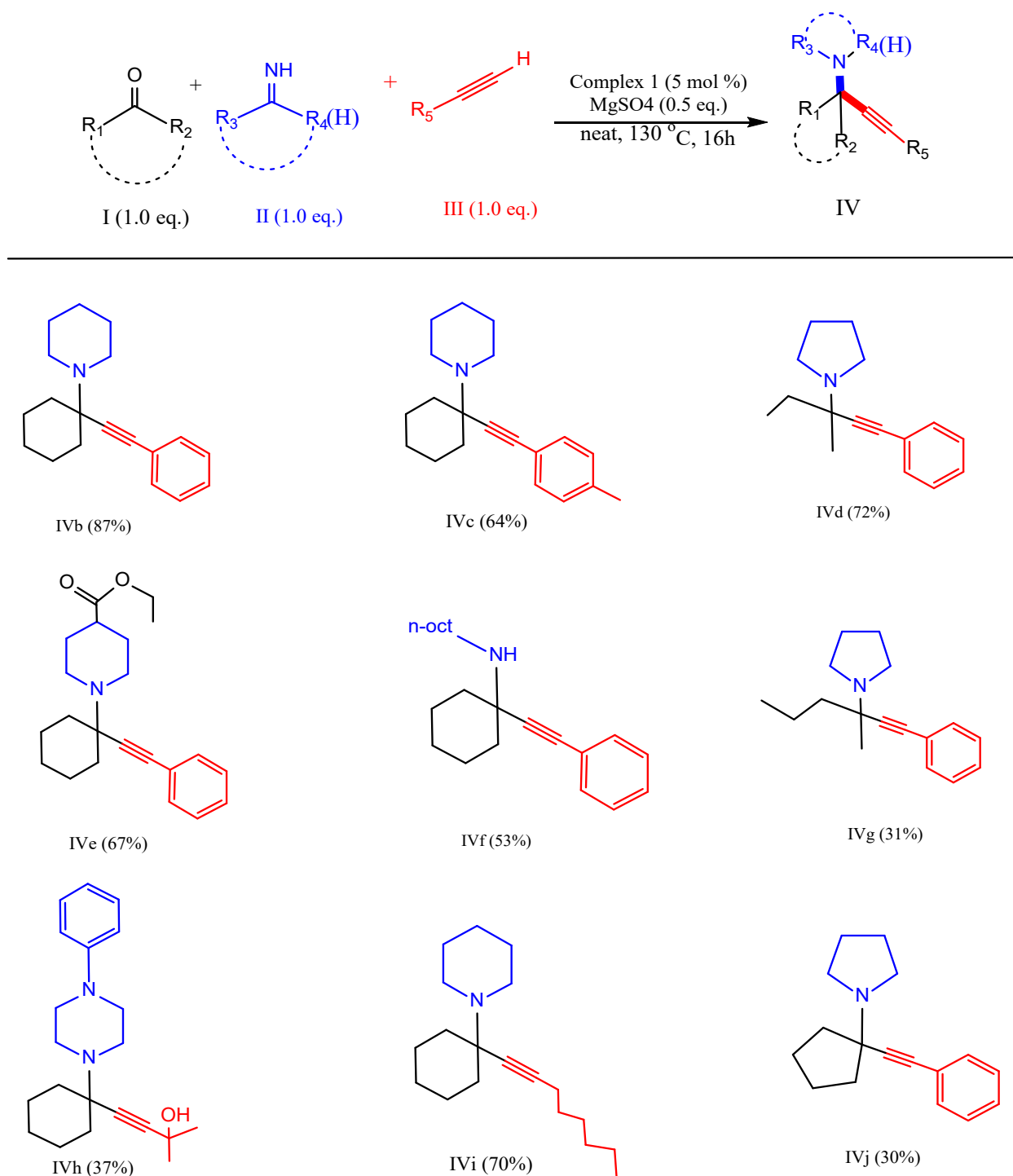
In summary, **1** permits a lower catalyst loading than straightforward zinc salts and exhibits enhanced resilience under challenging ambient conditions [35]. Nevertheless, it's important to note that the limitations and substrate scope trends observed in this coupling reaction still hold for complex **1**.

Table 12: Enhancement of the reaction conditions for **1-3**.

Entry	Catalyst	Temp.(°C)	Mol%	Solvent	Additive (0.5 eq.)	% Isolated Yield ¹
1	1	120	10	toluene (1 M)	-	85
2	HL¹Cl	120	10	toluene (1 M)	-	0
3	3	120	10	toluene (1 M)	-	67
4	HL³Cl	120	10	toluene (1 M)	-	0
5	2	120	10	toluene (1 M)	-	56
6	1	110	5	neat	-	51
7	1	110	10	neat	-	65
8	3	110	10	neat	-	57
9	1	130	5	neat	MgSO ₄	91
10	3	130	5	neat	MgSO ₄	61
11 ²	1	130	5	neat	MgSO ₄	33

All reactions were performed on a scale of 0.5 mmol, and the typical reaction duration was 16 hours unless otherwise stated. The progression of the reaction was monitored using GC/MS analysis, with n-octane utilized as an internal reference. The reported isolated yields denote the purified end product

obtained after chromatographic purification. In certain instances, the reaction was concluded after a 3-hour duration.



Scheme 18: The range of substrates investigated in the reaction system under the ideal conditions (pertaining to complex 1). All experiments were conducted using a 0.5 mmol scale, and the yields reported are those obtained after column chromatography (indicated in parentheses)

4.6.1 Computational results for complexes 1–3

DFT computations were performed to determine the geometries of 1-3 in the ground state. The calculations confirmed the experimental XRD results, Table 13. For **1** and **3**, the DFT calculations predicted five-fold coordination, with the tridentate ligands **HL**¹Cl and **HL**³Cl and a pair of N-atoms

from the thiocyanate ligands coordinating the Zn(II) ion. This corroborates the experimental results obtained from X-ray diffraction (XRD), reinforcing the observed structures in Figure 28.

According to the DFT findings, **2** demonstrated an octahedral geometry wherein the Zn(II) was coordinated to two molecules of the tridentate L^2 ligand *via* the N-atoms of thiazole, immine, as well as S-atoms of thiolate. This arrangement resulted in the creation of a complex with octahedral geometry containing four interconnected chelating rings with five members, consistent with data obtained from the experimental. Key bond lengths and valence angle values are outlined in Table 13 for reference.

Table 13: Average values of selected bond lengths (in Ångstroms) and angles, as calculated using DFT and compared to experimental data and angles ($^{\circ}$) for $[ZnL^1(NCS)_2]$ (complex **1**), $[Zn(L^2)_2]$ (complex **2**) and $[ZnL^3(NCS)_2]$ (complex **3**).

Compound	1		2		3	
	exp	DFT	exp	DFT	exp	DFT
Distances, Å						
Zn1–N6/Zn1–N6/Zn1–N6	1.955	1.953	2.149	2.159	1.965	1.962
Zn1–N5/Zn1–N5/Zn1–N5	1.959	1.912	2.186	2.207	1.965	1.924
Zn1–N2/Zn1–N2/Zn–N2	2.058	2.139	2.147	2.159	2.088	2.125
Zn1–O1/Zn1–N1/Zn1–O1	2.178	1.255	2.318	1.206	2.206	1.244
Zn1–N1/Zn1–S2/Zn1–N1	2.212	2.247	2.452	2.598	2.146	1.201
O1–C6 /Zn1–S4/N3–C8	1.265	1.288	2.411	2.596	1.322	1.339
Angles, $^{\circ}$						
N6–Zn1–N1/N1–Zn1–N5/ N1–Zn1–N	101.9	104.5	84.5	88.8	74.1	74.5
N5–Zn1–N1/N2–Zn1–N5/ N1–Zn1–N	97.9	95.2	103.1	105.2	100.5	106.2
N5–Zn1–N2/N6–Zn1–N5/ N1–Zn1–N	127.4	129.1	75.3	76.2	96.5	95.7
N6–Zn1–O1/N2–Zn1–N1/ N1–Zn1–O	96.9	91.6	73.6	76.2	147.9	145.7
N5–Zn1–O1/N2–Zn1–S4/ N2–Zn1–O	97.8	98.0	101.2	100.3	74.0	73.0

Table 13 shows a strong correlation between the calculated geometric parameters, including bond lengths and valence angles, and the XRD structures, demonstrating excellent agreement between the calculated and experimental values.

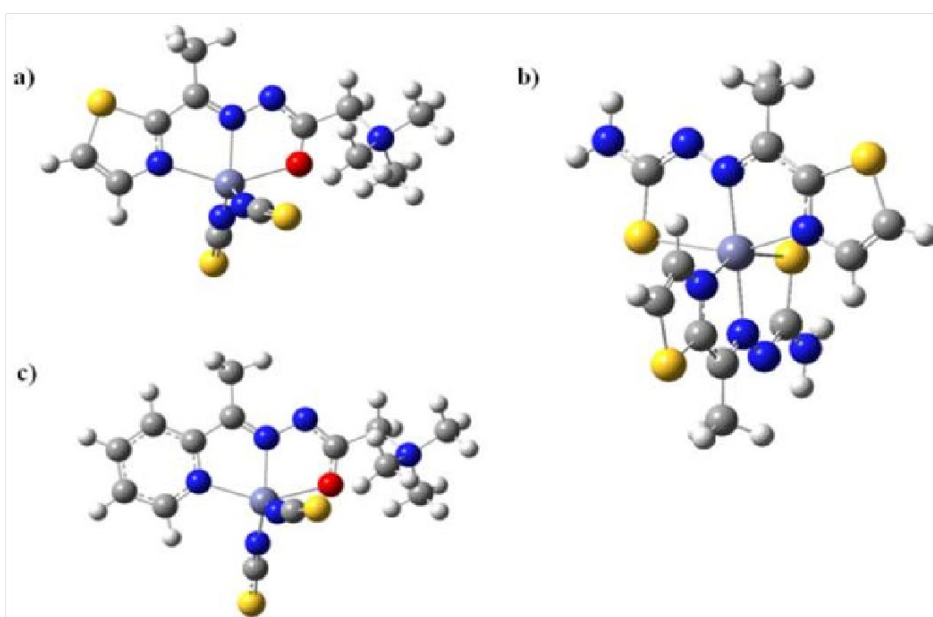


Figure 28: Geometries optimized using DFT for: (a) $[ZnL^1(NCS)_2]$ (complex **1**); (b) $[Zn(L^2)_2]$ (complex **2**); and (c) $[ZnL^3(NCS)_2]$ (complex **3**).

The HOMO-LUMO energies of these complexes offer essential insights into their energetic characteristics and stability. The difference in energy between the HOMO and LUMO levels serves as a determinant of the molecules' reactivity and kinetic stability [107-109].

E_{HOMO} and E_{LUMO} represent the energies of the HOMO and LUMO, respectively. The negative value of the chemical potential indicates the stability of the complex, indicating that it does not undergo spontaneous decomposition into its constituent elements. Hardness is a measure of the molecule's ability to resist changes in its electron distribution.

The HOMO-LUMO energies were calculated using time-dependent density functional theory (TD-DFT) at the B3LYP/6-31G level of theory in both vacuum and toluene. This functional is known for its accuracy and reasonable computational cost in reactivity studies [110]. Calculations were also performed using the B3LYP functional with a more extensive basis set, 6-311G(d,p), to examine the basis set dependence. Results are presented in Table 14. The differences in HOMO and LUMO energies between the two basis sets ranged from 0.07 to 0.22 eV. HOMO-LUMO gaps tend to exhibit low sensitivity to changes in the basis set [110].

Table 14: The E_{HOMO} (Energy of the Highest Occupied Molecular Orbital), E_{LUMO} (Energy of the Lowest Unoccupied Molecular Orbital), and the energy gaps between them, calculated using TD-DFT (Time-Dependent Density Functional Theory) in a vacuum at various levels of theory.

		[ZnL ¹ (NCS) ₂] (1)	[Zn(L ²) ₂] (2)	[ZnL ³ (NCS) ₂] (3)
B3LYP/6-31G	ΔE_{gap} (eV)	2.167	2.913	2.465
	E_{LUMO} (eV)	-2.803	-2.141	-2.438
	E_{HOMO} (eV)	-4.970	-5.054	-4.903
B3LYP/6-311G(d,p)	ΔE_{gap} (eV)	2.289	2.939	2.537
	E_{LUMO} (eV)	-2.874	-2.306	-2.587
	E_{HOMO} (eV)	-5.163	-5.245	-5.124
BVP86/6-311G(d,p)	ΔE_{gap} (eV)	0.908	1.760	1.077
	E_{LUMO} (eV)	-3.509	-2.871	-3.294
	E_{HOMO} (eV)	-4.417	-4.630	-4.371

The HOMO and LUMO orbitals and their corresponding energies were estimated to identify high and low regions of density in the complexes, as depicted in Figure 29. In complex **1** and **3**, the HOMOs are predominantly distributed over the linear NCS⁻ monodentate ligands and metal centers, while the LUMOs are spread across the Schiff base planar ring located in the equatorial plane. In **2**, the HOMOs are primarily distributed across the heterocyclic rings (with five members) containing NH₂ groups in terminal position, whereas the LUMOs are dispersed within the heterocyclic chelating rings containing five members of the two tridentate ligands.

Reactivity descriptors of the complexes, (Eqs 1-5, Section 3.6.3) such as hardness, chemical potential, electronegativity, softness, and electrophilicity index, were calculated and are presented in Table 15. The negative chemical potential values (-3.89, -3.60, and -3.67 eV) signify the stability of the complexes, suggesting their resistance to spontaneous decomposition. Among the three complexes, complex **1** has the smallest energy gap, with ΔE_{gap} measuring 2.17 eV in a vacuum and 2.98 eV in toluene, rendering it the most malleable molecule, or "softest." Chemical hardness, determined by the HOMO-LUMO energy gap, is 1.08 eV for **1**, 1.46 eV for **2**, and 1.232 eV for **3** (Table 15). **1** exhibits the lowest chemical hardness and the highest softness, indicating higher reactivity in accordance with the experimental catalytic data (previous Section). Complex **1** also has the lowest LUMO energy, signifying its capacity as a highly efficient electron acceptor. Additionally, the values for the electrophilicity index provided in Table 15 for complexes **1-3** (6.97, 4.44, and 5.47 eV, respectively) indicate that **1** rank as the most potent electrophile among all the compounds. Its elevated electronegativity value accounts for its superior catalytic activity compared to the other examined

complexes [35]. The GGA-type functional, BVP86/6-311G(d,p), yielded the lowest HOMO-LUMO energy gap for complex **1**, in agreement with the results obtained with the hybrid B3LYP functional, Table 15.

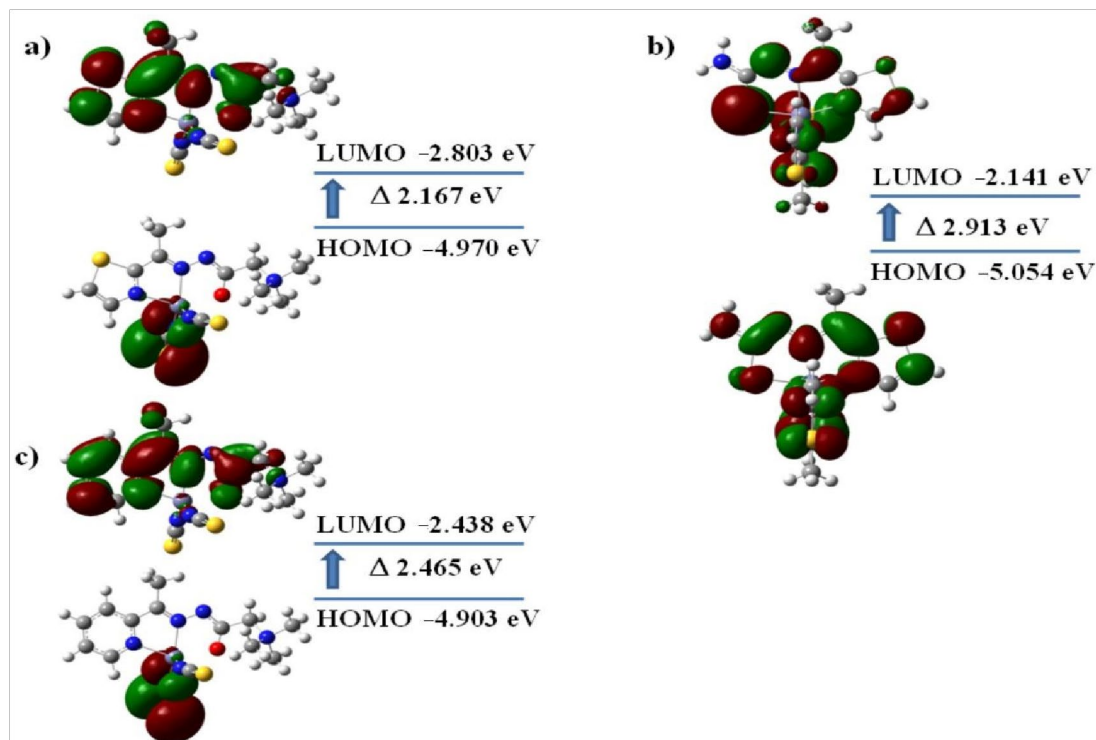


Figure 29: Molecular orbital diagrams and energy levels for the Highest Occupied Molecular Orbital (HOMO), the Lowest Unoccupied Molecular Orbital (LUMO), and the transitions between HOMO and LUMO for: (a) $[\text{ZnL}^1(\text{NCS})_2]$ (complex **1**); (b) $[\text{Zn}(\text{L}^2)_2]$ (complex **2**); and (c) $[\text{ZnL}^3(\text{NCS})_2]$ (complex **3**).

Table 15: Quantum chemical descriptors for complexes in vacuum and toluene (in brackets) calculated at B3LYP/6-31G level of theory.

	$[\text{ZnL}^1(\text{NCS})_2]$ (1)	$[\text{Zn}(\text{L}^2)_2]$ (2)	$[\text{ZnL}^3(\text{NCS})_2]$ (3)
ΔE_{gap} (eV)	2.167 (2.977)	2.913 (3.016)	2.465 (3.315)
E_{LUMO} (eV)	-2.803 (-2.695)	-2.141 (-2.252)	-2.438 (-2.330)
E_{HOMO} (eV)	-4.970 (-5.692)	-5.054 (-5.268)	-4.903 (-5.645)
η (eV)	2.166 (2.976)	2.912 (3.016)	2.464 (3.314)
μ (eV)	-3.886 (-4.193)	-3.597 (-3.76)	-3.670 (-3.987)
χ (eV)	3.886 (4.193)	3.597 (3.760)	3.670 (3.987)
S (eV)	0.461 (0.336)	0.343 (0.331)	0.405 (0.301)
ω (eV)	6.971 (5.908)	4.443 (4.687)	5.466 (4.797)

4.7 Assessment of the catalytic activity of complex **4-9** in the coupling reaction of KA^2

To examine the catalytic activity of **4-9** in the KA^2 reaction, cyclohexanone, piperidine, and phenylacetylene were selected as model substrates [38]. In the initial experiments, employing complex **4** in 5 mol% as the catalyst along with MgSO_4 as a desiccant, we achieved a successful reaction, yielding the desired propargylamine at an isolated yield of 80% (Table 16, Entry 1). Elevating the catalyst concentration to 10 mol% led to a decrease in the yield isolated (Table 16, Entry no. 2). Conducting the reaction under conditions of open-air still afforded a 70% yield of the

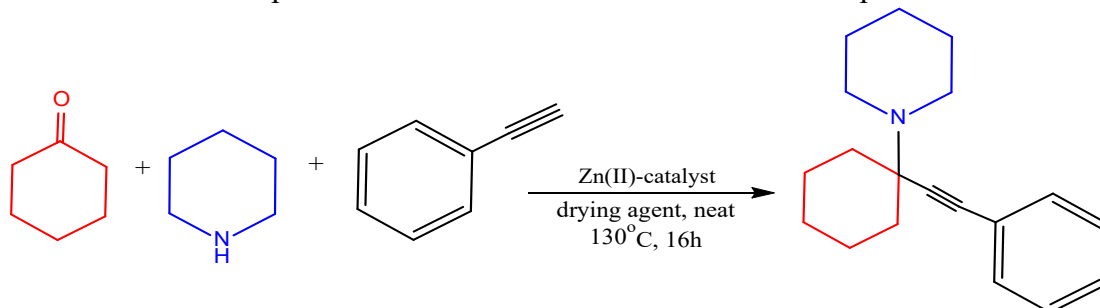
propargylamine (Table 16, Entry 3). Adding titanium ethoxide (0.5 equivalent) as a supplement, together with a catalyst concentration of 5 mol%, improved the yield to 86% (Table 16, Entry no. 4). However, augmenting the titanium ethoxide concentration to the equivalent of one adversely affected the reaction's outcome (Table 16, Entry 5).

We proceeded to assess the catalytic efficacy of **5-9** using refined conditions established for complex **4**, which involved a 5 mol% catalyst loading and the addition of Ti(OEt)₄ (0.5 equivalent). **6** displayed the greatest reactivity of all tested complexes, yielding the targeted propargylamine in a 92% isolated yield (Table 16, Entry no. 7). **5** and **9** provided the product **63** and 66% yield, respectively (Entry no. 6 and no. 11, Table 16), while **7** and **8** exhibited much lesser catalytic performance, with 56% and 54% yield isolated respectively (Table 16, Entry no. 9 and no. 10). To confirm that the ligand's attachment to the zinc is responsible for the improved catalytic performance seen in **6**, we performed a reaction utilizing zinc acetate (5 mol%) as the catalyst [35, 41]. This yielded a reduced output of 30%, as determined through GC-MS analysis. When the HL⁴Cl ligand was applied independently without a zinc source, we detected only minimal amounts of the propargylamine product (Entry 8, Table 16). This suggests a reaction with a very low yield attributed to the elevated temperature. In a control experiment conducted without complex **6** (Entry 12, Table 16), we recovered the initial reactants.

Then, we examined the reactivity of various substrates under optimized conditions, using a range of 2° aliphatic ketones, amines and alkynes (Scheme 19). This resulted in producing propargylamines with yields that varied from moderate to highly satisfactory. In contrast to piperidine, morpholine displayed diminished reactivity, yielding compound **Vb** with an isolated yield of 67%, which aligns with the performance of the ligand-free KA² system relying on zinc [38]. Primary amines, namely 1-octylamine and di-n-propylamine, yielded products **Vc** and **Vd**, respectively, with yields of 42% and 40%. The comparatively reduced yield of **Vc** can be ascribed to the heightened stability of the imine intermediate that is generated. In **Vd**, the generation of a byproduct of allene was also noted.

Products **Ve** and **Vf** were obtained in moderate yields when p-tolyl-acetylene and p-chloro-phenylacetylene were reacted with pyrrolidine and cyclohexanone, respectively. This is significant because p-tolyl-acetylene features an electron donor group in the para position. The reaction between cyclohexanone and p-methoxy-phenylacetylene with piperidine resulted in a 96% yield of compound **Vg**. This outcome was expected as the para-substituted alkyne carries a strongly electron-donating group, facilitating effective nucleophilic attack by the zinc acetylide on the ketiminium cation. Moderate yields of compound **Vh** were obtained when 1-octyne was used as the substrate. In terms of ketone reactivity, the combination of 3-pentanone, pyrrolidine and phenylacetylene yielded compound **Vi** with a yield of 75%. All in all, **6** exhibited commendable catalytic capability in KA² reaction, especially when considering the current advancements in the field.

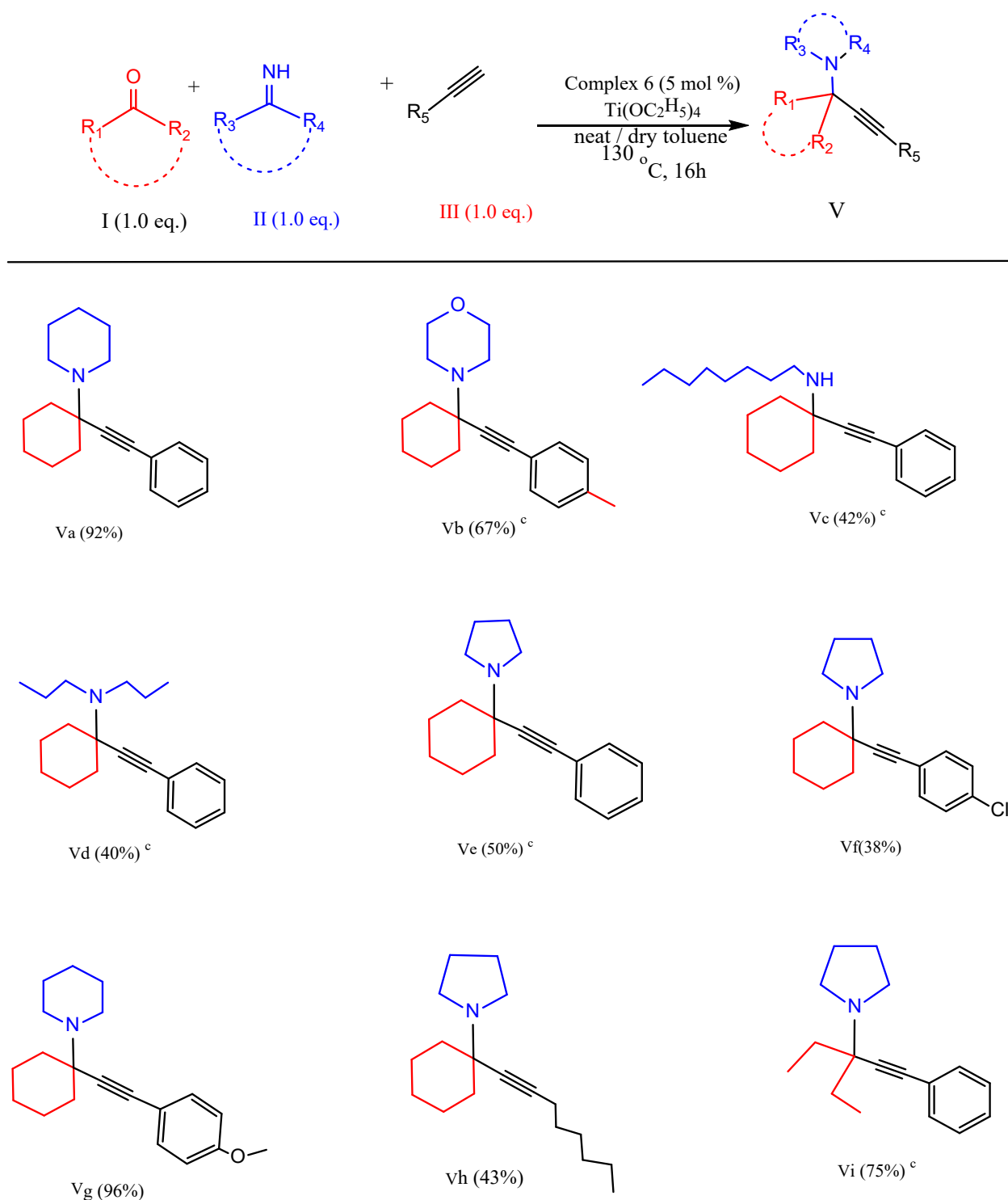
Table 16: Optimization of the reaction conditions for complexes 4-9.



Entry	Catalyst	Additives (0.5 eq)	Loading mol%	% Isolated Yield
1	4	MgSO ₄	5	80
2	4	MgSO ₄	10	62
3	4	MgSO ₄	5	70 ^l

4	4	Ti(OC ₂ H ₅) ₄	5	86
5	4	Ti(OC ₂ H ₅) ₄	5	82 ²
6	5	Ti(OC ₂ H ₅) ₄	5	63
7	6	Ti(OC₂H₅)₄	5	92
8	HL ⁴	Ti(OC ₂ H ₅) ₄	5	Traces ³
9	7	Ti(OC ₂ H ₅) ₄	5	56
10	8	Ti(OC ₂ H ₅) ₄	5	54
11	9	Ti(OC ₂ H ₅) ₄	5	66
12	Zn(OAc) ₂	Ti(OC ₂ H ₅) ₄	5	30 ³
13	-	Ti(OC ₂ H ₅) ₄	-	No reaction

All experiments were conducted within a flame-dried Schlenk apparatus under inert conditions, utilizing a 0.5 mmol scale. The drying reagent was introduced at a 0.5 equivalent (0.25 mmol) scale, unless specified otherwise. ¹The reaction took place under ambient atmospheric conditions. ²One equivalent (0.5 mmol) of Titanium(IV) ethoxide was used. ³Detection was accomplished through GC-MS analysis.



Scheme 19: Substrate scope of the reaction system under the optimal conditions (with respect to complex 6). Isolated yields are shown in parenthesis. ^bReaction conditions: catalyst (5 mol%), 0.5 mmol ketone, 0.5 mmol alkyne, 0.5 mmol amine, 0.25 mmol additive, neat (130 °C, 16 h). ^cIncorporation of 200 μ L of anhydrous toluene

4.7.1 Computational results for complexes 4–9

DFT computations were carried out to explore the electronic structure of **4–9** and establish relationships between their structural characteristics and reactivity. The XRD structures of the complexes served as the basis, and the calculations were performed at the CAM-B3LYP/TZP theoretical level.

Figure 30 displays the surfaces depicting the electrostatic potential for the complexes. These surfaces are represented using a "divergent colormap," where blue and red regions indicate areas charged positively and negatively, respectively. These visualizations offer valuable insights into the distribution of charges within the complexes. Across all complexes, we consistently observe negatively charged regions clustering around the anionic monodentate ligands. In **4**, and **6-9**, regions charged positively are predominantly located within the quaternary ammonium group.

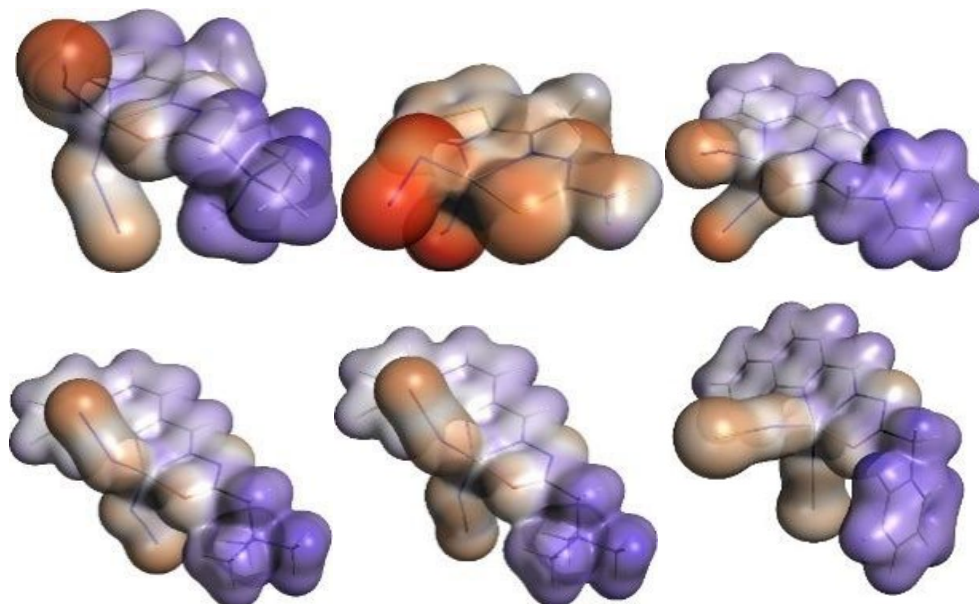


Figure 30: Electrostatic potential surfaces (at 0.01 au) of **4-9** respectively. A color map ranging from -0.20 (indicated in red) to +0.21 (represented in blue) atomic units (a.u.) is employed

Figure 31 presents the frontier HOMO and LUMO molecular orbitals of the examined complexes. HOMOs are predominantly situated on the monodentate anionic ligands, with a minor degree of delocalization towards the center metal. In **5**, the HOMO is distributed across both azide ligands. However, in complexes **4** and **6**, the HOMO is concentrated on a single azide ligand.

In the case of complexes **7**, **8**, and **9**, the HOMO exhibits delocalization within the two monodentate ligands, albeit in an asymmetric manner. Conversely, the LUMOs of complex **6** and **9** are primarily concentrated on the cationic pyridinium segment of the chelating ligands. In the remaining complexes, the LUMOs display delocalization across the tridentate ligands.

Table 17: Table providing the conceptual DFT reactivity descriptors, expressed in atomic units (a.u.), for complexes **4-9**. These descriptors were computed based on XRD geometries employing the theoretical level CAM-B3LYP/TZP. The calculations were executed utilizing both FDL and the FMO methods.

	4	5	6	7	8	9	
FDL	η	0.163	0.208	0.137	0.204	0.252	0.181
	μ	-0.13	-0.044	-0.156	-0.152	-0.166	-0.165
	S	6.137	4.801	7.311	4.898	3.971	5.531
	ω	0.052	0.005	0.089	0.056	0.055	0.075
FMO	η	0.122	0.173	0.090	0.169	0.218	0.137
	μ	-0.129	-0.044	-0.157	-0.151	-0.167	-0.168
	S	8.165	5.777	11.074	5.926	4.579	7.305
	ω	0.067	0.006	0.137	0.068	0.064	0.103

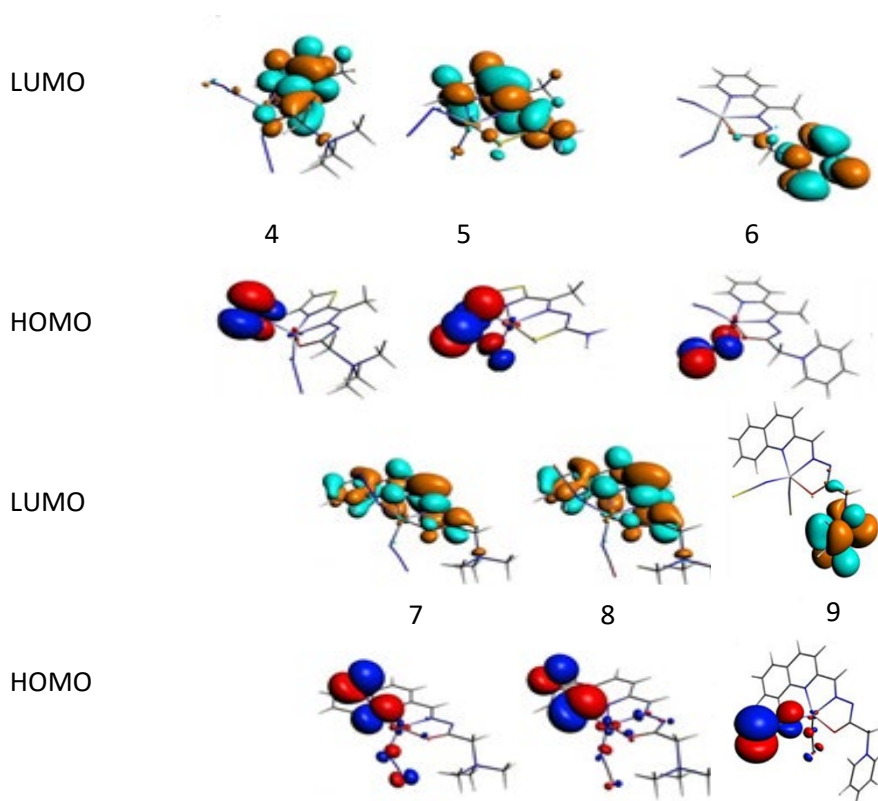


Figure 31: Frontier orbitals (HOMO, LUMO) of Zn(II) complexes **4–9** (isosurfaces 0.03 a.u.).

Table 17 showcases the conceptual DFT reactivity descriptors of complexes **4–9**, calculated using the FDL and FMO methodologies at the theoretical level CAM-B3LYP/TZP. Complex **6** stands out with the highest molecular softness, signifying its status as the most reactive among the examined complexes. Consequently, it boasts the lowest molecular hardness as per Equation 3, section 3.6.3. Remarkably, complex **6** also exhibits the highest catalytic performance, as evident in Table 17. Conversely, complex **8** is identified as the least reactive molecule among those investigated and demonstrates the least efficient catalytic performance. The molecular softness is the primary factor influencing the reactivity and catalytic activity of the complexes. A linear correlation becomes apparent when comparing the softness values (Table 17) to the catalytic performance, quantified by the % yield of isolation for the wanted propargylamine (Table 17). This relationship is graphically depicted in Figure 32, showing a strong correlation with an R-squared value of 0.8900. Hence, complexes with higher molecular softness tend to exhibit more significant catalytic efficiency.

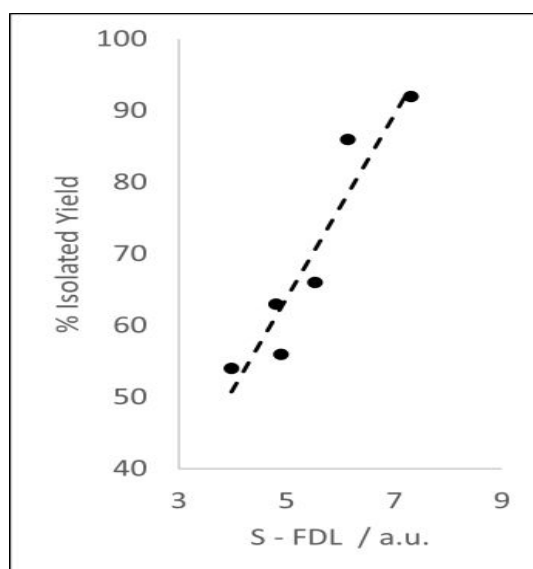


Figure 32: Linear correlation between the percentage yield of isolation for the propargylamine and the molecular softness(S) calculated using the FDL approach at theoretical level CAM-B3LYP/TZP.

Although the descriptor values obtained through the FDL and FMO approaches may vary, it's essential to emphasize that the trends they unveil remain consistent. This consistency holds significant value as it establishes a straight connection between both sets of data. This relationship is exemplified in Figure 33 for the descriptors μ , S , and ω , which exhibit high R-squared values of 0.9991, 0.9878, and 0.9630, respectively. The simpler FMO approximation is commonly favored due to its capacity to capture the essential trends and provide a dependable estimation of the reactivity descriptors.

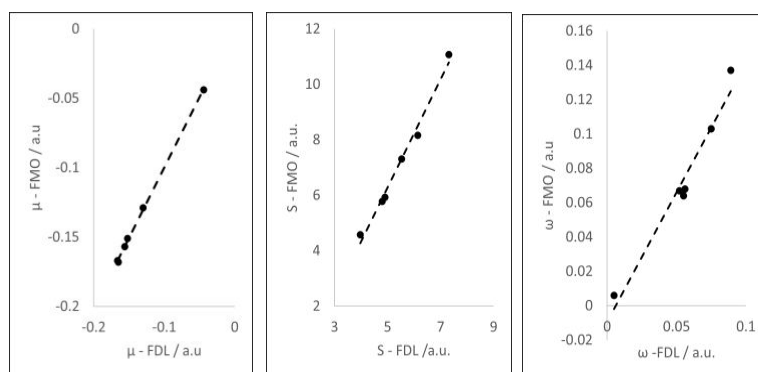


Figure 33: Linear relationship between a) electron chemical potential (μ) b) molecular softness (S), c) electrophilic index (ω), using FDL and FMO methods.

5. Conclusions

Four novel complexes were synthesized and characterized through FT-IR and NMR spectroscopy methods, as well as single-crystal XRD. Complex **1**, was obtained by reacting zinc acetate and HL¹Cl, in the presence of NH₄SCN. Complex **2**, was synthesized by reacting Zn(BF₄)₂·6H₂O with HL². Complex **5**, on the other hand, was formed through the reaction of Zn(BF₄)₂·6H₂O with HL², with NaN₃, in a. Furthermore, complex **6**, was synthesized by reacting Zn(BF₄)₂·6H₂O with HL⁴Cl, in the presence of NaN₃.

The structural analysis unveiled distinct geometries for each of the complexes. In complex **1**, the zinc ion exhibited a distorted square pyramidal geometry coordinated with a tridentate ligand L¹ and a pair of thiocyanate anions. Complex **2** featured a hexacoordinated Zn(II) ion, forming a distorted octahedral structure with two L² molecules. Complex **5** displayed a geometry that fell between a square pyramid and a trigonal bipyramid, with azide anions bridging Zn(II) ions in a $\mu_{1,3}$ fashion, resulting in the formation of polymeric chains, which are zigzag. In **6**, the zinc ion adopted a square pyramidal distorted geometry. Furthermore, through experimental and theoretical investigations, the study comprehensively explored five previously synthesized Zn(II) complexes, namely, 3, 4, 7, 8, and 9.

The catalytic capabilities of complexes **1-3** were accessed in the KA² reaction, in which complex **1** showed the highest catalytic activity with 91% isolated yield. In the evaluation of the catalytic capabilities of complexes **4-9**, complex **6** showed the highest catalytic capability with 92% isolated yield.

The observed catalytic activity trends align perfectly with the conclusions drawn from the DFT calculations. Notably, complexes with the highest softness and the lowest hardness are those with the highest catalytic activity. This correlation between theoretical and experimental findings is underscored by the relationship observed between the isolated yield of the desired propargylamine product and the calculated molecular softness for complexes **4-9**.

References

1. Singh, R. B.; Jain, P.; Singh, R. P. Hydrazones as analytical reagents: a review. *Talanta* **1982**, 29(2), 77-84. [https://doi.org/10.1016/0039-9140\(82\)80024-6](https://doi.org/10.1016/0039-9140(82)80024-6).
2. Romanović, Č. M.; Milenković, R. M.; Pevec, A.; Turel, I.; Spasojević, V.; Grubišič, S.; Radanović, D.; Anđelković, K.; Čobeljić, B. Crystal structures, magnetic properties and DFT study of cobalt(II) azido complexes with the condensation product of 2-quinolinecarboxaldehyde and Girard's T reagent. *Polyhedron* **2018**, 139, 142-147, <https://doi.org/10.1016/j.poly.2017.10.018>.
3. Romanović, Č. M.; Čobeljić, R. B.; Pevec, A.; Turel, I.; Spasojević, V.; Tsaturyan, A. A.; Shcherbakov, I. N.; Anđelković, K. K.; Milenković, M.; Radanović, D.; Milenković, M. R. Synthesis, crystal structure, magnetic properties and DFT study of dinuclear Ni(II) complex with the condensation product of 2-quinolinecarboxaldehyde and Girard's T reagent. *Polyhedron* **2017**, 128, 30-37, <https://doi.org/10.1016/j.poly.2017.02.039>.
4. Greenaway, A. M.; O'Connor, C. J.; Schrock, A.; Sinn, E. High-and low-spin interconversion in a series of (. alpha.-picolylamine) iron (II) complexes. *Inorganic Chemistry* **1979**, 18, 2692-2695, <https://doi.org/10.1021/ic50200a011>.
5. Koner, S.; Saha, S.; Mallah, T.; Okamoto, K. I. Unprecedented Low Cu-N(azide)-Cu Angles in End-On Double Azido Bridged Copper(II) Complex. *Inorganic Chemistry* **2004**, 43, 840-842, <https://doi.org/10.1021/ic034347p>.
6. Taberero, V.; Cuenca, T.; Herdtweck, E. Hydrazonide titanium derivatives: Synthesis, characterization and catalytic activity in olefin polymerization. Molecular structure of [Ti(η^5 -C₅H₄SiMe₃)Cl(μ -N₂CPh₂)]₂. *Journal of Organometallic Chemistry* **2002**, 663, 173-182, [https://doi.org/10.1016/S0022-328X\(02\)01733-3](https://doi.org/10.1016/S0022-328X(02)01733-3).
7. Cronin, S. P.; Al Mamun, A.; Toda, M. J.; Mashuta, M. S.; Losovyj, Y.; Kozlowski, P. M.; Buchanan, R. M.; Grapperhaus C. A. Utilizing Charge Effects and Minimizing Intramolecular Proton Rearrangement to Improve the Overpotential of a Thiosemicarbazonato Zinc HER Catalyst. *Inorganic Chemistry* **2019**, 58, 12986-12997, <https://doi.org/10.1021/acs.inorgchem.9b01912>.
8. Shakhofa, M. M. E.; Shtaiwi, M. H.; Morsy, N.; Abdel-rassel, T. M. A. Metal Complexes of Hydrazones and Their Biological, Analytical and Catalytic Applications: A Review. *Main Group Chemistry* **2014**, 13 (3), 187-218. <https://doi.org/10.3233/MGC-140133>.
9. Yang, W.; Fang-Lei, Z.; Zhen-Jiang, L.; Zhen-Jiang, L. Half-Sandwich Iridium Complexes with Hydrazone Ligands: Synthesis and Catalytic Activity in N-Alkylation of Anilines or Nitroarenes with Alcohols via Hydrogen Autotransfer. *Inorganic Chemistry* **2022**, 61(27), 10310-10320, <https://doi.org/10.1021/acs.inorgchem.2c00703>.
10. Vojinović-Ješić, L.; Novaković, S.; Leovac, V.; Česljević, V. Transition Metal Complexes with Girard Reagents and Their Hydrazones. *Journal of the Serbian Chemical Society* **2012**, 77 (9), 1129-1155, <https://doi.org/10.2298/JSC120704083V>.
11. Pousaneh, E.; Sadighian, S.; Bikas, R.; Hosseini-Monfared, H.; Sousaraei, A.; Siczek, M.; Lis, T. One-pot synthesis, crystal structure and theoretical calculations of a dinuclear Mn(III) complex with in-situ generated O,N,O- and O,N-donor chelating hydrazone ligand, *Journal of Molecular Structure* **2020**, 1199, <https://doi.org/10.1016/j.molstruc.2019.127023>.
12. Vojinović-Ješić, L. S.; Bogdanović, G. A.; Leovac, V. M.; Česljević, V. I.; Jovanović, L. S. Transition Metal Complexes with Girard Reagent-Based Ligands. Part IV. Synthesis and Characterization of Pyridoxilidene Girard-T Hydrazone Complexes. Crystal Structure of the Copper(II) Complex. *Structural Chemistry* **2008**, 19(5), 807-881. <https://doi.org/10.1007/s11224-008-9368-x>.
13. Pouralimardan, O.; Chamayou, A. C.; Janiak, C.; Hosseini-Monfared, H. Hydrazone Schiff base manganese(II) complexes: Synthesis, crystal structure and catalytic reactivity. *Inorganica Chimica Acta* **2007**, 360, 1599-1608, <https://doi.org/10.1016/j.ica.2006.08.056>.

14. Milenković, M.R.; Papastavrou, A.T.; Radanović, D.; Pevec, A.; Jagličić, Z.; Zlatar, M.; Gruden, M.; Vougioukalakis, G.C.; Turel, I.; Anđelković, K.; et al. Highly efficient N-arylation of imidazole catalyzed by Cu(II) complexes with quaternary ammonium-functionalized 2-acetylpyridine acylhydrazone. *Polyhedron*, **2019**, *165*, 22-30, <https://doi.org/10.1016/j.poly.2019.03.001>.
15. Nevena, S.; Mima, J.; Dragana, M.; Ivana, Z. M.; Marija Đ. C.; Miroslava, V.; Dušan, S.; Božidar, Č.; Katarina, A. Evaluation of antitumor potential of Cu(II) complex with hydrazone of 2-acetylthiazole and Girard's T reagent. *Journal of Serbian Chemical Society* **2002**, *87*(2), 181-192, <https://doi.org/10.2298/JSC211203114S>.
16. Keškić, T.; Jagličić, Z.; Pevec, A.; Čobeljić, B.; Radanović, D.; Gruden, M.; Turel, I.; Anđelković, K.; Brčeski, I.; Zlatar, M. Synthesis, X-Ray Structures and Magnetic Properties of Ni(II) Complexes of Heteroaromatic Hydrazone. *Polyhedron* **2020**, *191*, 114802, <https://doi.org/10.1016/j.poly.2020.114802>.
17. Stojičkov, M.; Zlatar, M.; Mazzeo, P. P.; Bacchi, A.; Radovanović, D., Stevanović, N.; Mima, J.; Novaković, I.; Anđelković, K.; Sladić, D.; Čobeljić, B.; Gruden, M. The interplay between spin states, geometries and biological activity of Fe(III) and Mn(II) complexes with thiosemicarbazone. *Polyhedron* **2023**, *237*, 116389, <https://doi.org/10.1016/j.poly.2023.116389>.
18. Darmanović, D.; Radanović, D.; Jevtović, M.; Turel, I.; Pevec, A.; Milčić, M.; Gruden, M.; Zlatar, M.; Đorđević, N.; Anđelković, K.; Čobeljić, B. Coordination preferences of NNO and NNS Schiff base ligands with Co(III) complexes: Synthesis, characterization and DFT calculation. *Journal of Molecular Structure* **2022**, *1266*, 133509, <https://doi.org/10.1016/j.molstruc.2022.133509>.
19. Čobeljić, B.; Pevec, A.; Stepanović, S.; Milenković, M. R.; Turel, I.; Gruden, M.; Radanović, D.; Anđelković, K. Structural Diversity of Isothiocyanato Cd(II) and Zn(II) Girard's T Hydrazone Complexes in Solution and Solid State: Effect of H-Bonding on Coordination Number and Supramolecular Assembly of Cd(II) Complex in Solid State. *Structural Chemistry* **2018**, *29* (6), 1797-1806, <https://doi.org/10.1007/s11224-018-1155-8>.
20. Čobeljić, B.; Turel, I.; Pevec, A.; Jagličić, Z.; Radanović, D.; Anđelković, K.; Milenković, M. R. Synthesis, Structures and Magnetic Properties of Octahedral Co(III) Complexes of Heteroaromatic Hydrazones with Tetraisothiocyanato Co(II) Anions. *Polyhedron* **2018**, *155*, 425-432, <https://doi.org/10.1016/j.poly.2018.08.070>.
21. Keskić, T.; Radanović, D.; Pevec, A.; Turel, I.; Gruden, M.; Andjelković, K.; Mitic, D.; Zlatar, M.; Čobeljić, B. Synthesis, X-Ray Structure and DFT Calculation of Magnetic Properties of Binuclear Ni(II) Complex with Tridentate Hydrazone-Based Ligand. *Journal of the Serbian Chemical Society* **2020**, *85* (10), 1279-1290, <https://doi.org/10.2298/JSC200625038K>.
22. Čobeljić, B.; Pevec, A.; Jagličić, Z.; Milenković, M.; Turel, I.; Radanović, D.; Milenković, M.; Anđelković, K. Synthesis, Characterization and Antimicrobial Activity of Isothiocyanato Fe(III) Girard's T Hydrazone Complex. *Journal of the Serbian Chemical Society* **2018**, *83* (12), 1327-1337, <https://doi.org/10.2298/JSC180828079C>.
23. Pelagatti, P.; Carcelli, M.; Pelizzi, C.; Costa, M. Polymerisation of phenylacetylene in water catalysed by Pd(NNO)Cl complexes. *Inorganica Chimica Acta* **2003**, *342*, 323, [https://doi.org/10.1016/S0020-1693\(02\)01161-1](https://doi.org/10.1016/S0020-1693(02)01161-1)
24. Álvarez-Casao, Y.; Monge, D.; Álvarez, E.; Fernández, R.; Lassaletta, J. Pyridine-Hydrazones as N,N'-Ligands in Asymmetric Catalysis: Pd(II)-Catalyzed Addition of Boronic Acids to Cyclic Sulfonylketimines. *Organic Letters* **2015**, *17*, 20, 5104-5107, <https://doi.org/10.1021/acs.orglett.5b02613>.
25. Bagherzadeh, M.; Zare, M.; Amani, V.; Ellern, A.; Woob, L. K. Dioxo and oxo-peroxo molybdenum(VI) complexes bearing salicylidene 2-picoloyl hydrazone: Structures and catalytic performances. *Polyhedron* **2013**, *53*, 223, <https://doi.org/10.1016/j.poly.2013.01.054>.

26. Mohammed, E.; Vasylyeva, V.; Janiak, C. Chirality and diastereoselection of Δ/Λ -configured tetrahedral zinc(II) complexes with enantiopure or racemic Schiff base ligands. *Inorganica Chimica Acta* **2013**, 408, 109, <https://doi.org/10.1016/j.ica.2013.08.016>.
27. Lei, Y. Two Oxidovanadium(V) Complexes with Hydrazone Ligands: Synthesis, Crystal Structures and Catalytic Oxidation Property. *Acta Chimica Slovenica* **2022**, 15(69), 235-242, <https://doi:10.17344/acsi.2021.7296>.
28. Lauder, K.; Toscani, A.; Scalacci, N.; Castagnolo, D. Synthesis and reactivity of propargylamines in organic chemistry. *Chemical Reviews* **2017**, 117, 14091-14200, <https://doi:10.1021/acs.chemrev.7b00343>.
29. Baranyi, M.; Porceddu, P. F.; Gölöncser, F.; Kulcsár, S.; Otrókocsi, L.; Kittel, Á.; Pinna, A.; Frau, L.; Huleatt, P. B.; Khoo, M. L.; Chai, C. L. L.; Dunkel, P.; Matyus, P.; Morelli, M.; Sperlágh, B. Novel (hetero)arylalkenyl propargylamine compounds are protective in toxin-induced models of Parkinson's disease. *Molecular Neurodegeneration* **2016**, 11, 1-21, <https://doi.org/10.1186/s13024-015-0067-y>.
30. Boulton, A. A.; Davis, B. A.; Durden, D. A.; Dyck, L. E.; Juorio, A. V.; Li, X. M.; Paterson, I. A.; Yu, P. H. Aliphatic propargylamines: new antiapoptotic drugs. *Drug Development Research* **1997**, 42, 150-156, [https://doi:10.1002/\(SICI\)1098-2299\(199711/12\)42:3/4<150::AID-DDR6>3.0.CO;2-P](https://doi:10.1002/(SICI)1098-2299(199711/12)42:3/4<150::AID-DDR6>3.0.CO;2-P).
31. Chen, J. J.; Swope, D. M. Clinical pharmacology of rasagiline: A novel, second-generation propargylamine for the treatment of Parkinson disease. *Journal of Clinical Pharmacology* **2005**, 45, 878-894, <https://doi:10.1177/0091270005277935>
32. Peshkov, V.A.; Pereshivko, O.P.; Van der Eycken, E.V. A walk around the A3-coupling. *Chemical Society Reviews* **2012**, 41, 3790-3807, <https://doi.org/10.1039/C2CS15356D>.
33. Zhao, X. B.; Ha, W.; Jiang, K.; Chen, J.; Yang, J. L.; Shi, Y. P. Efficient synthesis of camptothecin propargylamine derivatives in water catalyzed by macroporous adsorption resin-supported gold nanoparticles. *Green Chemistry* **2017**, 19, 1399-1406, <https://doi.org/10.1039/C6GC03119F>.
34. Shachat, N.; Bagnell, J. J. Reactions of propargyl alcohols and propargylamines with isocyanates. *Journal of Organic Chemistry* **1963**, 28, 991-995, <https://doi.org/10.1021/jo01039a028>.
35. Nikolaos V. T.; Stavros P. N.; Georgios C. V. Zn-Catalyzed Multicomponent KA² Coupling: One-Pot Assembly of Propargylamines Bearing Tetrasubstituted Carbon Centers. *American chemical society Omega* **2019**, 4, 6, 10279-10292, <https://doi.org/10.1021/acsomega.9b01387>
36. Wim, E. V.; Joren, V. S.; Philippe, F.; Kourosch, A. T. Copper(I)-Catalyzed Ketone, Amine, and Alkyne Coupling for the Synthesis of 2-Alkynylpyrrolidines and -piperidines, *Organic Letters* **2016**, 18, 19, 4782-4785, <https://doi.org/10.1021/acs.orglett.6b02127>.
37. Pierce, C. J.; Nguyen, M.; Larsen, C. H. Copper/titanium catalysis forms fully substituted carbon centers from the direct coupling of acyclic ketones, amines, and alkynes. *Angewandte Chemie International Edition* **2012**, 51, 12289-12292, <https://doi.org/10.1002/anie.201206674>.
38. Zorba, L.; Vougioukalakis, G. The Ketone-Amine-Alkyne (KA²) coupling reaction: Transition metal-catalyzed synthesis of quaternary propargylamines. *Coordination Chemistry Reviews* **2020**, 429, 213603, <https://doi.org/10.1016/j.ccr.2020.213603>;
39. Palchak, Z. L.; Lussier, D. J.; Pierce, C. J.; Larsen, C. H. Synthesis of tetrasubstituted propargylamines from cyclohexanone by solvent-free copper(II) catalysis. *Green Chemistry* **2015**, 17, 1802-1810, <https://doi.org/10.1039/C4GC02318H>.
40. Meyet, C. E.; Pierce, C. J.; Larsen, C. H. A single Cu(II) catalyst for the three-component coupling of diverse nitrogen sources with aldehydes and alkynes. *Organic Letters* **2012**, 14, 964-967, <https://doi.org/10.1021/ol2029492>.
41. Stavros P. N.; Nikolaos V. T.; Martin, P.; Enrique, G. B.; Georgios, C. V. Manganese-Catalyzed Multicomponent Synthesis of Tetrasubstituted Propargylamines: System

- Development and Theoretical Study. *Advanced synthesis and catalysis* **2020**, 18, 362, <https://doi.org/10.1002/adsc.202000566>.
42. Li, G.; Zhang, Q.; Yang, S.; Zhu, M.; Fu, Y.; Liu, Z.; Xing, N.; Shi, L. Three new zinc(II) complexes: design, synthesis, characterization and catalytic performance, *Journal of Coordination Chemistry* **2022**, 75, 1416-1433, <https://doi.org/10.1080/00958972.2022.2098472>.
 43. Stevanović, N.; Zlatar, M.; Novaković, I.; Pevec, A.; Radanović, D.; Matic, I. Z.; Đorđić Crnogorac, M.; Stanojković, T.; Vujčić, M.; Gruden, M.; Sladić, D.; Anđelković, K.; Turel, I.; Čobeljić, B. *Dalton Transaction* **2022**, 51, 185-196, <https://doi.org/10.1039/D1DT03169D>.
 44. Romanović, M. Č.; Čobeljić, B.; Pevec, A.; Turel, I.; Anđelković, K.; Milenković, M. M. R.; Radanović, D.; Belošević, S. Synthesis, Crystal Structures and Antimicrobial Activity of Azido and Isocyanato Zn(II) Complexes with the Condensation Product of 2-Quinolinecarboxaldehyde and Girard's T Reagent. *Journal of Coordination Chemistry* **2017**, 70, 2425-2435, <https://doi.org/10.1080/00958972.2017.1343945>.
 45. Stevanović, N.; Mazzeo, P. P.; Bacchi, A.; Matic, I. Z.; Đorđić Crnogorac, M.; Stanojković, T.; Vujčić, M.; Novaković, I.; Radanović, D.; Šumar-Ristović, M.; Sladić, D.; Čobeljić, B.; Anđelković, K. Characterization, Antimicrobial and Cytotoxic Activity and DNA-Binding Properties of d-Metal Complexes with Hydrazones of Girard's T and P Reagents. *Journal of Biological Inorganic Chemistry* **2021**, 26, 863-880, <https://doi.org/10.1007/s00775-021-01893-5>.
 46. Otwinowsky, Z.; Minor, W. Processing of X-ray Diffraction Data Collected in Oscillation Mode. *Methods in Enzymology* **1997**, 276, 307-326, [https://doi.org/10.1016/S0076-6879\(97\)76066-X](https://doi.org/10.1016/S0076-6879(97)76066-X).
 47. CrysAlis PRO. Oxford Diffraction; Oxford Diffraction Ltd.: Yarnton, UK, **2009**.
 48. Altomare, A.; Casciaro, G.; Giacovazzo, C.; Guagliardi, A. Completion and refinement of crystal structures with SIR92. *Journal of Applied Crystallography* **1993**, 26, 343-350, <https://doi.org/10.1107/S0021889892010331>.
 49. Sheldrick, G. M. A short history of SHELX. *Acta Crystallographica* **2008**, A64, 112-122, <https://doi.org/10.1107/S0108767307043930>.
 50. Agilent, **2014**.
 51. Sheldrick, G. M. Crystal structure refinement with SHELXL. *Acta crystallographica Section C, Structural chemistry* **2015**, 71, 3-8, <https://doi.org/10.1107/S2053229614024218>.
 52. Cheng, M.; Zhang, Q.; Hu, X.; Li, B.; Ji, J.; Chan, A. Gold-catalyzed direct intermolecular coupling of ketones, secondary amines, and alkynes: A facile and versatile access to propargylic amines containing a quaternary carbon center. *Advance Synthesis and Catalysis* **2011**, 353, 1274-1278, <https://doi.org/10.1002/adsc.201000914>.
 53. Pierce, C. J.; Larsen, C. H. Copper(II) catalysis provides cyclohexanone-derived propargylamines free of solvent or excess starting materials: Sole by-product is water. *Green Chemistry* **2012**, 14, 2672-2676, <https://doi.org/10.1039/C2GC35713E>.
 54. Schlimpen, F.; Plaçais, C.; Starck, E.; Bénétiau, V.; Pale, P.; Chassaing, S. α -Tertiary Propargylamine Synthesis via KA^2 -Type Coupling Reactions under Solvent-Free CuI-Zeolite Catalysis. *Journal of Organic Chemistry* **2021**, 86, 23, 16593-16613, <https://doi.org/10.1021/acs.joc.1c01893>.
 55. Frisch, M. J.; Trucks, G. W.; Schlegel, H. B.; Scuseria, G. E.; Robb, M. A.; Cheeseman, J. R.; Scalmani, G.; Barone, V.; Mennucci, B.; Petersson, G. A.; Nakatsuji, H.; Caricato, M.; Li, X.; Hratchian, H. P.; Izmaylov, A. F.; Bloino, J.; Zheng, G.; Sonnenberg, J. L.; Hada, M.; Ehara, M.; Toyota, K.; Fukuda, R.; Hasegawa, J.; Ishida, M.; Nakajima, T.; Honda, Y.; Kitao, O.; Nakai, H.; Vreven, T.; Montgomery Jr., J. A.; Peralta, J. E.; Ogliaro, F.; Bearpark, M.; Heyd, J. J.; Brothers, E.; Kudin, K. N.; Staroverov, V. N.; Kobayashi, R.; Normand, J.; Raghavachari, K.; Rendell, A.; Burant, J. C.; Iyengar, S. S.; Tomasi, J.; Cossi, M.; Rega, N.; Millam, J. M.; Klene, M.; Knox, J. E.; Cross, J. B.; Bakken, V.; Adamo, C.; Jaramillo, J.; Gomperts, R.; Stratmann, R. E.; Yazyev, O.; Austin, A. J.; Cammi, R.; Pomelli, C.; Ochterski, J. W.; Martin,

- R. L.; Morokuma, K.; Zakrzewski, V. G.; Voth, G. A.; Salvador, P.; Dannenberg, J. J.; Dapprich, S.; Daniels, A. D.; Farkas, O.; Foresman, J. B.; Ortiz, J. V.; Cioslowski, J.; Fox, D. J. Gaussian 09, Revision B.01., *Gaussian Inc. Wallingford* **2010**.
56. Becke, A. D. Density-functional thermochemistry. III. The role of exact exchange. *Journal of Chemical Physics* **1993**, *98*, 5648-5652, <https://doi.org/10.1063/1.464913>.
 57. Lee, C.; Yang, W.; Parr, R. G. Development of the Colle-Salvetti correlation-energy formula into a functional of the electron density. *Physical Review B: Condensed Matter and Materials Physics* **1988**, *37*, 785, <https://doi.org/10.1103/physrevb.37.785>.
 58. Hehre, J.; Ditchfield, R.; Pople, J. A. Self-Consistent Molecular Orbital Methods. XII. Further Extensions of Gaussian-Type Basis Sets for Use in Molecular Orbital Studies of Organic Molecules. *Journal of Chemical Physics* **1972**, *56*, 2257-2261, <https://doi.org/10.1063/1.1677527>.
 59. Hariharan, P. C.; Pople, J. A. The influence of polarization functions on molecular orbital hydrogenation energies. *Theoretica chimica acta* **1973**, *28*, 213-222, <https://doi.org/10.1007/BF00533485>.
 60. Institute of Physics Belgrade. PARADOX Cluster User Guide v2.1: PARADOX IV Cluster; Institute of Physics Belgrade: Belgrade, Serbia, **2018**.
 61. Te Velde, G.; Bickelhaupt, F. M.; Baerends, E. J.; Guerra, C. F.; Van Gisbergen, S. J. A.; Snijders, J. G.; Ziegler, T. Chemistry with ADF. *Journal of Computational Chemistry*, **2001**, *22*, 931-967.
 62. Baerends, E. J.; Ziegler, T.; Atkins, A. J.; Autschbach, J.; Bashford, D.; Baseggio, O.; Bérces, A.; Bickelhaupt, F. M.; Bo, C.; Boerritger, P. M.; Cavallo, L.; Daul, C.; Chong, D. P.; Chulhai, D.; Deng, L.; Dickson, R. M.; Dieterich, J. M.; Ellis, D. E.; Faassen, M.; Ghysels, A.; Giammona, A.; Gisbergen, S. J. A.; Goetz, A.; Götz, A. W.; Gusarov, S.; Harris, F. E.; Van den Hoek, P.; Hu, Z.; Jacob, C. R.; Jacobsen, H.; Jensen, L.; Joubert, L.; Kaminski, J. W.; Van Kessel, G.; König, C.; Kootstra, F. A, ADF 2022.1, SCM, Theoretical Chemistry, Vrije Universiteit, Amsterdam, The Netherlands.
 63. Rüger, T. N. R.; Franchini, M.; Trnka, T.; Yakovlev, A.; Van Lenthe, E.; Philipsen, P.; Van Vuren, T.; Klumpers, B.; Soini, T. AMS 2022.1, SCM, Theoretical Chemistry, Vrije Universiteit, Amsterdam
 64. Van Lenthe, E.; Baerends, E. J.; Snijders, J. G. Relativistic regular two-component Hamiltonians. *Journal of Chemical Physics* **1993**, *99*, 4597-4610, <https://doi.org/10.1063/1.466059>.
 65. Van Lenthe, E.; Baerends, E. J.; Snijders, J. G. Relativistic total energy using regular approximations. *Journal of Chemical Physics* **1994**, *101*, 9783-9792, <https://doi.org/10.1063/1.467943>.
 66. Van Wüllen, C. *Journal of Chemical Physics* **1998**, *109*, 392-399, <https://doi.org/10.1063/1.476576>.
 67. Bitzek, E.; Koskinen, P.; Gähler, F.; Moseler, M.; Gumbusch, P. Structural Relaxation Made Simple. *Physical Review Letters* **2006**, *97*, 170201, <https://doi.org/10.1103/PhysRevLett.97.170201>.
 68. Becke, A. D. Density-functional exchange-energy approximation with correct asymptotic behavior. *Physical Review A* **1988**, *38*, 3098-3100, <https://doi.org/10.1103/PhysRevA.38.3098>.
 69. Perdew, J. P. Density-functional approximation for the correlation energy of the in homogeneous electron gas. *Physical Review B* **1986**, *33*, 8822-8824, <https://doi.org/10.1103/PhysRevB.33.8822>; erratum: *Physical Review B* *34*, 7406 (1986), <https://doi.org/10.1103/PhysRevB.34.7406>.
 70. Caldeweyher, E.; Ehlert, S.; Hansen, A.; Neugebauer, H.; Spicher, S.; Bannwarth, C.; Grimme, S. A generally applicable atomic-charge dependent London dispersion correction. *Journal of Chemical Physics* **2019**, *150*, 154122, <https://doi.org/10.1063/1.5090222>.

71. Geerlings, P.; De Proft, F.; Langenaeker, W. Conceptual Density Functional Theory. *Chemical Reviews* **2003**, 103, 1793-1874, <https://doi.org/10.1021/cr990029p>.
72. Chermette, H. Chemical reactivity indexes in density functional theory, *Journal of Computational Chemistry* **1999**, 20, 129-154
73. Hoffmann, G., Tognetti, V., Joubert, L. Can molecular and atomic descriptors predict the electrophilicity of Michael acceptors? *Journal of Molecular Modeling* **2018**, 24, 281, <https://doi.org/10.1007/s00894-018-3802-9>.
74. Dostanić, J.; Lončarević, D.; Zlatar, M.; Vlahović, F.; Jovanović, D. M. Quantitative structure-activity relationship analysis of substituted arylazo pyridone dyes in photocatalytic system: Experimental and theoretical study. *Journal of Hazard Mater* **2016**, 316, 26-33
75. Govindarajan, M.; Karabacak, M.; Periandy, S.; Tanuja, D. Spectroscopic (FT-IR, FT-Raman, UV and NMR) investigation and NLO, HOMO-LUMO, NBO analysis of organic 2,4,5-trichloroaniline. *Spectrochimica Acta, Part A: Molecular and Biomolecular Spectroscopy*. **2012**, 97, 231-245, <https://doi.org/10.1016/j.saa.2012.06.014>.
76. Vosko, S. H.; Wilk, L.; Nusair, M. Accurate spin-dependent electron liquid correlation energies for local spin density calculations: A critical analysis. *Canadian Journal of Physics* **1980**, 58 1200-11. <https://doi.org/10.1139/p80-159>
77. Caricato, M.; Mennucci, B.; Tomasi, J.; Ingrosso, F.; Cammi, R.; Corni, S.; Scalmani, G. Formation and relaxation of excited states in solution: A new time dependent polarizable continuum model based on time dependent density functional theory. *Journal of Chemical Physics* **2006**, 124, 124520-124532, <https://doi.org/10.1063/1.2183309>.
78. Yanai, T.; Tew, D. P.; Handy, N. C. A new hybrid exchange–correlation functional using the Coulomb-attenuating method (CAM-B3LYP). *Chemical Physics Letters* **2004**, 393, 51-57, <https://doi.org/10.1016/j.cplett.2004.06.011>.
79. Marques, M. A. L.; Oliveira, M. J. T. ; Burnus, T. A library of exchange and correlation functionals for density functional theory. *Computer Physics Communications* **2012**, 183, 2272-2281.
80. Nakamoto, K. Infrared and Raman Spectra of Inorganic and Coordination Compounds, 4th Edition, *Wiley-Interscience New York* **1998**, 283.
81. Mandewale, M. C.; Thorat, B.; Shelke, D.; Yamgar, R. Synthesis and Biological Evaluation of New Hydrazone Derivatives of Quinoline and Their Cu(II) and Zn(II) Complexes against Mycobacterium tuberculosis. *Bioinorganic Chemistry and Applications*. **2015**, 14, <https://doi.org/10.1155/2015/153015>.
82. Kargol, J. A.; Crecely, R.W.; Burmeister, J. L. Carbon-13 nuclear magnetic resonance study of coordinated thiocyanate, selenocyanate, and cyanate, *Inorganic Chemistry* **1979**, 18, 2532, <https://doi.org/10.1021/ic50199a040>.
83. Addison, A. W.; Rao, T. N.; Reedijk, J.; Van Rijn, J.; Verschoor, G. C. Synthesis, structure, and spectroscopic properties of copper(II) compounds containing nitrogen-sulphur donor ligands; the crystal and molecular structure of aqua [1,7-bis(N-methylbenzimidazol-20-yl)-2,6-dithiaheptane]copper(II) perchlorate. *Journal of the Chemical Society. Dalton transactions* **1984**, 1349-1356, <https://doi.org/10.1039/DT9840001349>.
84. Moroz, Y. S.; Sliva, T. Y.; Kulon, K.; Kozłowski, H.; Fritsky, I. O. Di-chlorido{2-hydroxyimino-N0-[1-(2-pyridyl)ethylidene]propanohydrazide-K³N,N',O} zinc(II) hemihydrate. *Acta Crystallographica* **2008**, 64, 353-354, <https://doi.org/10.1107/S160053680706535X>.
85. Chaur, M. N. Dichlorido{(E)-4-dimethylamino-N'-[(pyridin-2-yl)methylidene-κN]benzohydrazide-κO}zinc. *Acta Crystallographica* **2013**, E69, m27, <https://doi.org/10.1107/S1600536812049355>.
86. Reena, T. A.; Seená, E. B.; Prathapachandra Kurup, M. R. Zinc(II) complexes derived from di-2-pyridyl ketone N4-phenyl-3-semicarbazone: Crystal structures and spectral studies. *Polyhedron* **2008**, 27, 3461-3466, <https://doi.org/10.1016/j.poly.2008.08.014>.

87. Despaigne, A. A. R.; Da Silva, J. G.; Do Carmo, A. C. M.; Sives, F.; Piro, O. E.; Castellano, E. E.; Beraldo, H. Copper(II) and zinc(II) complexes with 2-formylpyridine-derived hydrazones. *Polyhedron* **2009**, 28, 3797-3803, <https://doi.org/10.1016/j.poly.2009.07.059>.
88. Li, L.; Zhang, Y. Z.; Liu, E.; Yang, C.; Golen, J. A.; Rheingold, A. L.; Zhang, G. Synthesis and structural characterization of zinc(II) and cobalt(II) complexes based on multidentate hydrazone ligands. *Journal of Molecular Structure* **2016**, 1110, 180-184, <https://doi.org/10.1016/j.molstruc.2016.01.051>.
89. Anđelković, K.; Pevec, A.; Grubišić, S.; Turel, I.; Čobeljić, B.; Milenković, M. R.; Keškić, T.; Radanović, D. Crystal structures and DFT calculations of mixed chloride-azide zinc(II) and chloride-isocyanate cadmium(II) complexes with the condensation product of 2-quinolinecarboxaldehyde and Girard's Treagent. *Journal of Molecular Structure* **2018**, 1162, 63-70, <https://doi.org/10.1016/j.molstruc.2018.02.074>.
90. Steiner, T. The Hydrogen Bond in the Solid State. *Angewandte Chemie International Edition* **2002**, 41, 48-76, [https://doi.org/10.1002/1521-3773\(20020104\)41:1<48::AID-ANIE48>3.0.CO;2-U](https://doi.org/10.1002/1521-3773(20020104)41:1<48::AID-ANIE48>3.0.CO;2-U).
91. Afkhami, F. A.; Khandar, A. A.; Mahmoudi, G.; Maniukiewicz, W.; Lipkowski, J.; White, J. M.; Waterman, R.; García-Granda, S.; Zangrando, E.; Bauzái, A.; Frontera, A. Synthesis, X-ray characterization, DFT calculations and Hirshfeld surface analysis of Zn(II) and Cd(II) complexes based on isonicotinoylhydrazone ligand. *Crystal Engineering and Communication* **2016**, 18, 4587-4596, <https://doi.org/10.1039/C6CE00877A>.
92. Venkatraman, R.; Fronczek, F. R. Experimental Crystal Structure Determination. *Cambridge Crystallographic Data Centre* **2015**, CCDC 1058780. <https://doi.org/10.5517/CC14JR6M>.
93. Bermejo, E.; Castiñeiras, A.; Fostiak, L. M.; Santos, I. G.; Swearingen, J. K.; West, D. X. Spectral and structural studies of Zn and Cd complexes of 2-pyridineformamide N(4)-ethylthiosemicarbazone. *Polyhedron* **2004**, 23, 2303-2313, <https://doi.org/10.1016/j.poly.2004.07.010>.
94. Stacy, A. E.; Palanimuthu, D.; Bernhardt, P. V.; Kalinowski, D. S.; Jansson, P. J.; Richardson, D. R. Zinc(II)-Thiosemicarbazone Complexes Are Localized to the Lysosomal Compartment Where They Transmetallate with Copper Ions to Induce Cytotoxicity. *Journal of Medicinal Chemistry*, **2016**, 59, 4965-4984, <https://doi.org/10.1021/acs.jmedchem.6b00238>.
95. Kasuga, N. C.; Hara, Y.; Koumo, C.; Sekino, K.; Nomiya, K. Two novel zinc(II) complexes of N'-[1-(2-pyridyl)ethylidene]morpholine-4-carbothiohydrazide. *Acta Crystallographica Section C Crystal Structure and Communication* **1999**, 55, 1264-1267, <https://doi.org/10.1107/S0108270199004199>.
96. Bresolin, L.; Burlow, R. A.; Hörner, M.; Bermejo, E.; Castiñeiras, A. Synthesis and crystal structure of di [(μ-acetato)(2-acetylpyridine-4N-ethylthiosemicarbazonato)zinc(II)]. *Polyhedron*, **1997**, 16, 3947-3951, [https://doi.org/10.1016/S0277-5387\(97\)00194-0](https://doi.org/10.1016/S0277-5387(97)00194-0).
97. Nfor, E. N.; Liu, W.; Zuo, J. L.; You, X. Z.; Offiong, O. E. Di-μ-acetatobis[(2-acetylpyridinethiosemicarbazonato) Zinc (II)]. *Acta Crystallographica Section C Crystal Structure and Communication* **2006**, 62, m211-m213, <https://doi.org/10.1107/S0108270106009152>.
98. Mirza, A. H.; Hamid, M. H. S. A.; Aripin, S.; Karim, M. R.; Arifuzzaman, M.; Ali, M. A.; Bernhardt, P. V. Synthesis, Spectroscopy and X-Ray Crystal Structures of Some Zinc(II) and Cadmium(II) Complexes of the 2-Pyridinecarboxaldehyde Schiff Bases of S-Methyl- and S-Benzylthiocarbazates. *Polyhedron*, **2014**, 74, 16-23, <https://doi.org/10.1016/j.poly.2014.02.016>.
99. Bermejo, E.; Castiñeiras, A.; García-Santos, I.; West, D. X. Structural and Coordinative Variability in Zinc(II), Cadmium(II), and Mercury(II) Complexes of 2-Pyridineformamide 3-Hexamethyleneiminylthiosemicarbazone. *Z. Anorg. Allg. Chem.*, **2004**, 630, 1096-1109, <https://doi.org/10.1002/zaac.200400097>.
100. Cavalcante, C. Q. O.; Arcanjo, D. S.; Silva, G. G.; Oliveira, D. M.; Gatto, C. C. Solution and solid behavior of mono and binuclear zinc(ii) and nickel(ii) complexes with dithiocarbazates.

- X-ray analysis, mass spectrometry and cytotoxicity against cancer cell lines. *New Journal Chemistry* **2019**, 43, 11209-11221, <https://doi.org/10.1039/C9NJ01814J>.
101. Afkhami, F. A.; Khandar, A. A.; Mahmoudi, G.; Amini, M.; Molins, E.; Garczarek, P.; Lipkowski, J.; White, J. M.; Kirillov, A. M. New cadmium(II) and zinc(II) coordination polymers derived from a pyridine-hydrazone block: Self-assembly generation, structural and topological features, and theoretical analysis. *Inorganica Chimica Acta* **2017**, 458, 68-76, <https://doi.org/10.1016/j.ica.2016.12.020>.
 102. Hong, X. J.; Zhan, Q. G.; Huang, Z. P.; Du, Y. Q.; Wei, L. M.; Li, T.; Zheng, Z. P.; Cai, Y. P. Construction of two Zn (II) complexes based on the oxime-containing Schiff base ligand with NO and N₂O donor sets. *Inorganic Chemistry Communications* **2014**, 44, 53-57, <https://doi.org/10.1016/j.inoche.2014.03.001>.
 103. Sy, A.; Dieng, M.; Thiam, I. E.; Gaye, M.; Retailleau, P. Dichlorido{N'-[phen-yl(pyridin-2-yl-κN)methyl-idene]isonicotinohydrazide-κ2 N',O}zinc. *Acta Crystallogrica Section E Crystal Structure* **2013**, 69, m108-m108, <https://doi.org/10.1107/S1600536813001281>.
 104. Despaigne, A. A. R.; Da Silva, J. G.; do Carmo, A. C. M.; Piro, O. E.; Castellano, E. E.; Beraldo, H. Structural studies on zinc(II) complexes with 2-benzoylpyridine-derived hydrazones. *Inorganica Chimica Acta* **2009**, 362, 2117-2122, <https://doi.org/10.1016/j.ica.2008.09.040>.
 105. Afkhami, F. A.; Mahmoudi, G.; Khandar, A. A.; White, J. M.; Maniukiewicz, W. Design and construction of Zn(II) coordination polymers made by pincer type pyridine-hydrazine based ligands. *Journal of Molecular Structure* **2019**, 1197, 555-563, <https://doi.org/10.1016/j.molstruc.2019.07.090>.
 106. H. Yu, S. Guo, J.-Y. Cheng, G. Jiang, Z. Li, W. Zhai, A. Li, Y. Jiang and Z. You, Synthesis and crystal structures of cobalt(III), copper(II), nickel(II) and zinc(II) complexes derived from 4-methoxy-N'-(pyridin-2-ylmethylene)benzohydrazide with urease inhibitory activity. *Journal of Coordination Chemistry* **2018**, 71, 4164-4179, <https://doi.org/10.1080/00958972.2018.1533959>.
 107. Kosar, B.; Albayrak, C. Spectroscopic investigations and quantum chemical computational study of (E)-4-methoxy-2-[(p-tolylimino)methyl]phenol. *Spectrochimica Acta A* **2011**, 78, 160-167, <https://doi.org/10.1016/j.saa.2010.09.016>.
 108. Rauk, A. Orbital Interaction Theory of Organic Chemistry, 2nd edition. JohnWiley & Sons: New York, NY, USA **2001**, 34.
 109. Tabares-Mendoza, C.; Guadarrama, P. Predicting the catalytic efficiency by quantum-chemical descriptors: Theoretical study of pincer metallic complexes involved in the catalytic Heck reaction. *Journal of Organometallic Chemistry* **2006**, 691, 2978-2986, [10.1016/j.jorganchem.2006.03.007](https://doi.org/10.1016/j.jorganchem.2006.03.007)
 110. Domingo, L. R.; Ríos-Gutiérrez, M.; Pérez, P. Applications of the Conceptual Density Functional Theory Indices to Organic Chemistry Reactivity. *Molecules* **2016**, 21, 748, <https://doi.org/10.3390/molecules21060748>.
 111. Zhan, C. G.; Nichols, J. A.; Dixon, D. A. Ionization Potential, Electron Affinity, Electronegativity, Hardness, and Electron Excitation Energy: Molecular Properties from Density Functional Theory Orbital Energies. *Journal of Physical Chemistry A* **2003**, 107, 4184-4195, <https://doi.org/10.1021/jp0225774>.

Appendix

PICTURE 1: IR Spectra for ligand **HL¹Cl** (E)-N,N,N-trimethyl-2-oxo-2-(2-(1-(thiazol-2-yl)ethylidene)hydrazinyl)ethan-1-aminium chloride

PICTURE 2: ¹H NMR Spectra for ligand **HL¹ Cl** (E)-N,N,N-trimethyl-2-oxo-2-(2-(1-(thiazol-2-yl)ethylidene)hydrazinyl)ethan-1-aminium chloride

PICTURE 3: ¹³C NMR Spectra for ligand **HL¹ Cl** (E)-N,N,N-trimethyl-2-oxo-2-(2-(1-(thiazol-2-yl)ethylidene)hydrazinyl)ethan-1-aminium chloride

PICTURE 4: IR Spectra for ligand **HL²** (E)-2-(1-(thiazol-2-yl)ethylidene)hydrazine-1-carbothioamide

PICTURE 5: ¹H NMR Spectra for ligand **HL²** (E)-2-(1-(thiazol-2-yl)ethylidene)hydrazine-1-carbothioamide

PICTURE 6: ¹³C NMR Spectra for ligand **HL²** (E)-2-(1-(thiazol-2-yl)ethylidene)hydrazine-1-carbothioamide

PICTURE 7: IR Spectra for ligand **HL⁴Cl** (E)-1-(2-oxo-2-(2-(1-(pyridin-2-yl)ethylidene)hydrazinyl)ethyl)-pyridine-1-ium chloride

PICTURE 8: ¹H NMR Spectra for ligand **HL⁴Cl** (E)-1-(2-oxo-2-(2-(1-(pyridin-2-yl)ethylidene)hydrazinyl)ethyl)-pyridine-1-ium chloride

PICTURE 9: ¹³C NMR Spectra for ligand **HL⁴Cl** (E)-1-(2-oxo-2-(2-(1-(pyridin-2-yl)ethylidene)hydrazinyl)ethyl)-pyridine-1-ium chloride

PICTURE 10: IR Spectra for complex **1 [ZnL¹(NCS)₂]·2H₂O**

PICTURE 11: ¹H NMR Spectra for complex **1 [ZnL¹(NCS)₂]·2H₂O**

PICTURE 12: ¹³C NMR Spectra for complex **1 [ZnL¹(NCS)₂]·2H₂O**

PICTURE 13: IR Spectra for complex **2 [Zn(L²)₂]**

PICTURE 14: ¹H NMR Spectra for complex **2 [Zn(L²)₂]**

PICTURE 15: ¹³C NMR Spectra for complex **2 [Zn(L²)₂]**

PICTURE 16: IR Spectra for complex **5 [ZnL²(N₃)₂]**

PICTURE 17: ¹H NMR Spectra for complex **5 [ZnL²(N₃)₂]**

PICTURE 18: ¹³C NMR Spectra for complex **5 [ZnL²(N₃)₂]**

PICTURE 19: COSY NMR Spectra for complex **5 [ZnL²(N₃)₂]**

PICTURE 20: HSQC NMR Spectra for complex **5 [ZnL²(N₃)₂]**

PICTURE 21: IR Spectra for complex **6 [ZnL⁴(N₃)₂]**

PICTURE 22: ¹H NMR Spectra for complex **6 [ZnL⁴(N₃)₂]**

PICTURE 23: ¹³C NMR Spectra for complex **6 [ZnL⁴(N₃)₂]**

PICTURE 24: COSY NMR Spectra for complex **6 [ZnL⁴(N₃)₂]**

PICTURE 25: HSQC NMR Spectra for complex **6 [ZnL⁴(N₃)₂]**

PICTURE 26: ¹H NMR for *1-(1-(phenylethynyl)cyclohexyl)pyrrolidine 4a*

PICTURE 27: ¹³C NMR for *1-(1-(phenylethynyl)cyclohexyl)pyrrolidine 4a*

PICTURE 28: ¹H NMR for *1-(1-(phenylethynyl)cyclohexyl)piperidine 4b*

PICTURE 29: ^{13}C NMR for *1-(1-(phenylethynyl)cyclohexyl)piperidine* 4b

PICTURE 30: ^1H NMR for *1-(1-(p-tolyethynyl)cyclohexyl)piperidine* 4c

PICTURE 31: ^{13}C NMR for *1-(1-(p-tolyethynyl)cyclohexyl)piperidine* 4c

PICTURE 32: ^1H NMR for *1-(3-methyl-1-phenylpent-1-yn-3-yl)pyrrolidine* 4d

PICTURE 33: ^{13}C NMR for *1-(3-methyl-1-phenylpent-1-yn-3-yl)pyrrolidine* 4d

PICTURE 34: ^1H NMR for *1-(1-(phenylethynyl)cyclohexyl)piperidine-4-carboxylate* 4e

PICTURE 35: ^{13}C NMR for *1-(1-(phenylethynyl)cyclohexyl)piperidine-4-carboxylate* 4e.

PICTURE 36: ^1H NMR for *N-octyl-1-(phenylethynyl)cyclohexanamine* 4f

PICTURE 37: ^{13}C NMR for *N-octyl-1-(phenylethynyl)cyclohexanamine* 4f

PICTURE 38: ^1H NMR for *1-(3-methyl-1-phenylhex-1-yn-3-yl)pyrrolidine* 4g

PICTURE 39: ^{13}C NMR for *1-(3-methyl-1-phenylhex-1-yn-3-yl)pyrrolidine* 4g

PICTURE 40: ^1H NMR for *2-methyl-4-(1-(4-phenylpiperazin-1-yl)cyclohexyl)but-3-yn-2-ol* 4h

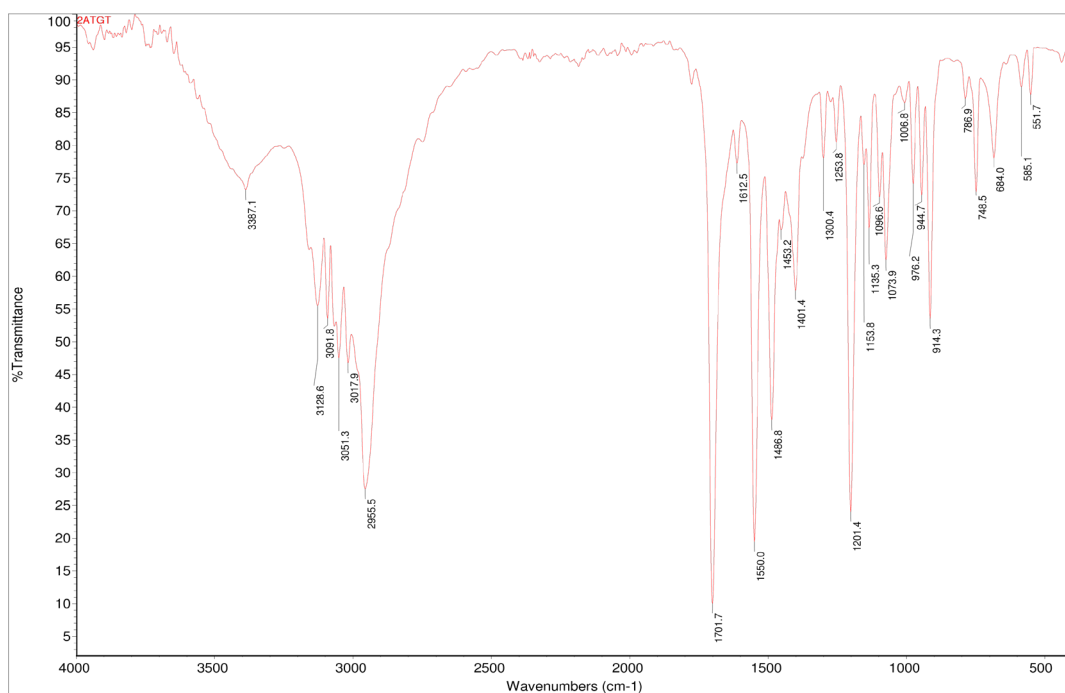
PICTURE 41: ^{13}C NMR for *2-methyl-4-(1-(4-phenylpiperazin-1-yl)cyclohexyl)but-3-yn-2-ol* 4h

PICTURE 42: ^1H NMR for *1-(1-(oct-1-yn-1-yl)cyclohexyl)piperidine* 4i.

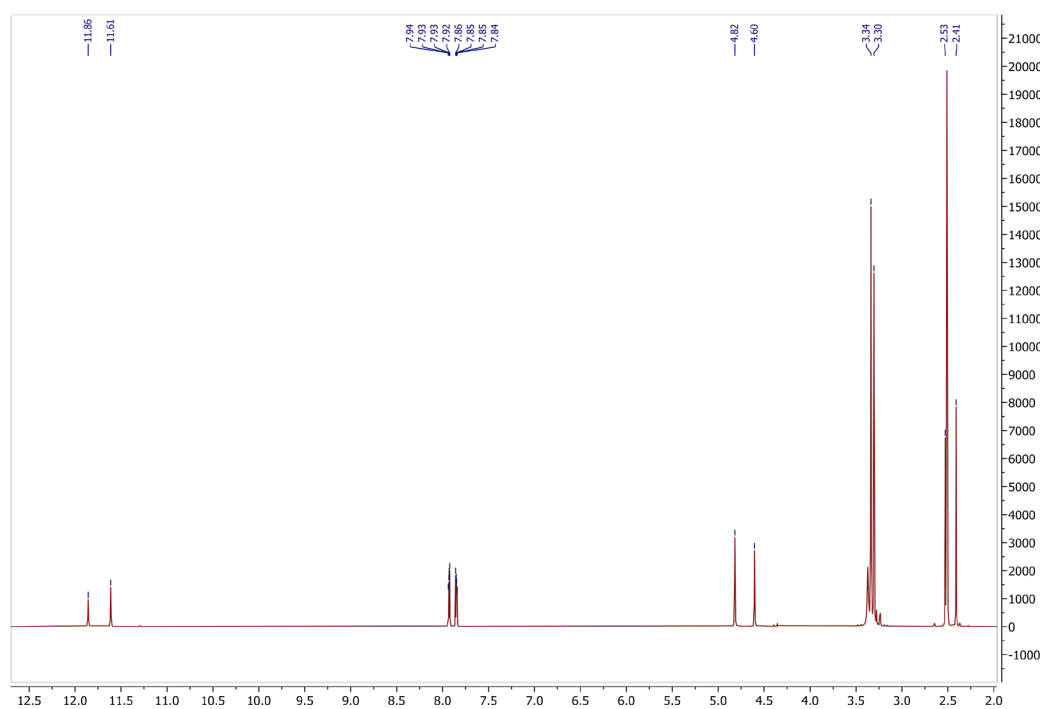
PICTURE 43: ^{13}C NMR for *1-(1-(oct-1-yn-1-yl)cyclohexyl)piperidine* 4i

PICTURE 44: ^1H NMR for *1-(1-(phenylethynyl)cyclopentyl)piperidine* 4j

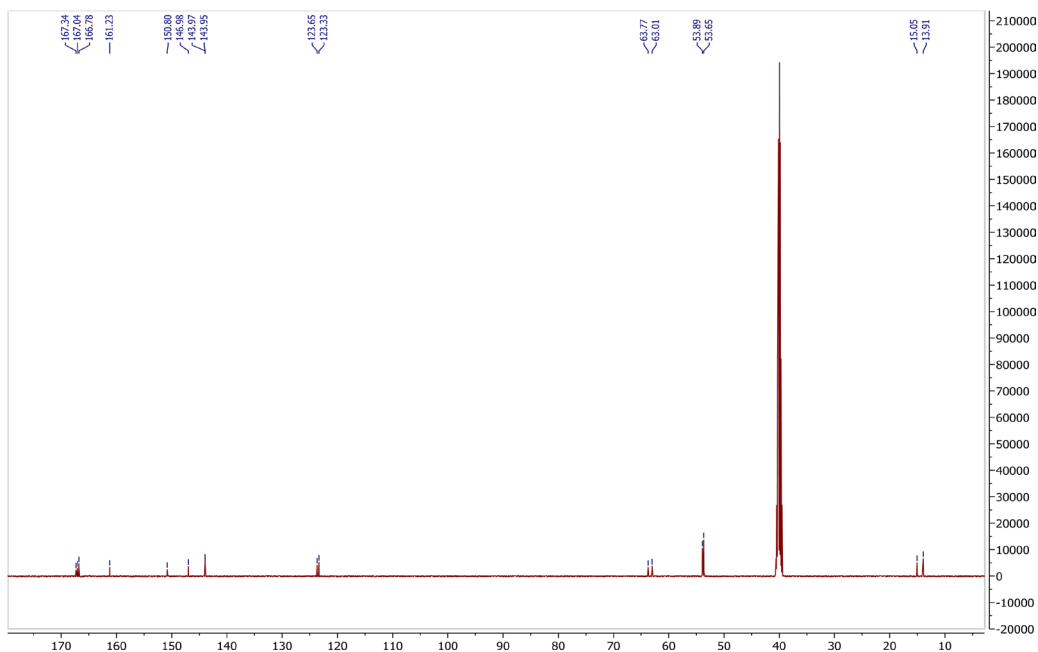
PICTURE 45: ^{13}C NMR for *1-(1-(phenylethynyl)cyclopentyl)piperidine* 4j



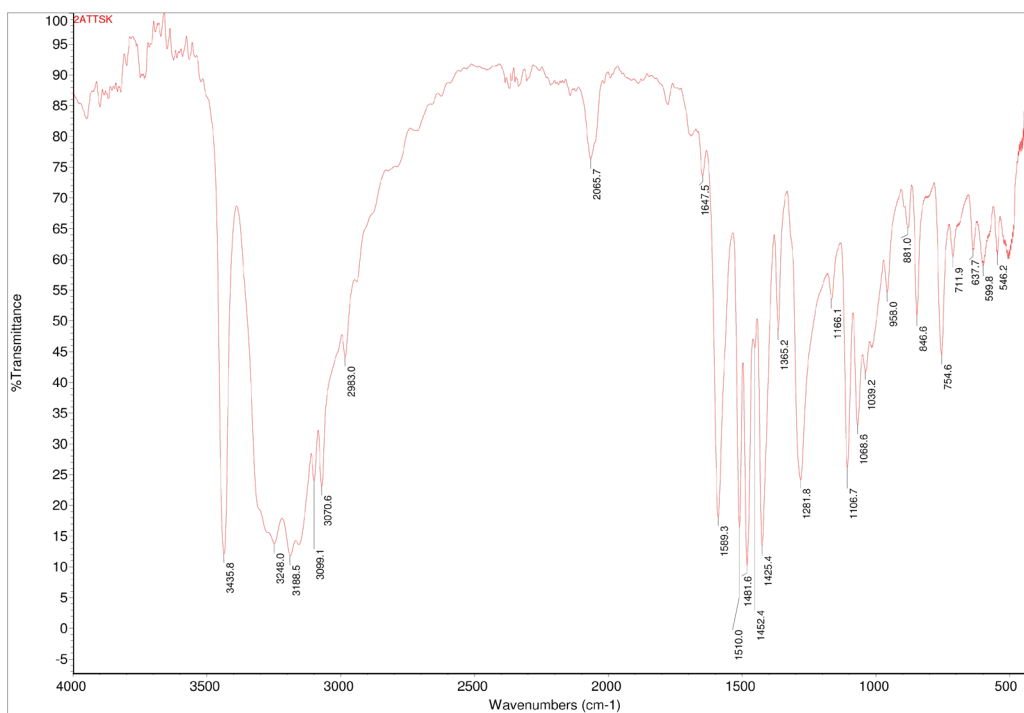
PICTURE 1: IR Spectra for ligand **HL¹Cl** (E)-N,N,N-trimethyl-2-oxo-2-(2-(1-(thiazol-2-yl)ethylidene)hydrazinyl)ethan-1-aminium chloride



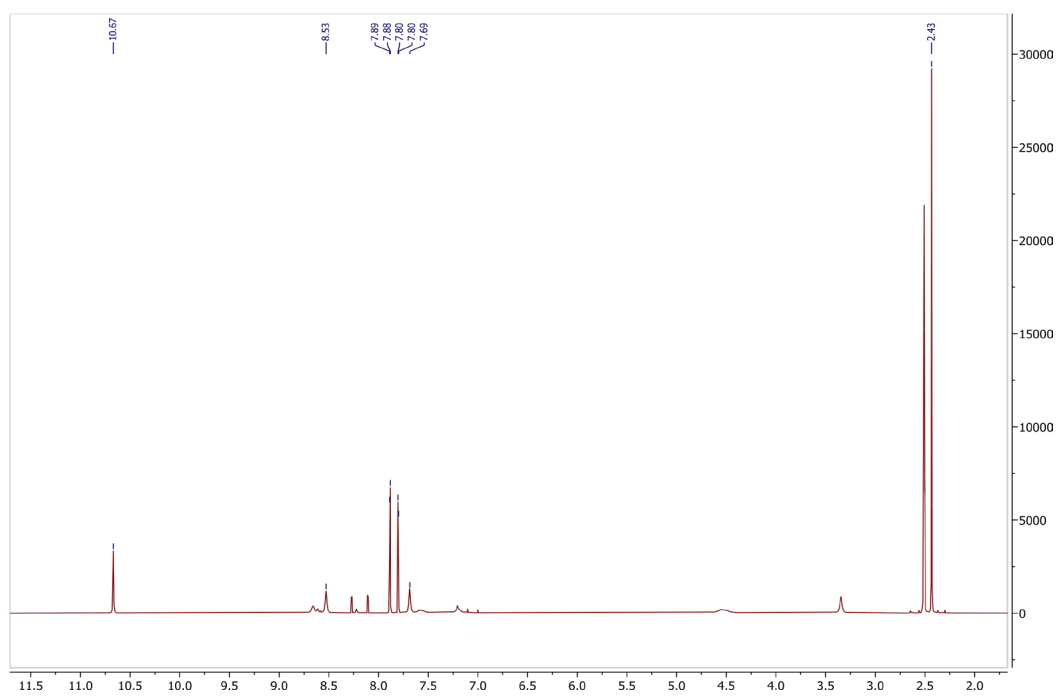
PICTURE 2: ¹H NMR Spectra for ligand **HL¹Cl** (E)-N,N,N-trimethyl-2-oxo-2-(2-(1-(thiazol-2-yl)ethylidene)hydrazinyl)ethan-1-aminium chloride



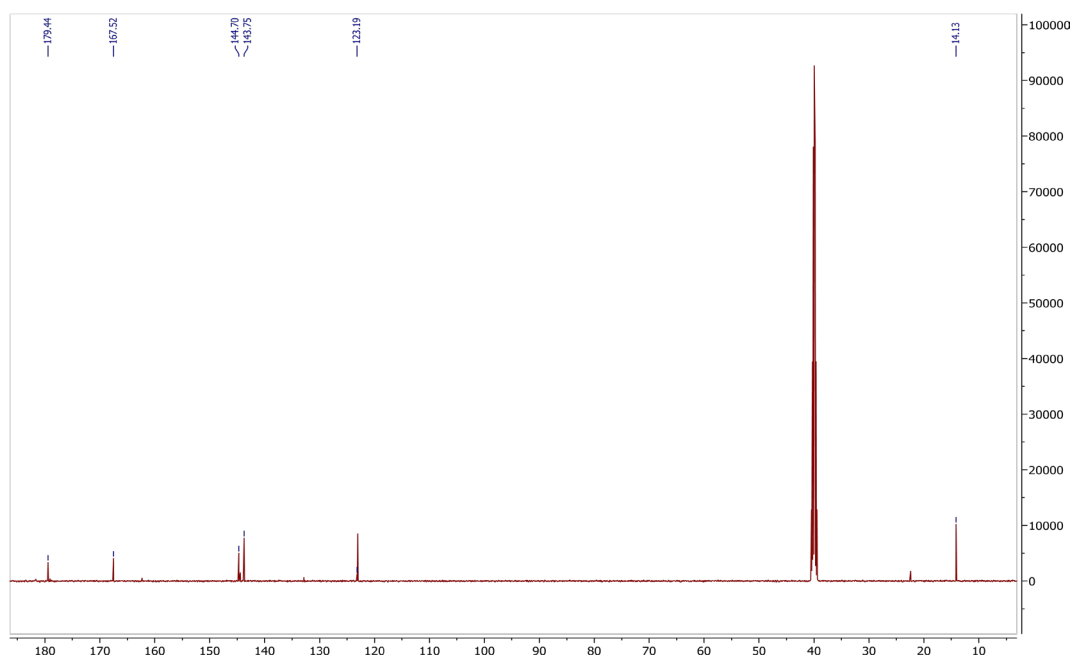
PICTURE 3: ^{13}C NMR Spectra for ligand **HL¹ Cl** (E)-N,N,N-trimethyl-2-oxo-2-(2-(1-(thiazol-2-yl)ethylidene)hydrazinyl)ethan-1-aminium chloride



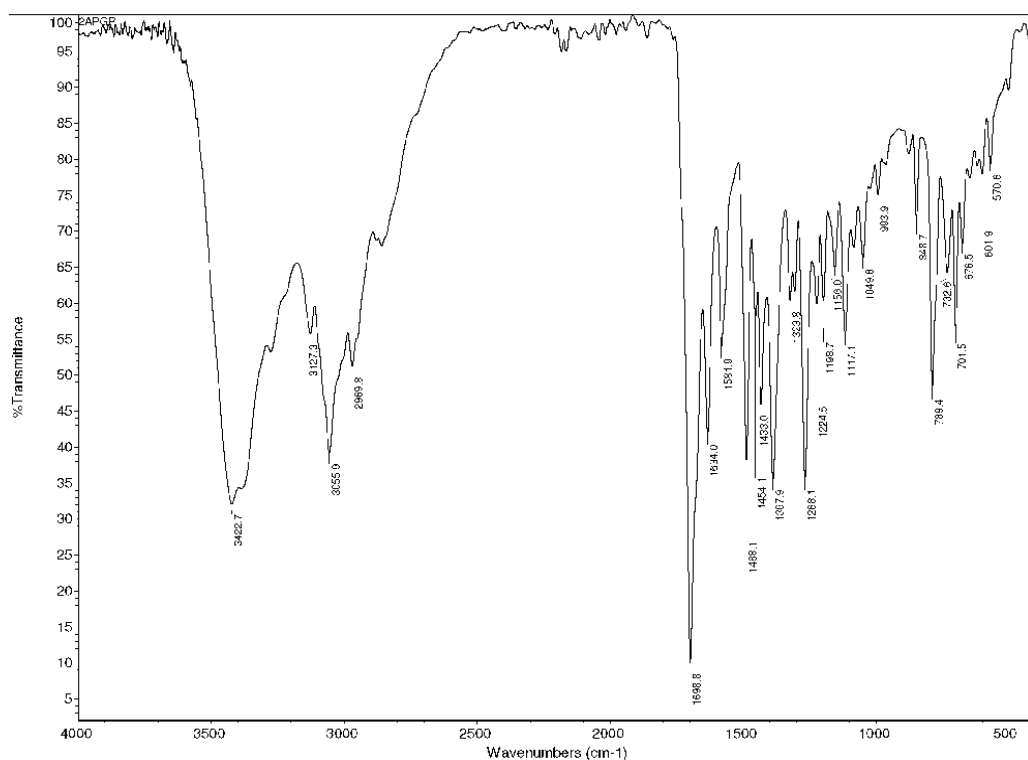
PICTURE 4: IR Spectra for ligand **HL²** (E)-2-(1-(thiazol-2-yl)ethylidene)hydrazine-1-carbothioamide



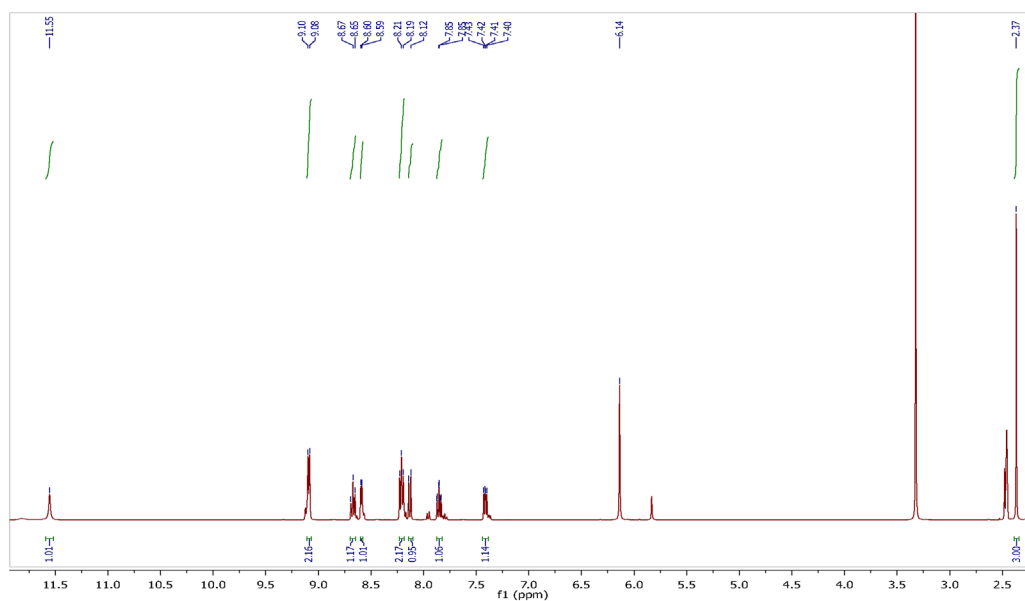
PICTURE 5: ^1H NMR Spectra for ligand **HL²** (E)-2-(1-(thiazol-2-yl)ethylidene)hydrazine-1-carbothioamide



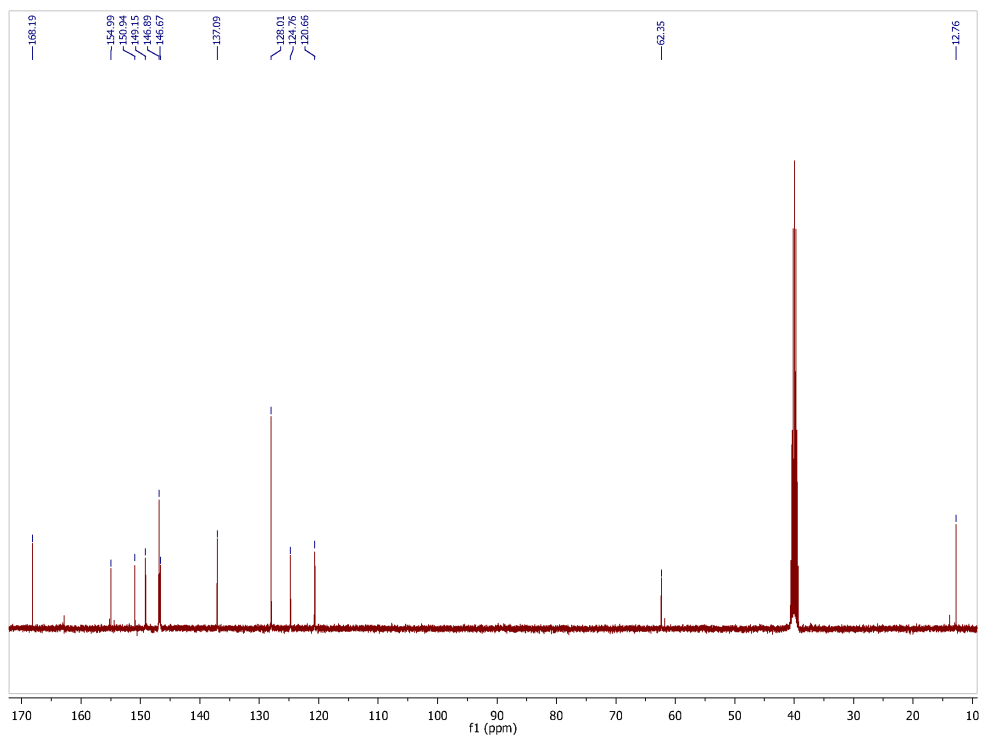
PICTURE 6: ^{13}C NMR Spectra for ligand **HL²** (E)-2-(1-(thiazol-2-yl)ethylidene)hydrazine-1-carbothioamide



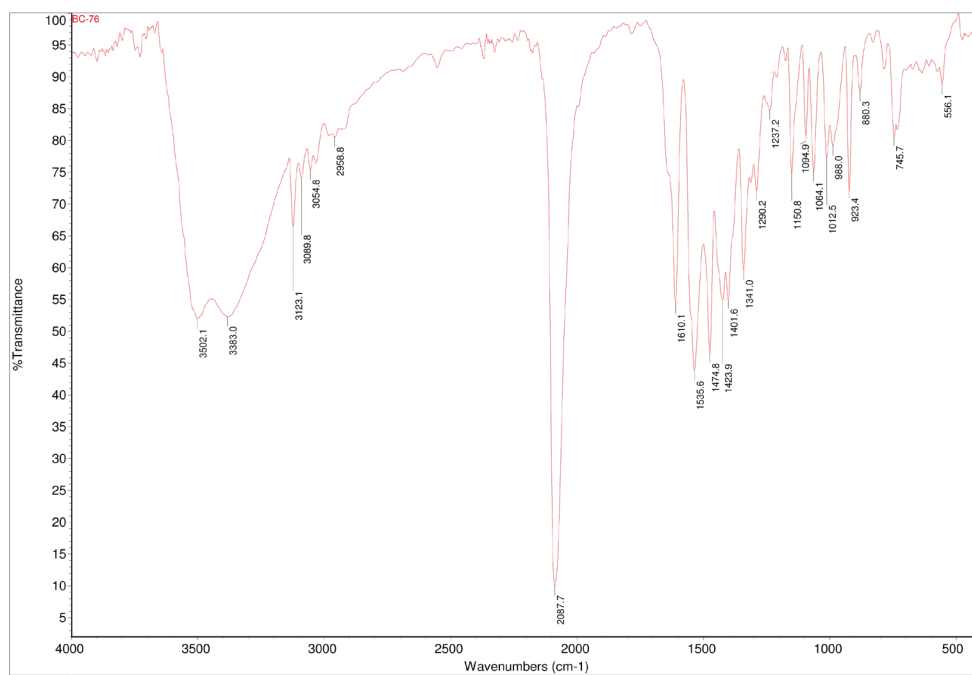
PICTURE 7: IR Spectra for ligand **HL⁴Cl** (E)-1-(2-oxo-2-(2-(1-(pyridin-2-yl)ethylidene)hydrazinyl)ethyl)-pyridine-1-ium chloride



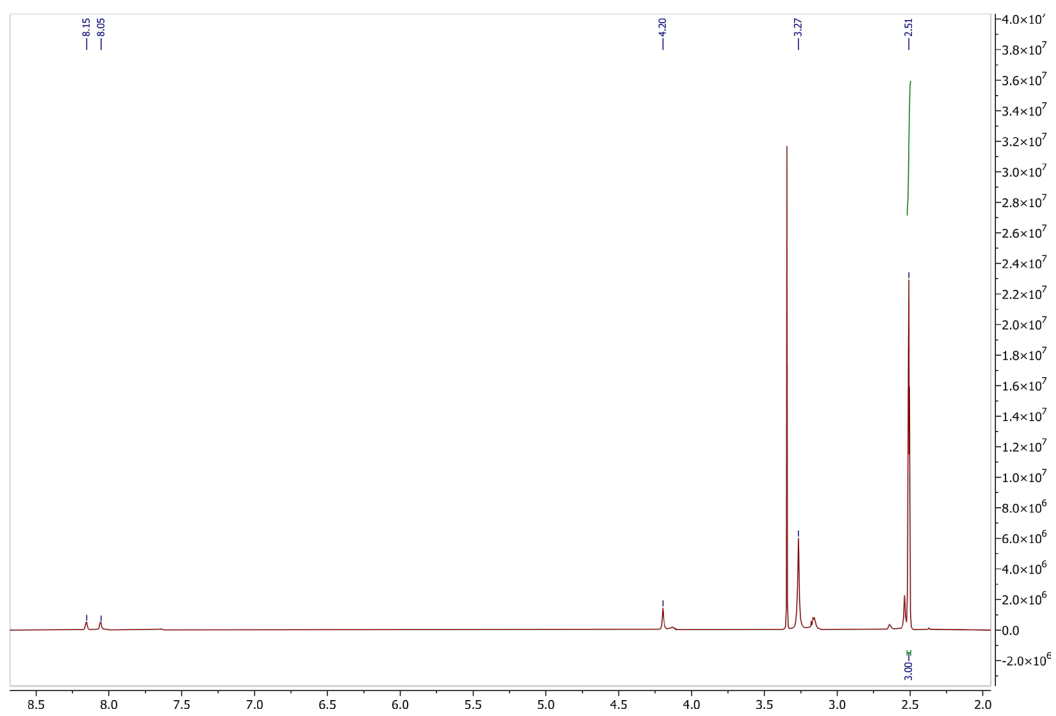
PICTURE 8: ¹H NMR Spectra for ligand **HL⁴Cl** (E)-1-(2-oxo-2-(2-(1-(pyridin-2-yl)ethylidene)hydrazinyl)ethyl)-pyridine-1-ium chloride



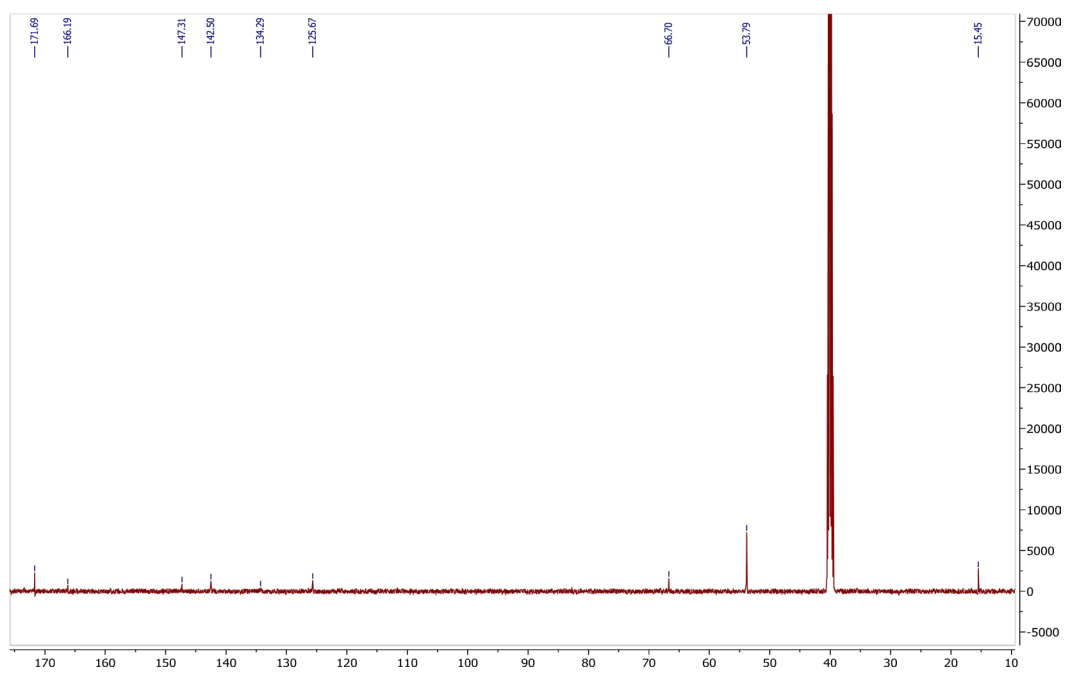
PICTURE 9: ^{13}C NMR Spectra for ligand HL^4Cl (E)-1-(2-oxo-2-(2-(1-(pyridin-2-yl)ethylidene)hydrazinyl)ethyl)-pyridine-1-ium chloride



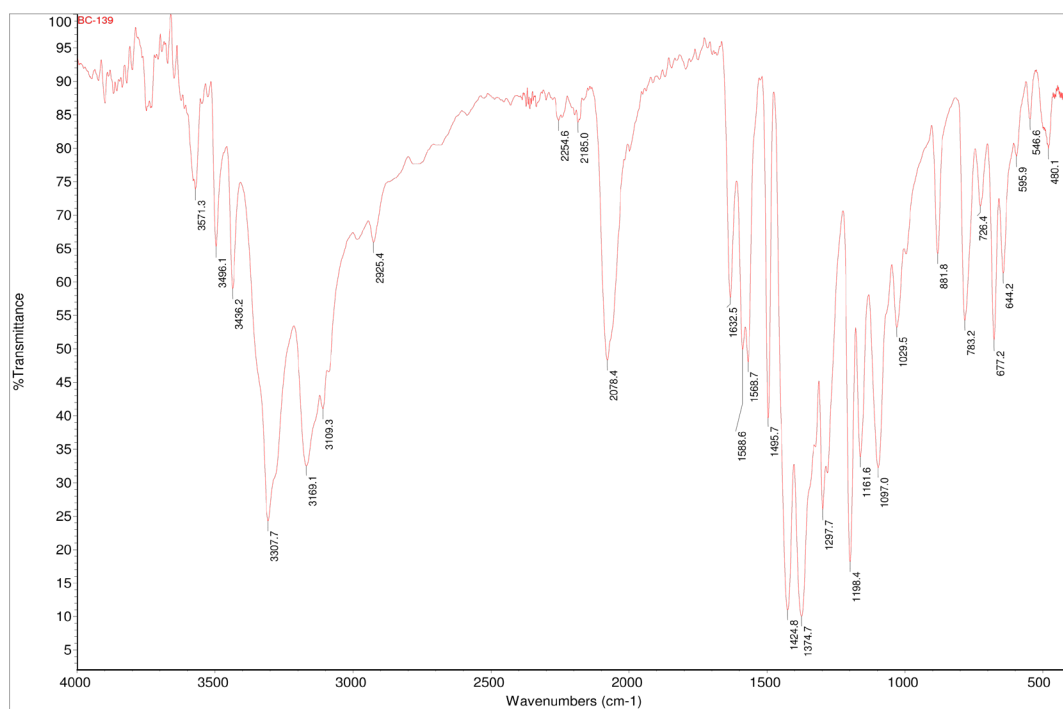
PICTURE 10: IR Spectra for complex 1 $[\text{ZnL}^1(\text{NCS})_2] \cdot 2\text{H}_2\text{O}$



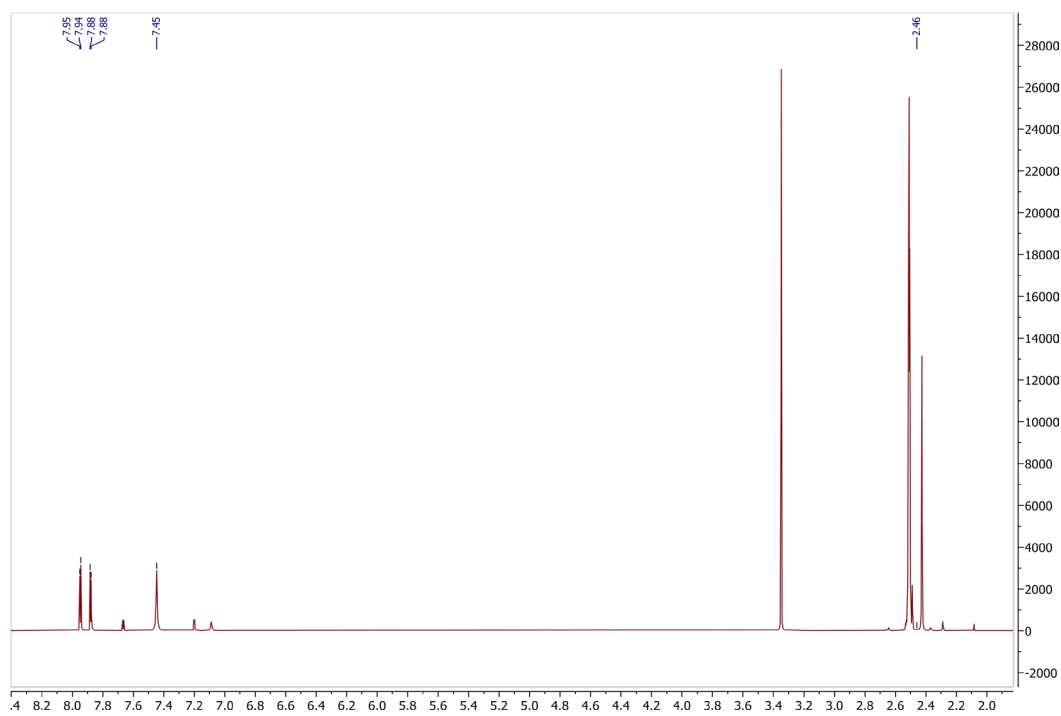
PICTURE 11: ^1H NMR Spectra for complex 1 $[\text{ZnL}^1(\text{NCS})_2] \cdot 2\text{H}_2\text{O}$



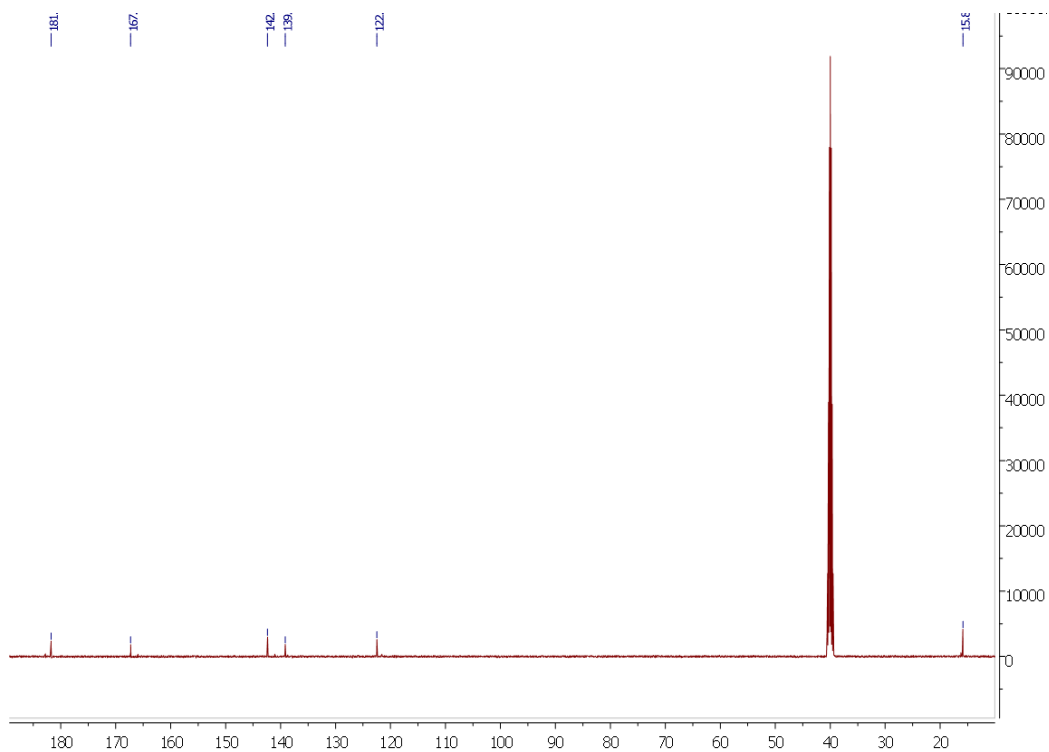
PICTURE 12: ^{13}C NMR Spectra for complex 1 $[\text{ZnL}^1(\text{NCS})_2] \cdot 2\text{H}_2\text{O}$



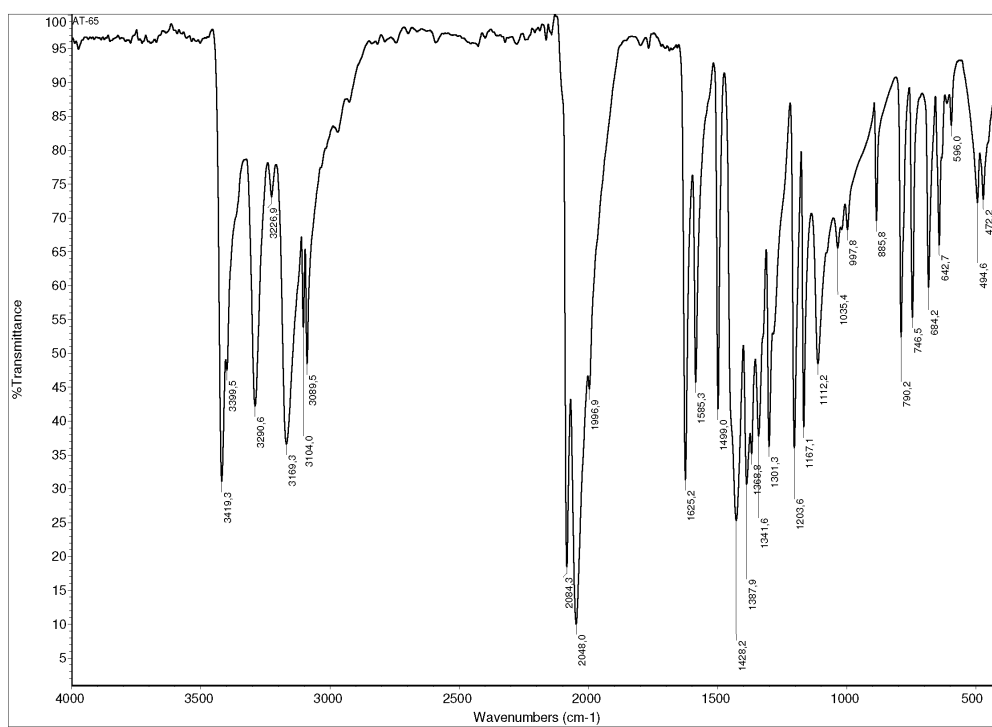
PICTURE 13: IR Spectra for complex 2 [Zn(L²)₂]



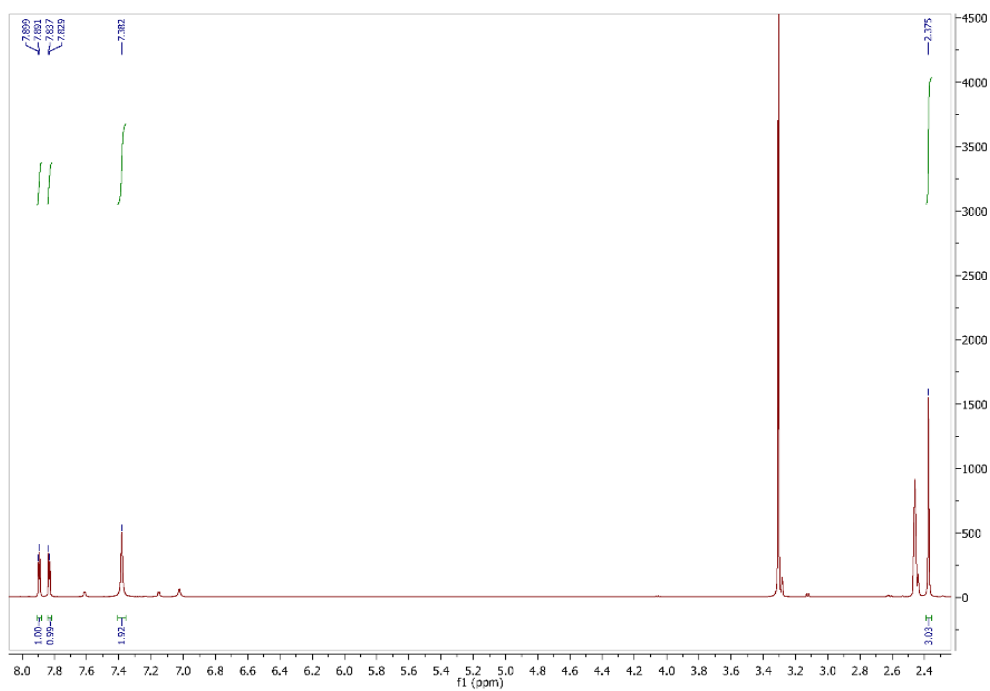
PICTURE 14: ¹H NMR Spectra for complex 2 [Zn(L²)₂]



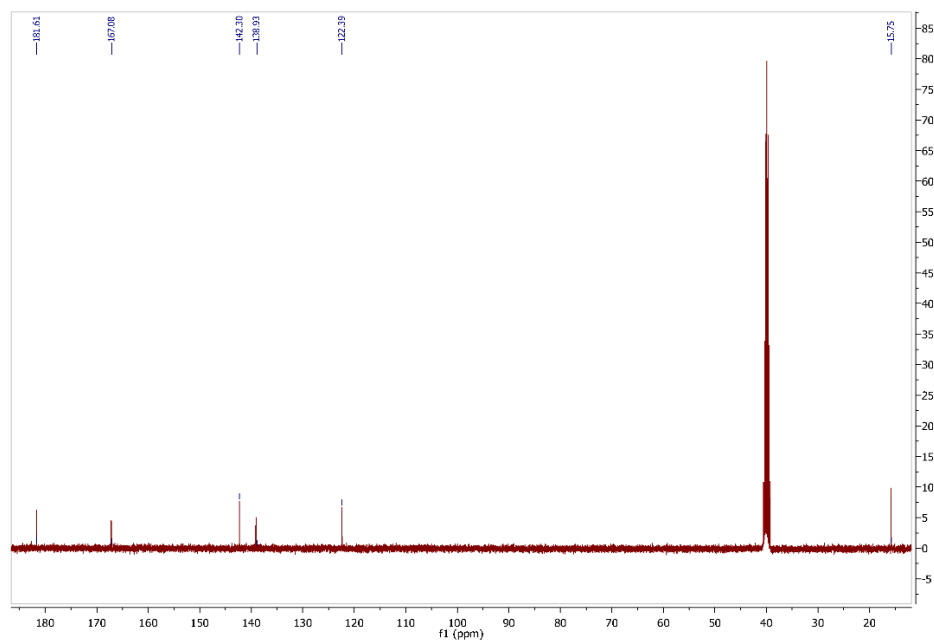
PICTURE 15: ¹³C NMR Spectra for complex 2 [Zn(L²)₂]



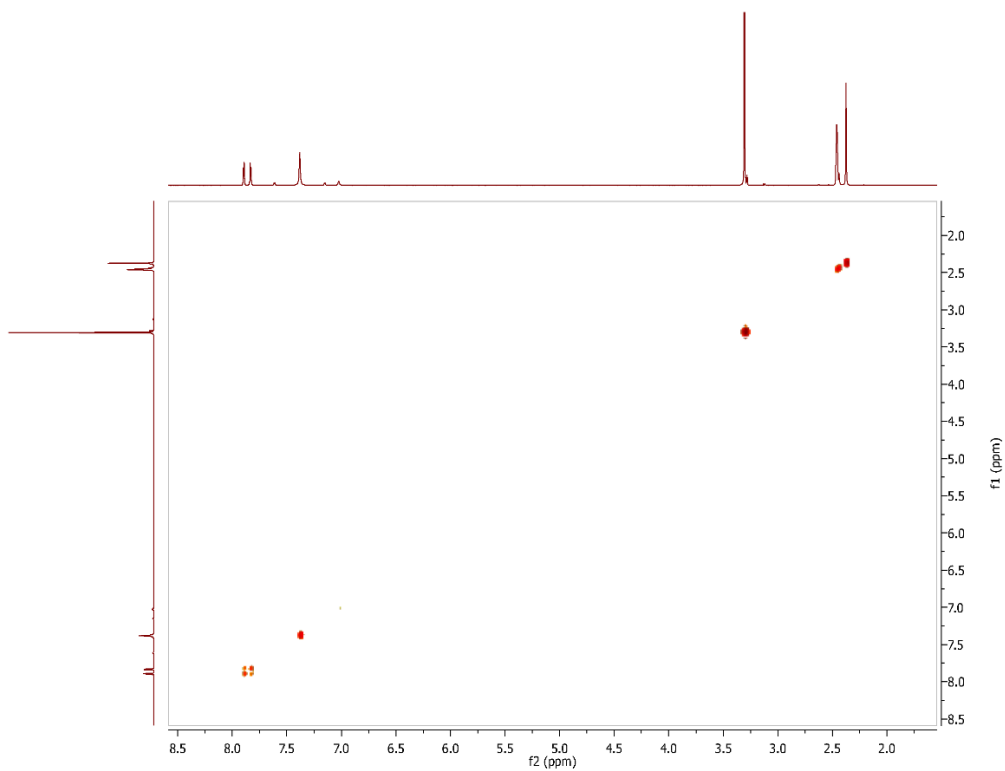
PICTURE 16: IR Spectra for complex 5 [ZnL²(N₃)₂]



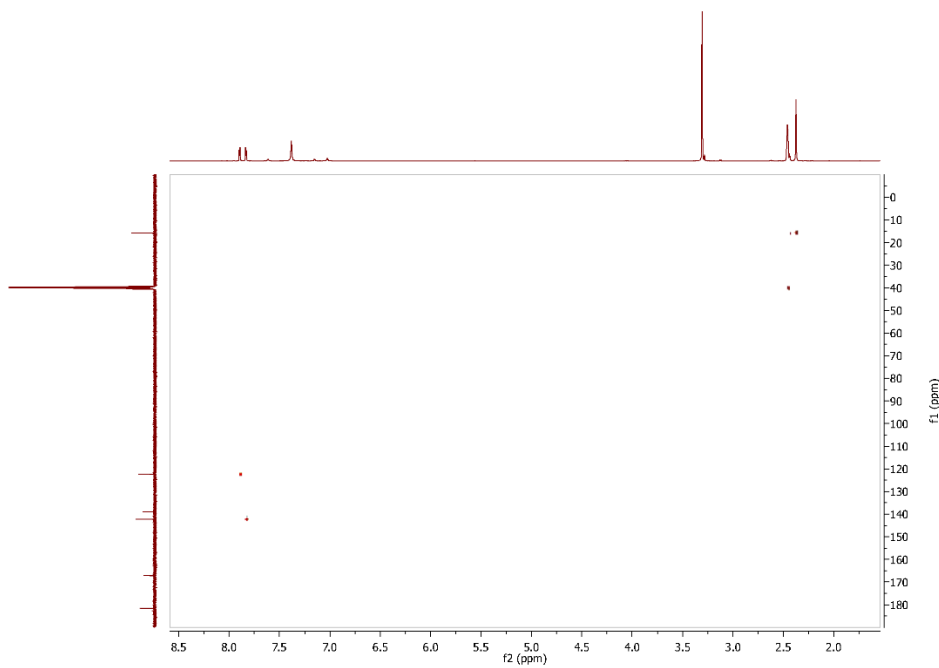
PICTURE 17: ¹H NMR Spectra for complex 5 [ZnL²(N₃)₂]



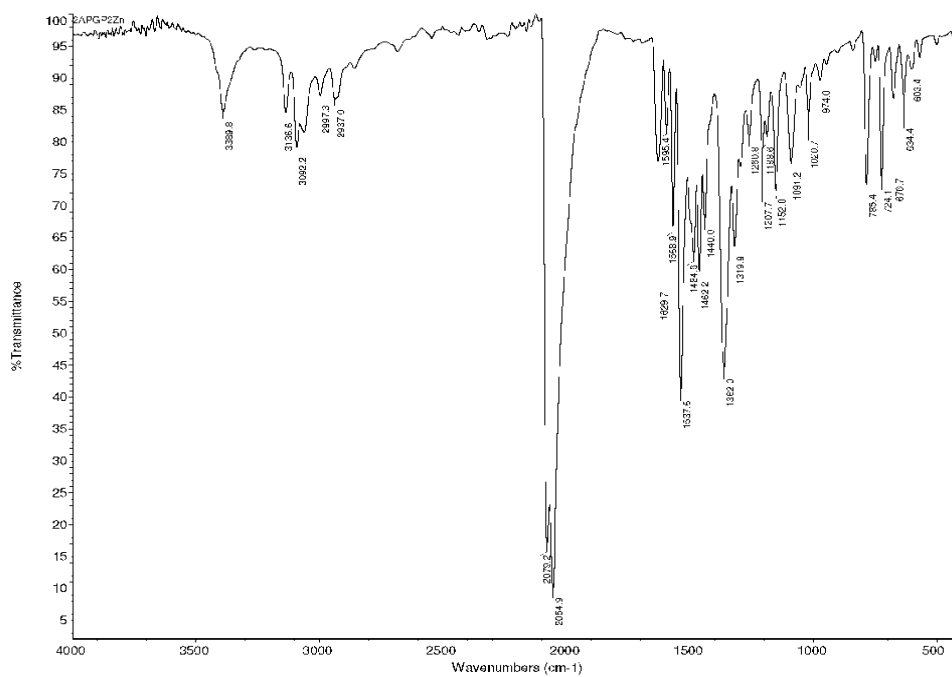
PICTURE 18: ¹³C NMR Spectra for complex 5 [ZnL²(N₃)₂]



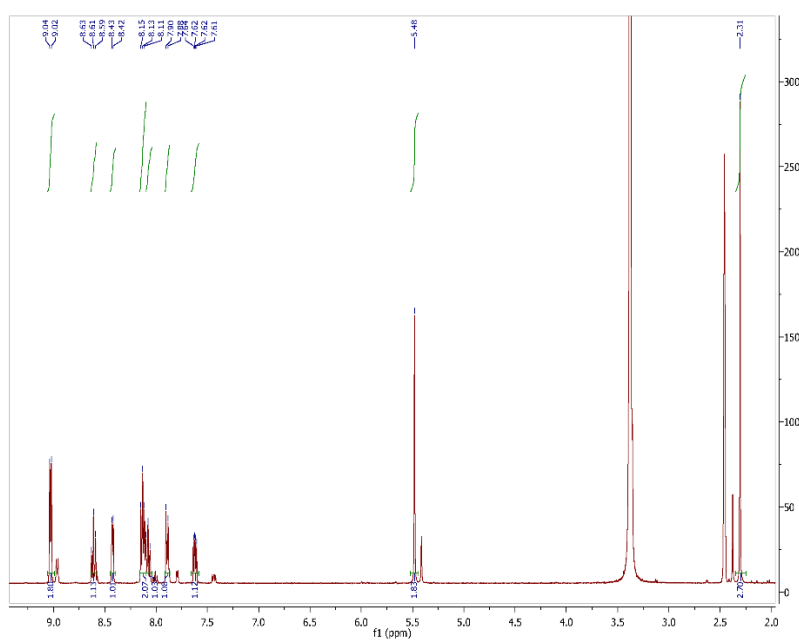
PICTURE 19: COSY NMR Spectra for complex 5 $[\text{ZnL}^2(\text{N}_3)_2]$



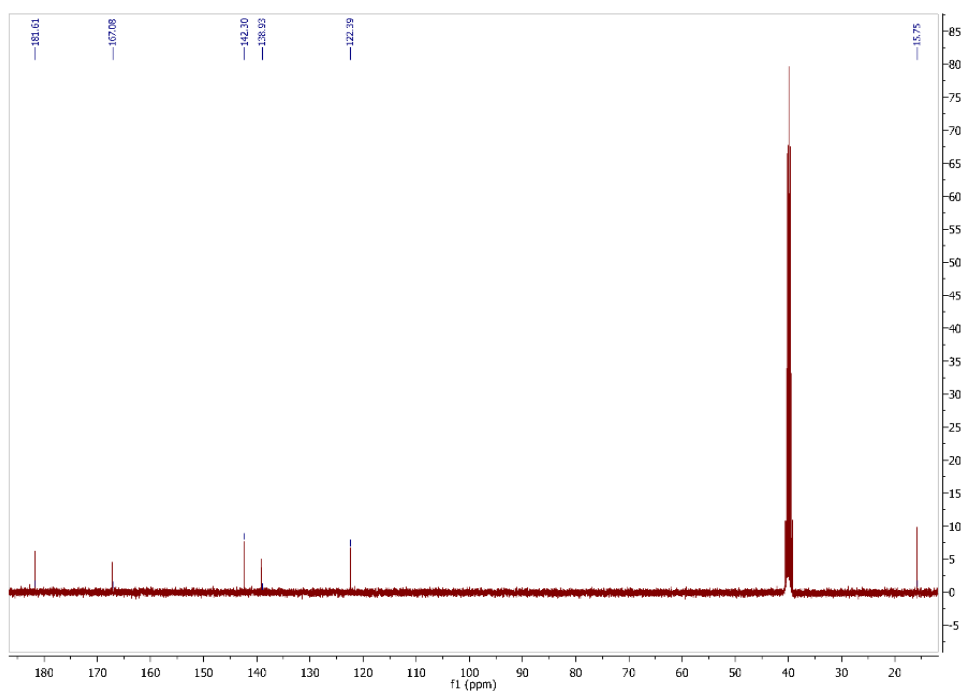
PICTURE 20: HSQC NMR Spectra for complex 5 $[\text{ZnL}^2(\text{N}_3)_2]$



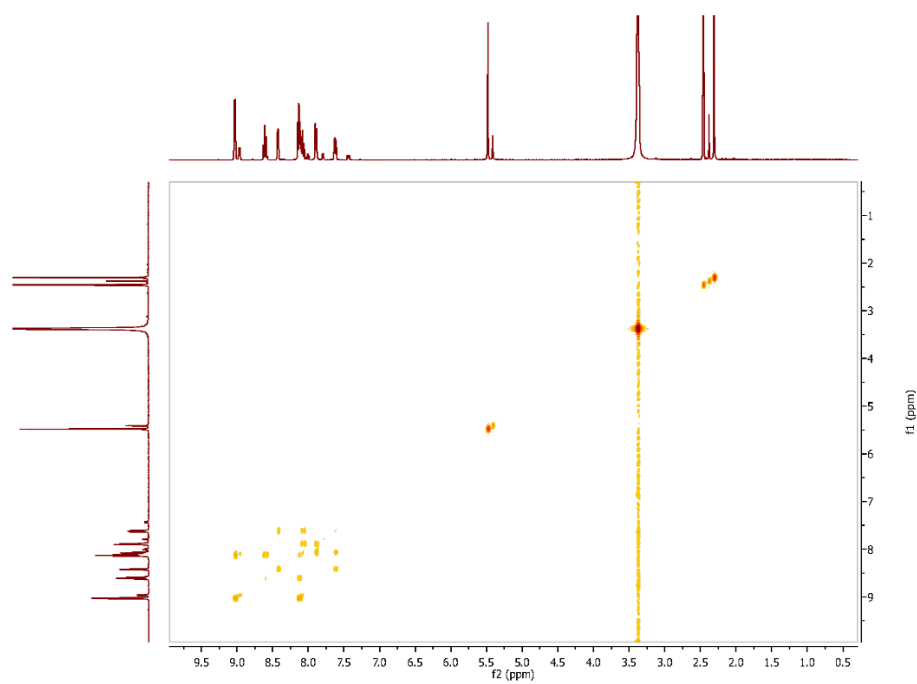
PICTURE 21: IR Spectra for complex 6 [ZnL⁴(N₃)₂]



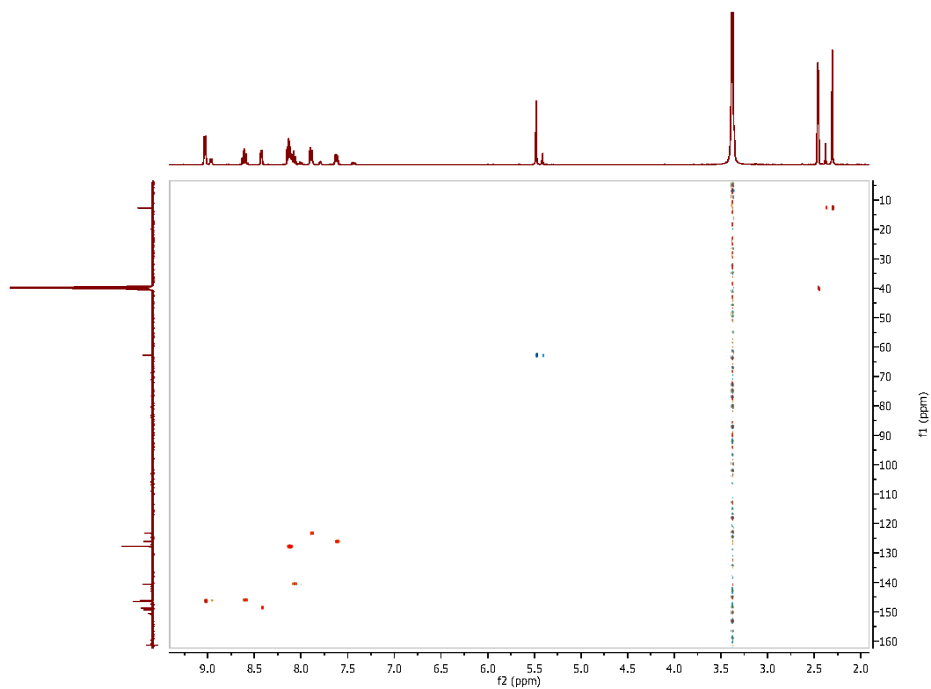
PICTURE 22: ¹H NMR Spectra for complex 6 [ZnL⁴(N₃)₂]



PICTURE 23: ^{13}C NMR Spectra for complex 6 $[\text{ZnL}^4(\text{N}_3)_2]$

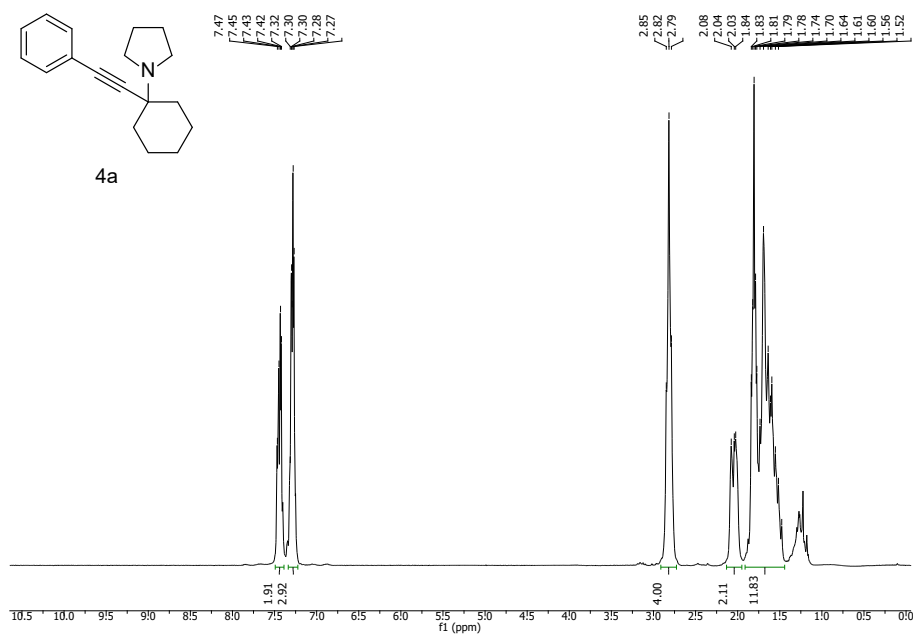


PICTURE 24: COSY NMR Spectra for complex 6 $[\text{ZnL}^4(\text{N}_3)_2]$

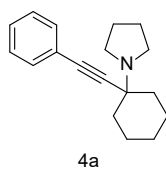


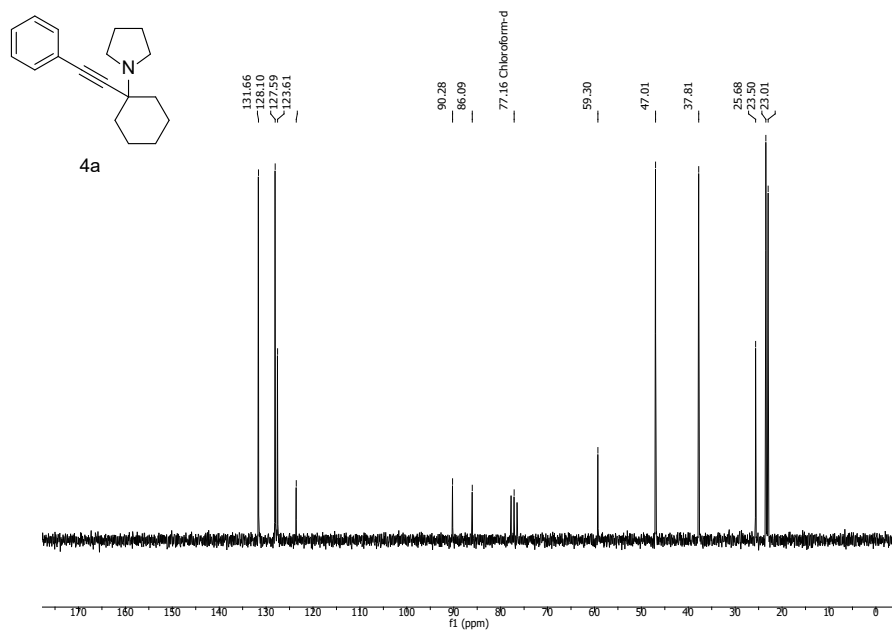
PICTURE 25: HSQC NMR Spectra for complex 6 $[\text{ZnL}^4(\text{N}_3)_2]$

^1H and $^{13}\text{C}\{^1\text{H}\}$ NMR spectra of the synthesized propargylamines

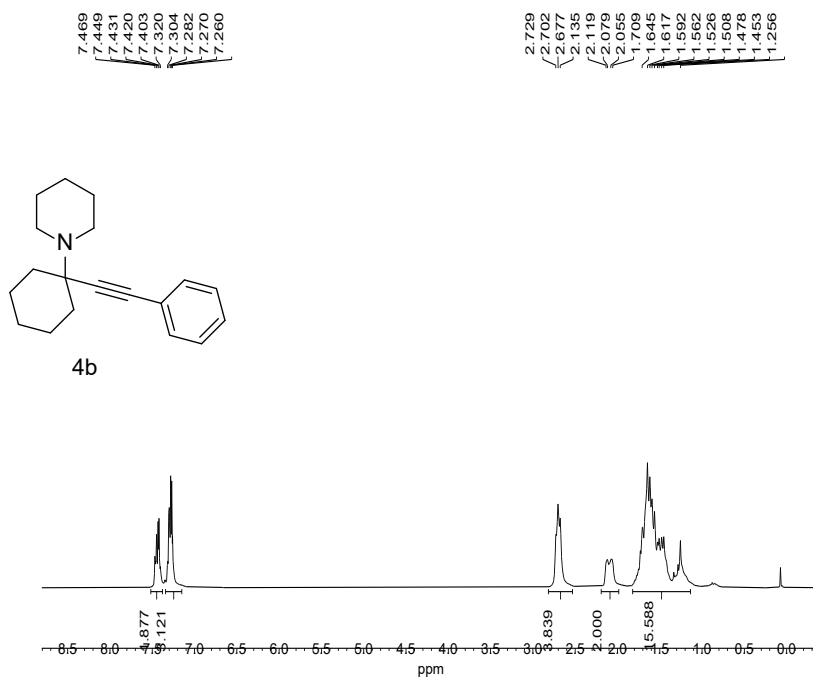


PICTURE 26: ^1H NMR for 1-(1-(phenylethynyl)cyclohexyl)pyrrolidine 4a

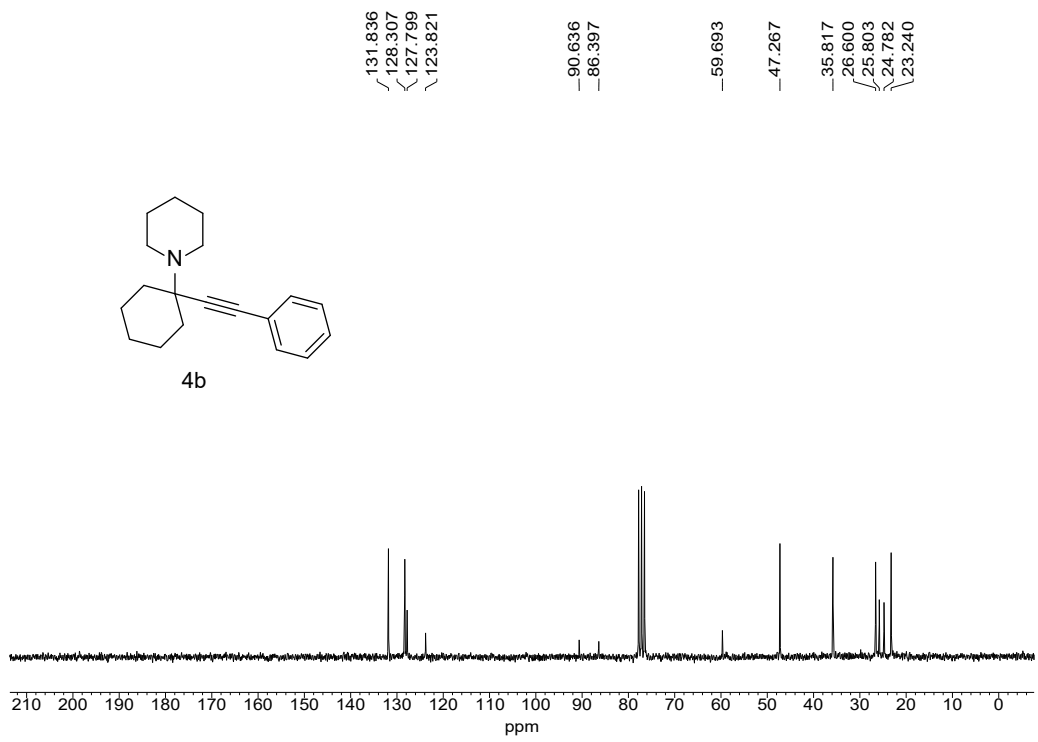




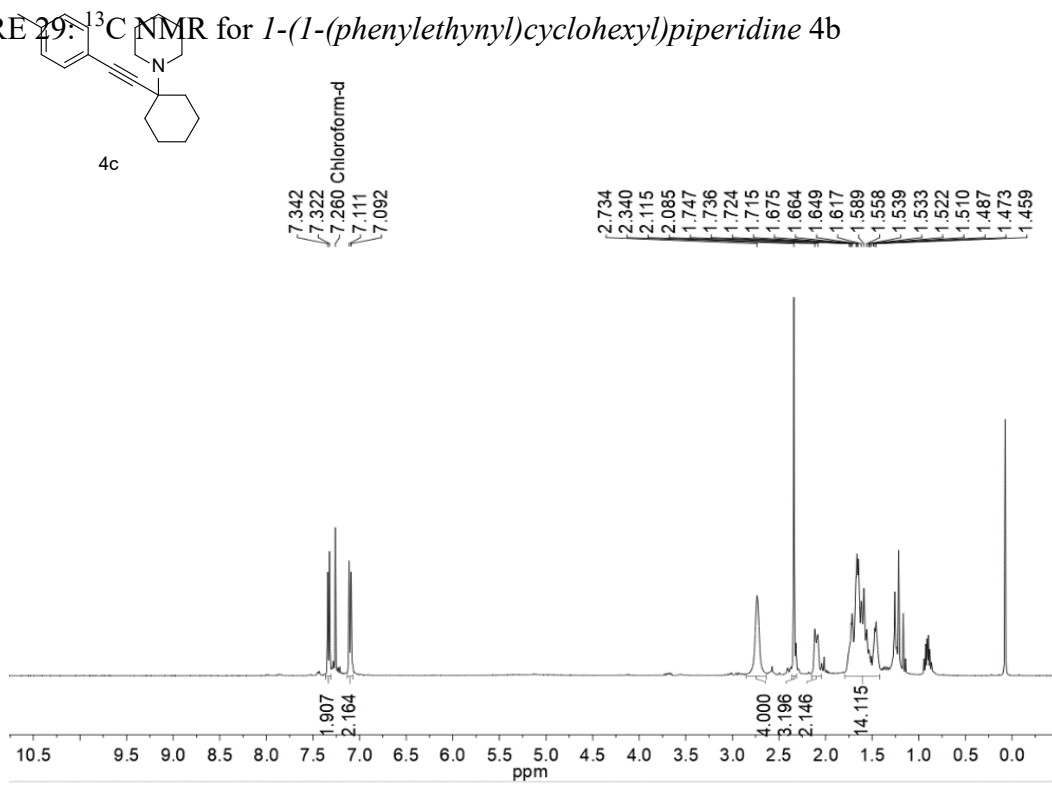
PICTURE 27: ¹³C NMR for 1-(1-(phenylethynyl)cyclohexyl)pyrrolidine 4a



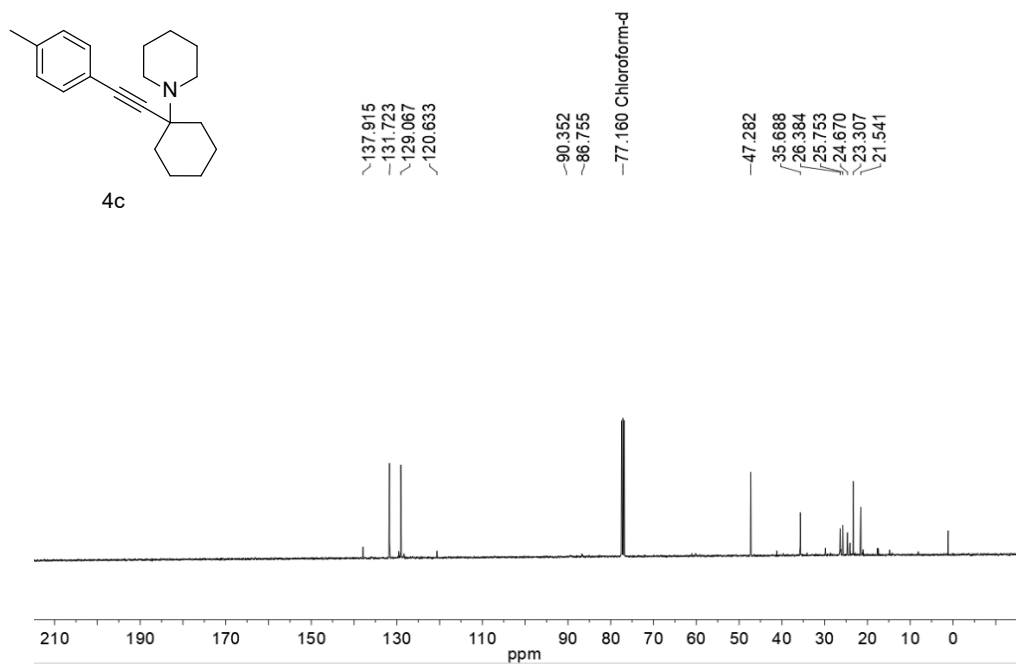
PICTURE 28: ¹H NMR for 1-(1-(phenylethynyl)cyclohexyl)piperidine 4b



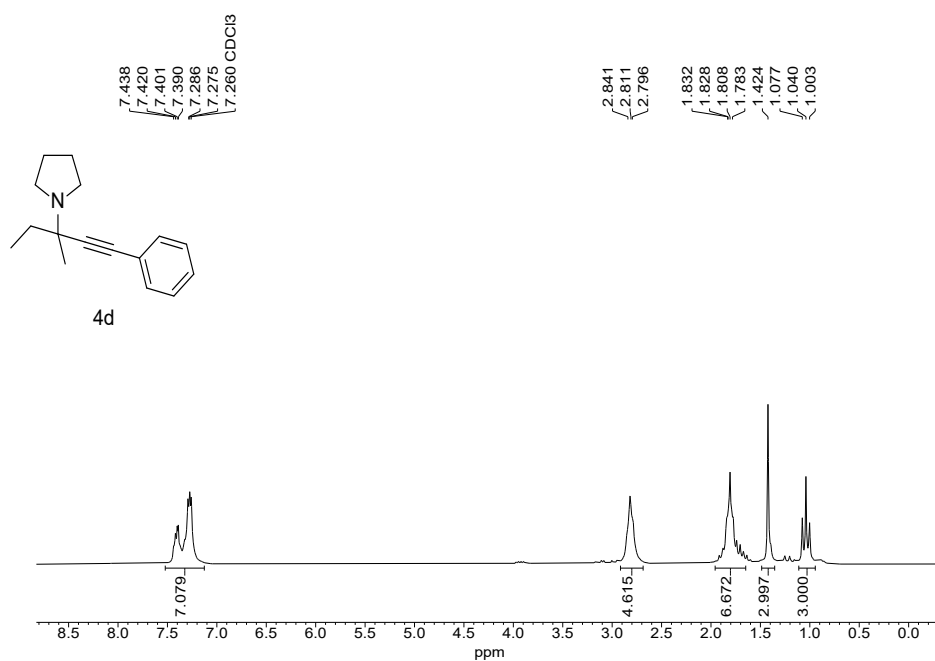
PICTURE 29: ¹³C NMR for 1-(1-(phenylethynyl)cyclohexyl)piperidine 4b



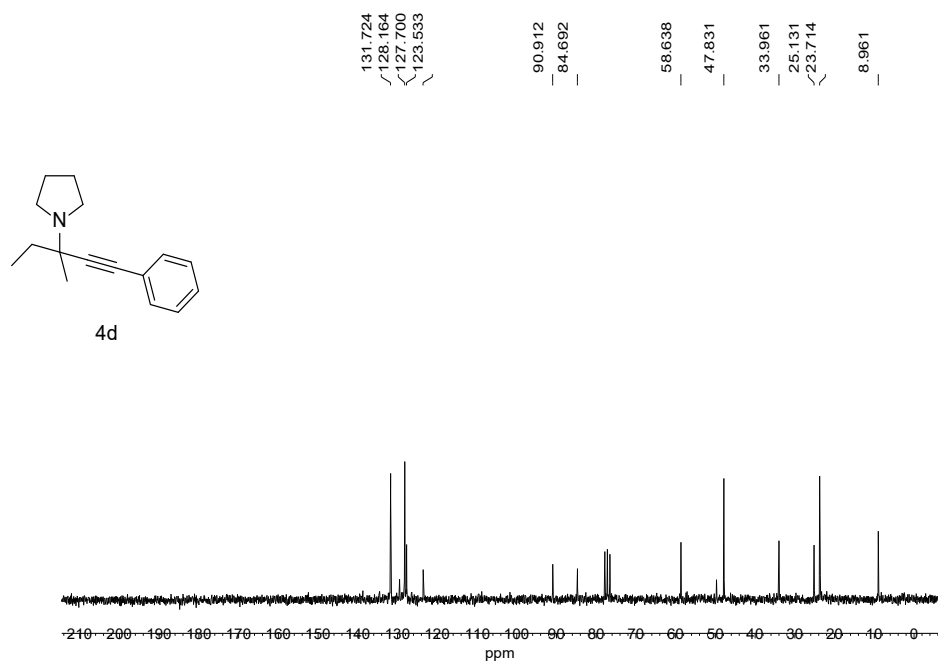
PICTURE 30: ¹H NMR for 1-(1-(p-tolylethynyl)cyclohexyl)piperidine 4c



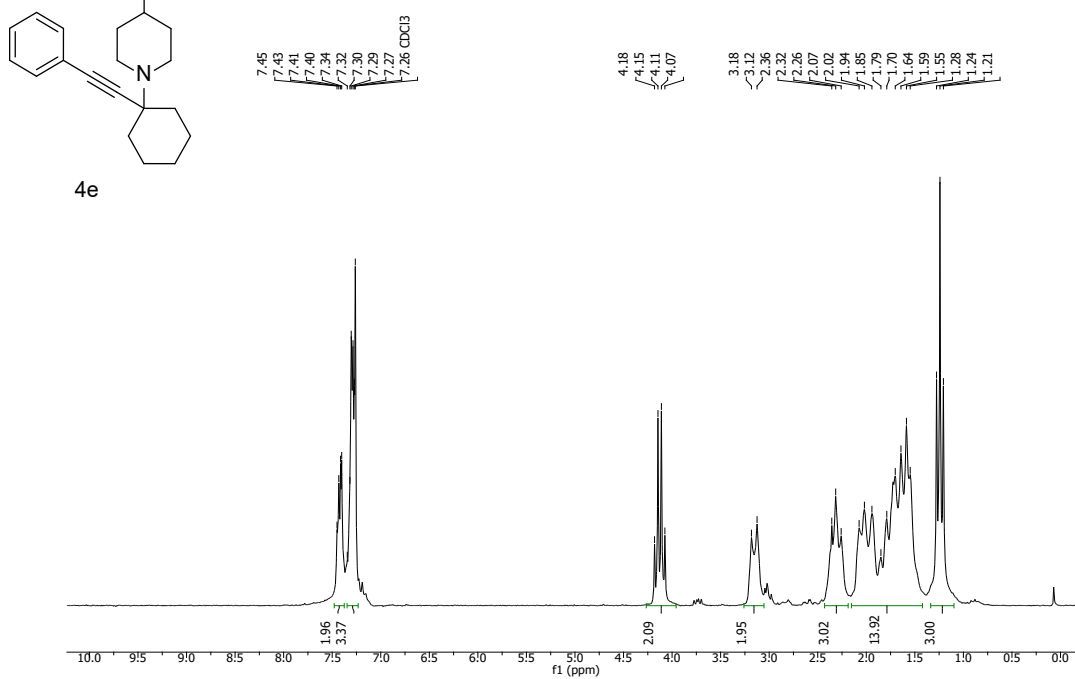
PICTURE 31: ¹³C NMR for *1-(1-(p-tolylethynyl)cyclohexyl)piperidine 4c*



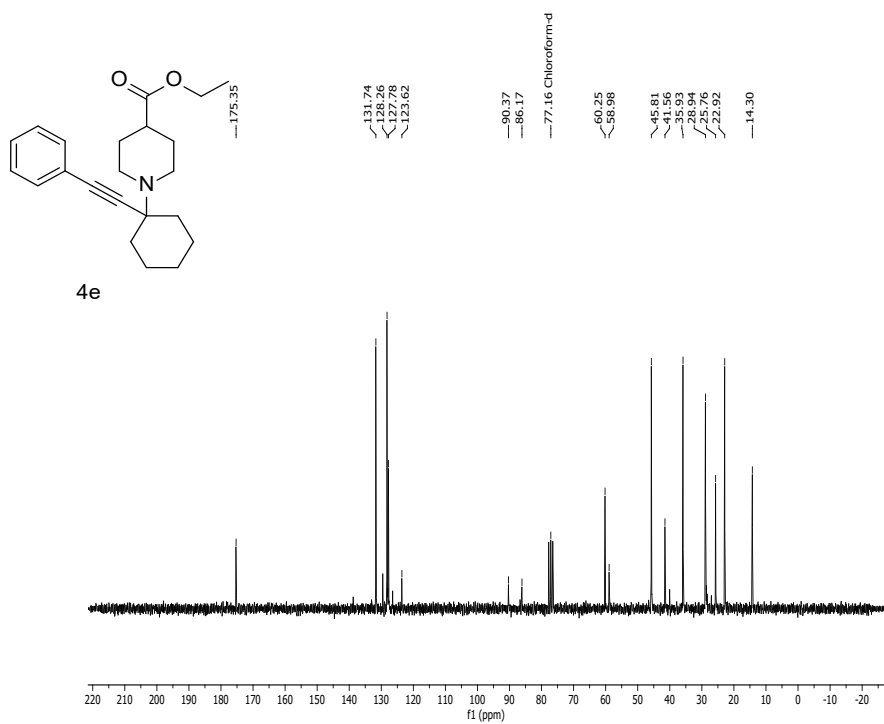
PICTURE 32: ¹H NMR for *1-(3-methyl-1-phenylpent-1-yn-3-yl)pyrrolidine 4d*



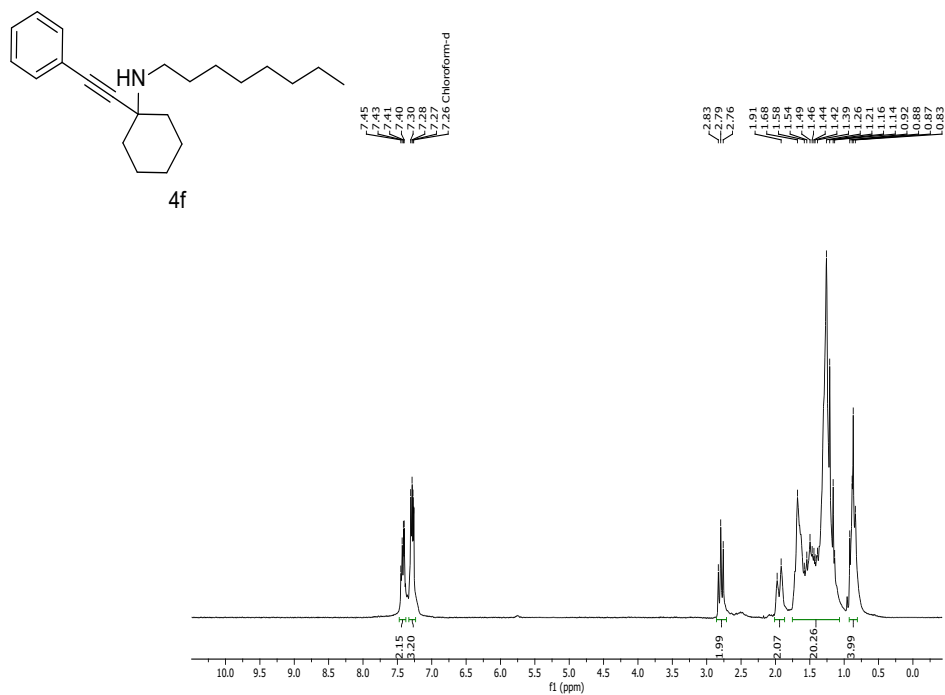
PICTURE 33: ¹³C NMR for 1-(3-methyl-1-phenylpent-1-yn-3-yl)pyrrolidine 4d



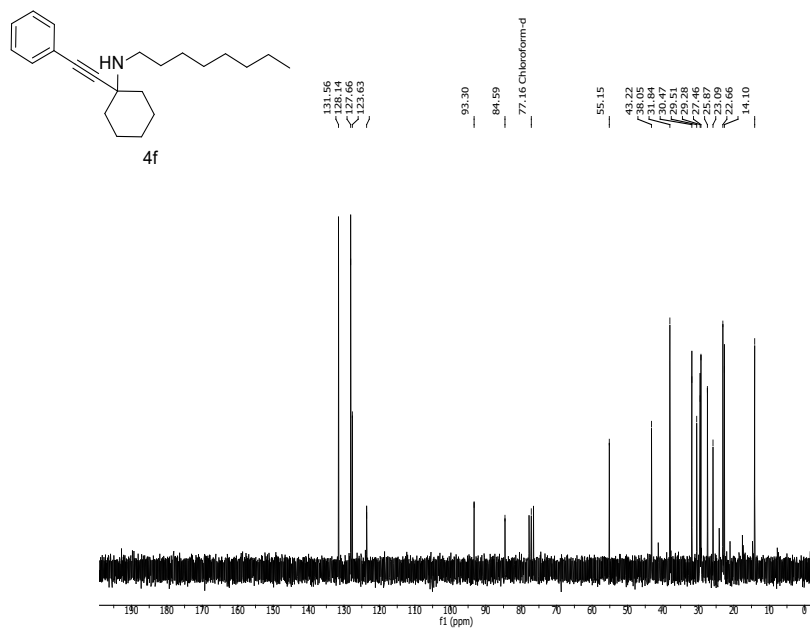
PICTURE 34: ¹H NMR for 1-(1-(phenylethynyl)cyclohexyl)piperidine-4-carboxylate 4e



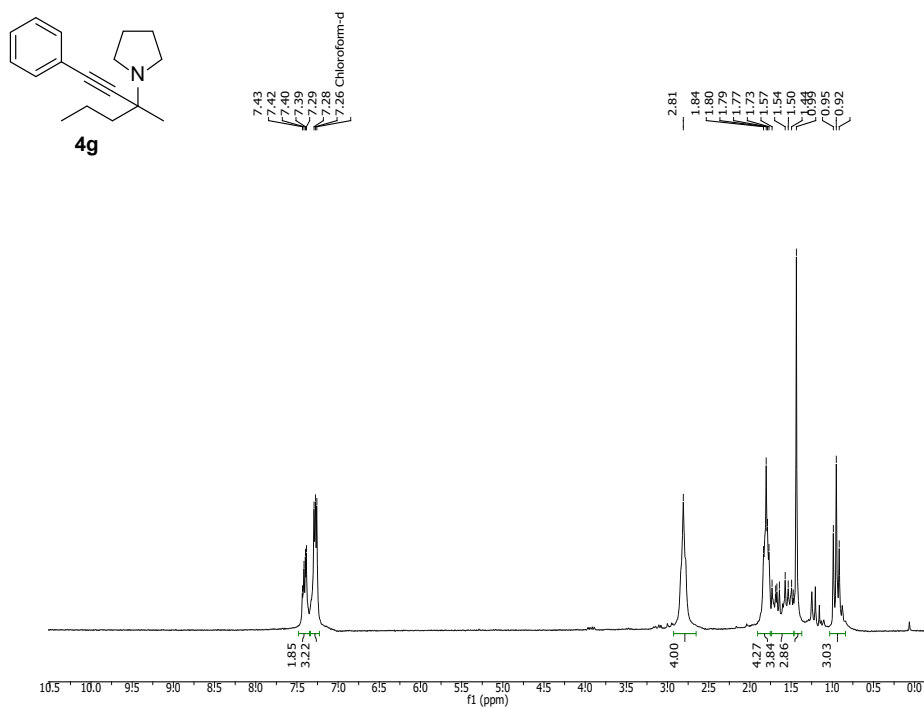
PICTURE 35: ^{13}C NMR for 1-(1-(phenylethynyl)cyclohexyl)piperidine-4-carboxylate 4e.



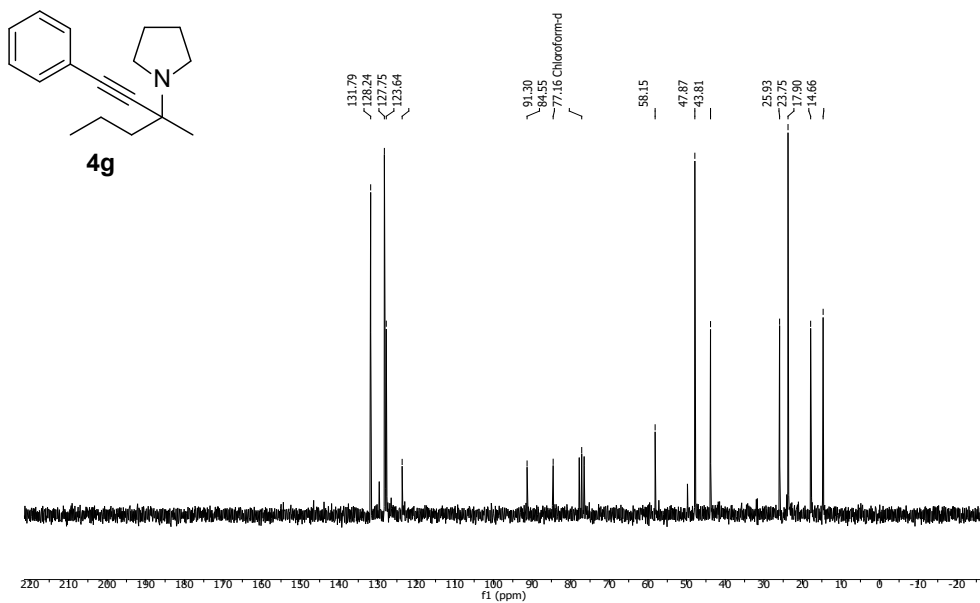
PICTURE 36: ^1H NMR for N-octyl-1-(phenylethynyl)cyclohexanamine 4f



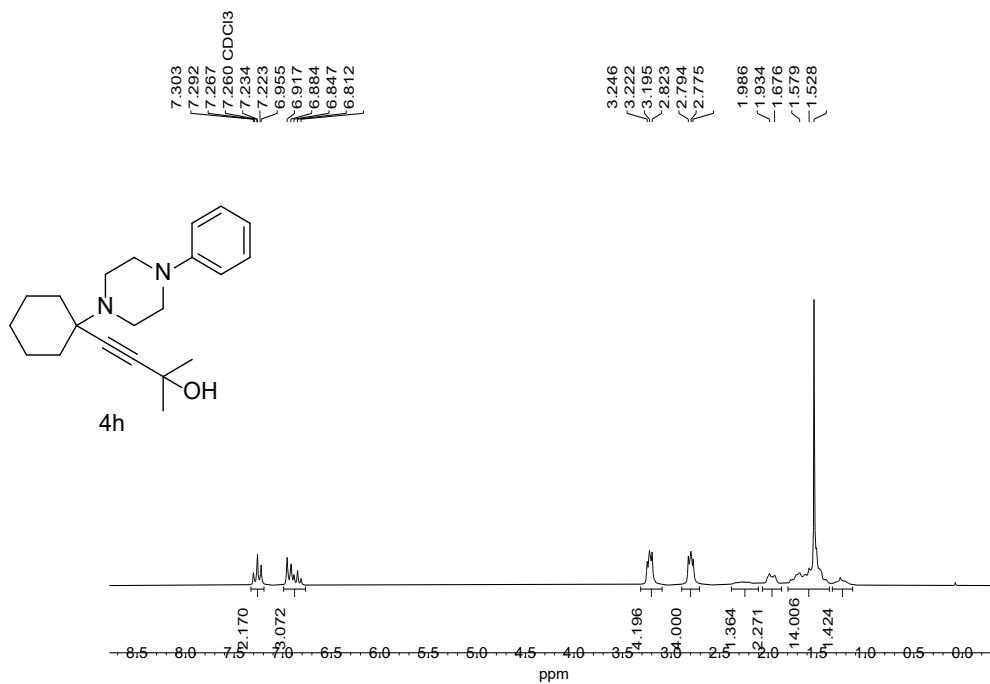
PICTURE 37: ^{13}C NMR for *N*-octyl-1-(phenylethynyl)cyclohexanamine **4f**



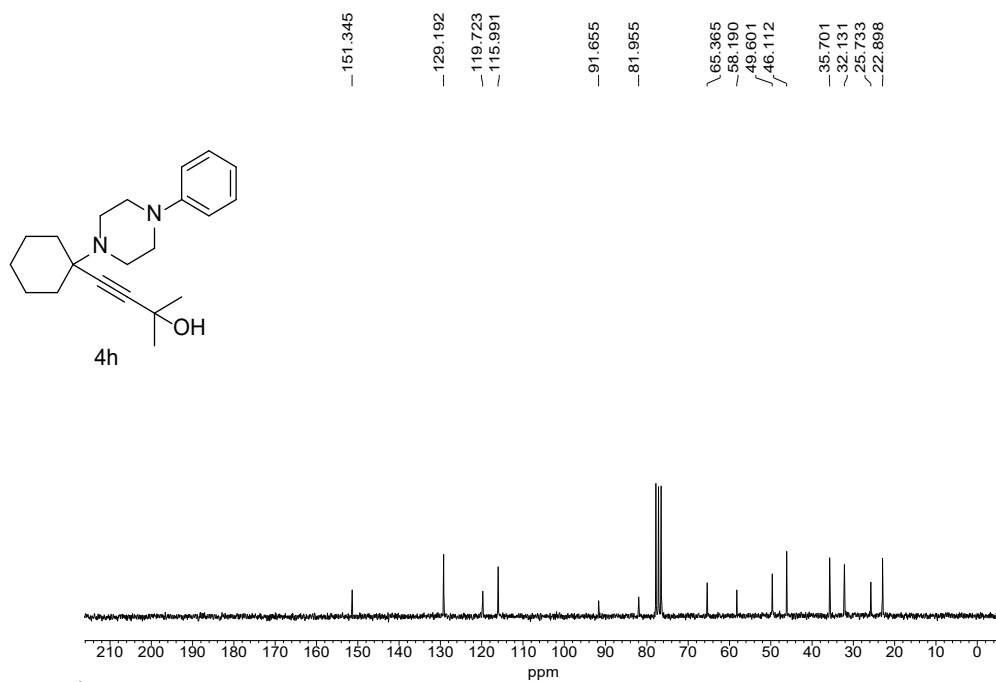
PICTURE 38: ^1H NMR for 1-(3-methyl-1-phenylhex-1-yn-3-yl)pyrrolidine **4g**



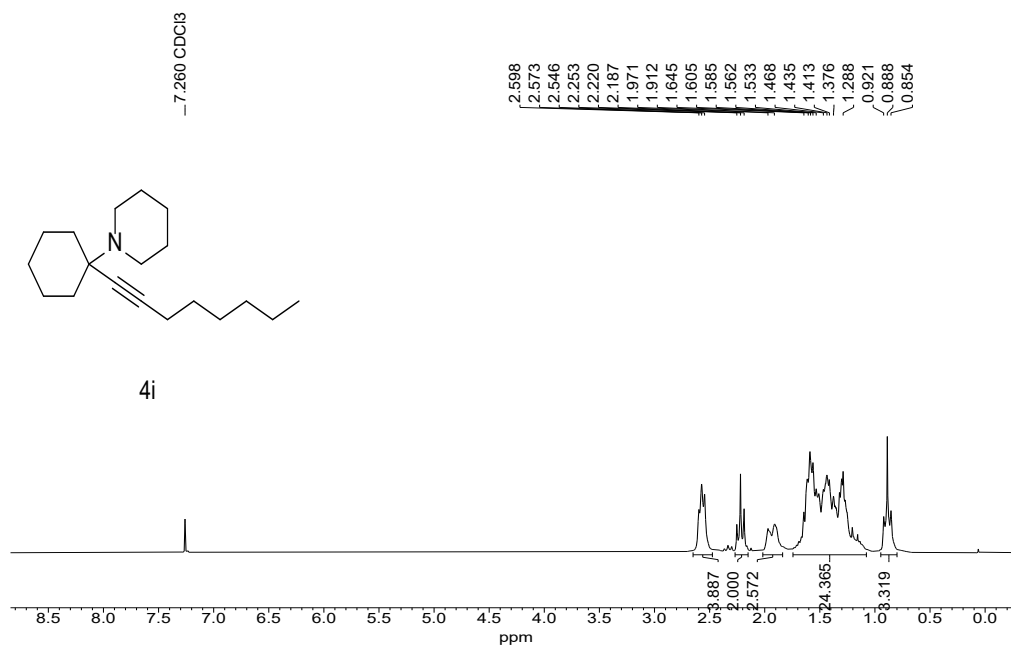
PICTURE 39: ^{13}C NMR for 1-(3-methyl-1-phenylhex-1-yn-3-yl)pyrrolidine 4g



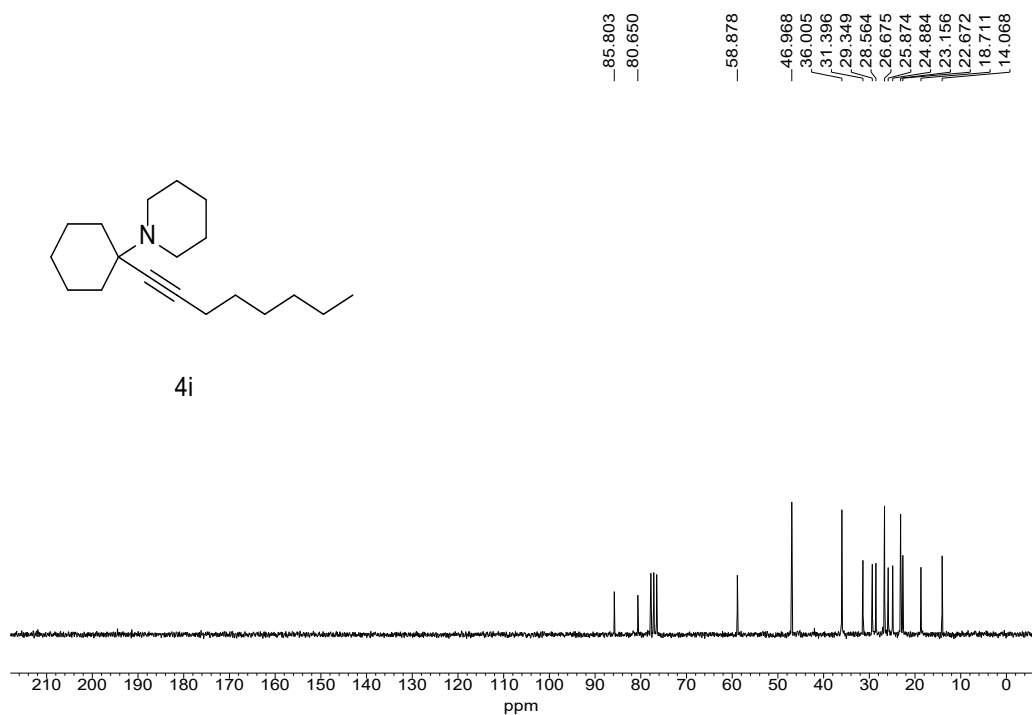
PICTURE 40: ^1H NMR for 2-methyl-4-(1-(4-phenylpiperazin-1-yl)cyclohexyl)but-3-yn-2-ol 4h



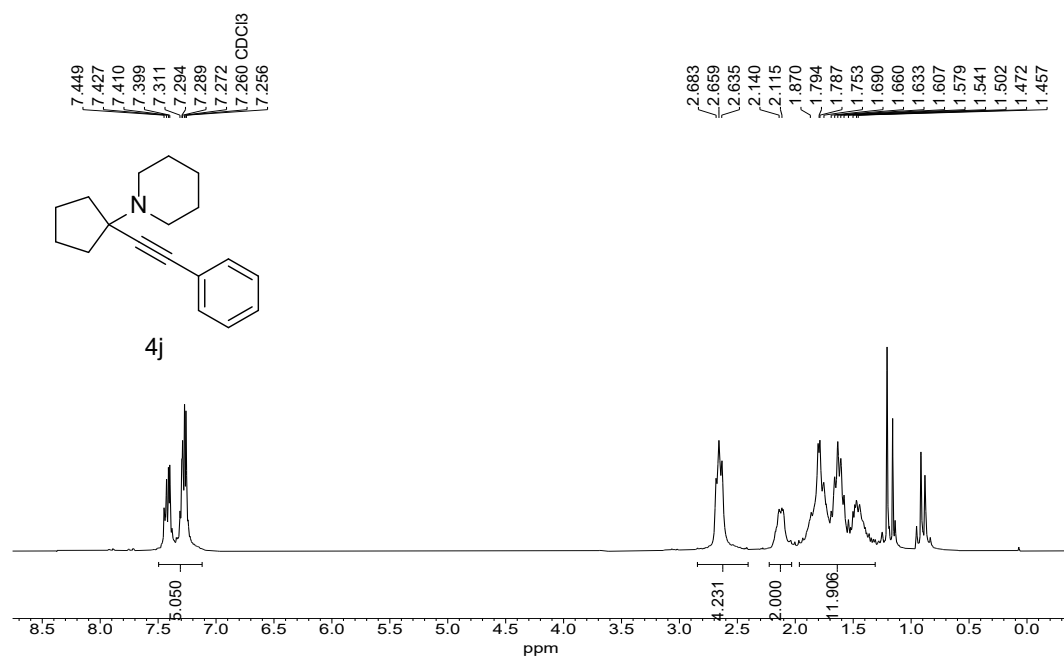
PICTURE 41: ¹³C NMR for 2-methyl-4-(1-(4-phenylpiperazin-1-yl)cyclohexyl)but-3-yn-2-ol 4h



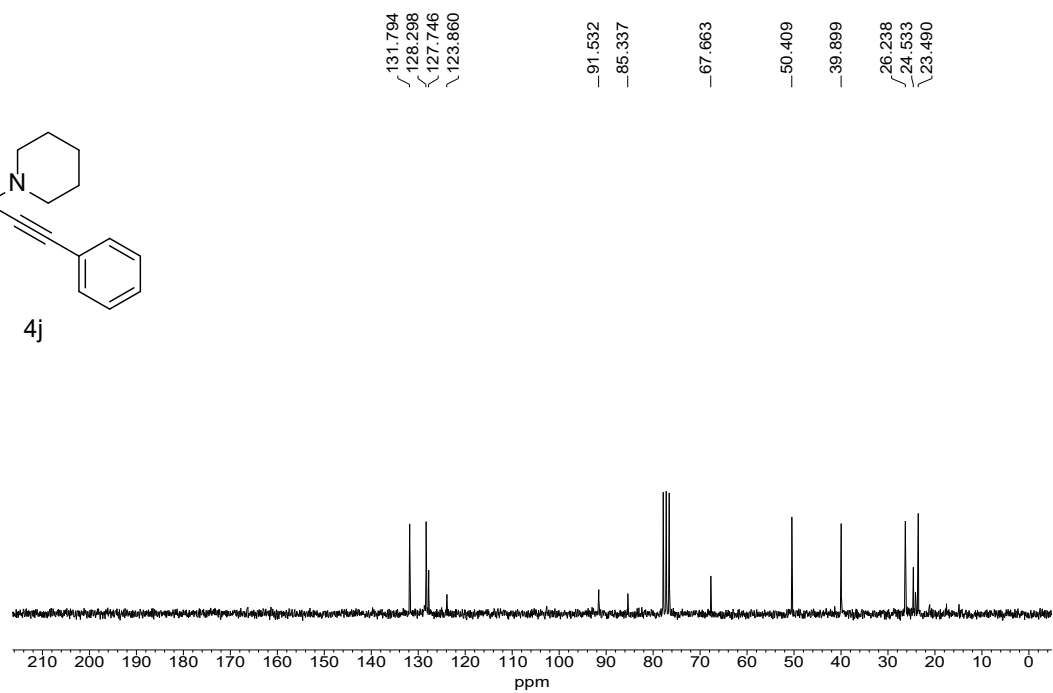
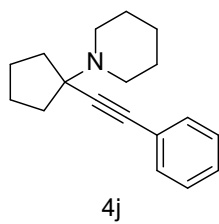
PICTURE 42: ¹H NMR for 1-(1-(oct-1-yn-1-yl)cyclohexyl)piperidine 4i.



PICTURE 43: ¹³C NMR for 1-(1-(oct-1-yn-1-yl)cyclohexyl)piperidine 4i



PICTURE 44: ¹H NMR for 1-(1-(phenylethynyl)cyclopentyl)piperidine 4j



PICTURE 45: ^{13}C NMR for 1-(1-(phenylethynyl)cyclopentyl)piperidine 4j

Personal and Academic Background

Adejumo Temiloluwa Timothy was born in the year 1994 in Iwo, Osun state, Nigeria. He completed his secondary education at Anglican School of Science, Gbongan. Subsequently, he pursued his undergraduate studies in Industrial Chemistry at Osun State University, graduating in 2012 with an impressive GPA of 4.10 out of 5.0.

Following his undergraduate degree, he furthered his academic journey by enrolling in the Master of Academic Studies program at the University of Ilorin, specializing in Industrial Chemistry. In 2015, he successfully completed his master's degree with a commendable average grade of 69%. His master's thesis, titled "Synthesis, Characterization, and Antimicrobial Activity of Au(II) Schiff Base Complexes," showcased his dedication to in-depth research and academic excellence.

A significant turning point in his educational pursuit was marked by his selection for a prestigious scholarship under the Bilateral Education Agreement (BEA) facilitated by the Federal Scholarship Board of Nigeria. This scholarship granted him the opportunity to pursue his doctoral studies abroad. In 2018, he embarked on his doctoral journey at the Department of General and Inorganic Chemistry within the Chemistry study program at the University of Belgrade, Faculty of Chemistry. He had the privilege of being mentored by Dr. Božidar Čobeljić, a respected personality in the field.

Since then, Adejumo Temiloluwa Timothy has been deeply engaged in impactful scientific research endeavors. His dedication and hard work have resulted in the publication of scientific papers in esteemed international journals. Notably, his research efforts have been financially supported by esteemed institutions including the Ministry of Science, Technological Development and Innovation of Republic of Serbia (Contract number: 451-03-47/2023-01/200168), the European Union, Greek national funds through the Operational Program "Human Resources Development, Education and Lifelong Learning", the Slovenian Research Agency, and the Ministry of Education of the Federal Republic of Nigeria. Also, this research was supported by the Science Fund of the Republic of Serbia, #7750288, Tailoring Molecular Magnets and Catalysts Based on Transition Metal Complexes – **TMMagCat**. All of these notable achievements have stemmed from the foundation of his doctoral dissertation.

Изјава о ауторству

Име и презиме аутора _____

Број индекса _____

Изјављујем

да је докторска дисертација под насловом

- резултат сопственог истраживачког рада;
- да дисертација у целини ни у деловима није била предложена за стицање друге дипломе према студијским програмима других високошколских установа;
- да су резултати коректно наведени и
- да нисам кршио/ла ауторска права и користио/ла интелектуалну својину других лица.

Потпис аутора

У Београду, _____

**Изјава о истоветности штампане и електронске верзије докторског
рада**

Име и презиме аутора _____

Број индекса _____

Студијски програм _____

Наслов рада _____

Ментор _____

Изјављујем да је штампана верзија мог докторског рада истоветна електронској верзији коју сам предао/ла ради похрањивања у **Дигиталном репозиторијуму Универзитета у Београду**.

Дозвољавам да се објаве моји лични подаци везани за добијање академског назива доктора наука, као што су име и презиме, година и место рођења и датум одбране рада. Ови лични подаци могу се објавити на мрежним страницама дигиталне библиотеке, у електронском каталогу и у публикацијама Универзитета у Београду.

Потпис аутора

У Београду, _____

Изјава о коришћењу

Овлашћујем Универзитетску библиотеку „Светозар Марковић“ да у Дигитални репозиторијум Универзитета у Београду унесе моју докторску дисертацију под насловом:

која је моје ауторско дело.

Дисертацију са свим прилозима предао/ла сам у електронском формату погодном за трајно архивирање.

Моју докторску дисертацију похрањену у Дигиталном репозиторијуму Универзитета у Београду и доступну у отвореном приступу могу да користе сви који поштују одредбе

садржане у одабраном типу лиценце Креативне заједнице (Creative Commons) за коју сам се одлучио/ла.

1. Ауторство (CC BY)
2. Ауторство – некомерцијално (CC BY-NC)
3. Ауторство – некомерцијално – без прерада (CC BY-NC-ND)
4. Ауторство – некомерцијално – делити под истим условима (CC BY-NC-SA)
5. Ауторство – без прерада (CC BY-ND)
6. Ауторство – делити под истим условима (CC BY-SA)

(Молимо да заокружите само једну од шест понуђених лиценци.

Кратак опис лиценци је саставни део ове изјаве).

Потпис аутора

У Београду, _____

Published and published works that are part of the dissertation:

- **Adejumo Temiloluwa *et al.***, (2023). "Correlating Structure and KA^2 Catalytic Activity of Zn(II) Hydrazone Complexes", *European journal of inorganic chemistry*, e202300193, <https://doi.org/10.1002/ejic.202300193>
- **Adejumo Temiloluwa *et al.***, (2020). Synthesis, characterization, catalytic studies and DFT calculations of Zn(II) hydrazone complexes. *Molecules*, volume 25 issue 18, <https://doi.org/10.3390/molecules25184043>

Conferences/Presentations

- Temiloluwa T. Adejumo, Katarina K. Anđelković, Dragana Mitić, Božidar Čobeljić. "Synthesis and characterization of Fe(III) and Mn(II) complexes with 2-acetylthiazolethiosemicarbazone." Presented at the Seventh Conference Of the Young Chemists Of Serbia, November 2nd, 2019, Belgrade, Serbia. Abstract published in Book of Abstracts CS PP 11, p 89. (ISBN: 978-86-7132-076-4)
- Nevena Stevanović, Snežana Selaković, Temiloluwa Adejumo, Maja Šumar-Ristović, Božidar Čobeljić, Katarina Anđelković. "Synthesis and characterization of Zn(II) and Bi(III) complexes with N-substituted glycine hydrazones." Presented at the Twenty-second Annual Conference "YUCOMAT 2021", August 30 - September 3, 2021, Herceg Novi, Montenegro. Abstract published in Book of Abstracts P.S.III.17, p 125. (ISBN: 978-86-919111-6-4).
- T. Adejumo, D. Radanović, M. Zlatar, M. Gruden, K. Anđelković, B. Čobeljić. "Synthesis, characterization and DFT calculations of dinuclear Schiff base Mn(II) complex." Presented at the 27th Conference of the Serbian Crystallographic Society, September 16–17, 2021, Kragujevac, Serbia. Abstract published in Book of Abstracts, pp 24–25. (ISBN: 978-86-6009-085-2)